Titre: Title:	Modelling and analysis of gain-coupled DFB semiconductor lasers
Auteur: Author:	Jianyao Chen
Date:	1997
Type:	Mémoire ou thèse / Dissertation or Thesis
Référence: Citation:	Chen, J. (1997). Modelling and analysis of gain-coupled DFB semiconductor lasers [Thèse de doctorat, École Polytechnique de Montréal]. PolyPublie. https://publications.polymtl.ca/6797/

UNIVERSITÉ DE MONTRÉAL

MODELLING AND ANALYSIS OF GAIN-COUPLED DFB SEMICONDUCTOR LASERS

JIANYAO CHEN

DÉPARTEMENT DE GÉNIE PHYSIQUE

ÉCOLE POLYTECHNIQUE DE MONTRÉAL

THÈSE PRÉSENTÉE EN VUE DE L'OBTENTION

DU GRADE DE PHILOSOPHIAE DOCTOR (Ph.D.)

(GÉNIE PHYSIQUE)

Février 1997

National Library of Canada
Acquisitions and Bibliographic Services
395 Wellington Street
Ottawa ON K1A 0N4
Canada

Bibliothèque nationale du Canada
Acquisitions et services bibliographiques
395, rue Wellington
Ottawa ON K1A 0N4
Canada

Your file Votre référence

Our file Notre référence

0-612-32994-1

Canada

UNIVERSITÉ DE MONTRÉAL

ÉCOLE POLYTECHNIQUE DE MONTRÉAL

Cette thèse intitulée:

MODELLING AND ANALYSIS OF GAIN-COUPLED DFB SEMICONDUCTOR LASERS

présentée par: CHEN Jianyao

en vue de l'obtention du grade de: Philosophiae Doctor

a été dûment acceptée par le jury d'examen constitué de:

M. YELON Arthur, Ph.D., président rapporteur

M. MACIEJKO Romain, Ph.D., directeur de recherche

M. HUANG Wei-Ping, Ph.D., membre

M. WU Ke, Ph.D., membre

Acknowledgements

I would like to thank sincerely my supervisor, Prof. Roman Maciejko, for his encouragement, advice and guidance throughout the course of this thesis work. His kindness, understanding, and patience during my last four years at Ecole Polytechnique deserve my deepest gratitude.

My special gratitude is also due to Dr. Toshihiko Makino, manager of semiconductor laser design group at Nortel Technologies Inc., for his invaluable suggestions and warm encouragement to bring me to pass through this Ph. D. research program.

I am also grateful to Dr. Alain Champagne for his wonderful cooperation, fruitful discussions and indispensable assistance on many computer issues during this study.

I wish especially to thank my former supervisor, Prof. Jing-Ren Qian of the University of Science and Technology of China (USTC), for his invaluable advice, clear guidance and personal help during my studies and work in USTC and his interest and encouragement throughout my studies in Canada.

I must also thank my fellow colleagues for their encouragement and help. In particular, the contributions from Jie Gao, Benoit Reid, Michele Goano, Michel Abou-Khalil, and Kim Ryel are gratefully acknowledged.

I would like to express my special love and gratitude to Weiwen Zhang for her love, understanding and sacrifice and to my parents, my sister and brother for their constant blessing and unyielding support.

Résumé

Les lasers à semi-conducteurs à rétroaction distribuée (DFB) sont présentement les sources les plus prometteuses pour les systèmes de télécommunication par fibres optiques, en partie grâce à leur faible dimension et à leur sélectivité fréquentielle. L'introduction récente du couplage par gain et de la modulation par électrodes multiples ouvre de nouvelles possibilités pour l'amélioration de ces lasers. Le but de cette thèse est de développer un outil numérique suffisamment complet et versatile pour modéliser efficacement et avec précision ces dispositifs complexes, et en suivant une modélisation et une analyse soignées, de présenter les caractéristiques importantes des lasers DFB à couplage par gain.

Suivant le formalisme des ondes stationnaires, la méthode des modes couplés et l'analyse par les fonctions de Green sont utilisées pour étudier les lasers DFB à couplage par gain. Puisqu'elle permet de séparer les dépendances temporelle et spatiale des champs modaux, cette approche possède l'avantage unique d'obtenir des résultats analytiques qui aident à clarifier le fonctionnement de ces lasers. Grâce aux équations d'évolution avec dépendance spatiale, un modèle auto-consistant et multimodal a été développé pour les lasers DFB à couplage complexe et modulé par électrodes multiples. L'analyse détaillée de cette thèse couvre un large spectre de la physique des lasers DFB à couplage par gain. En utilisant l'analyse par ondes de Bloch, les conditions d'oscillation unimodale des lasers DFB à couplage par gain ont été expliquées intuitivement, et l'effet très important des longueurs inégales du

réseau de gain sur la marge de gain unimodal a été démontré pour la première fois. En s'appuyant sur les équations d'évolution multimodales avec dépendance spatiale développées dans cette thèse, les caractéristiques statiques et dynamiques du mode principal et des modes secondaires des lasers DFB à couplage par gain ont été étudiées en détail. L'étude a aussi été étendue aux lasers DFB à électrodes multiples du type *push-pull* pour la première fois. En étudiant le rôle du coefficient de couplage complexe et de divers phénomènes spatiaux, une compréhension en profondeur du rendement élévé, de la puissance élevée, de la vitesse élevée, de la grande suppression des modes secondaires, du faible seuil, de la faible dérive en fréquence et de la faible distortion harmonique dans les lasers DFB à couplage par gain a été atteinte.

Abstract

With the unique features of compact size and a built-in frequency selective element, the distributed feedback (DFB) semiconductor lasers are presently the most promising light sources in optical fiber communications systems. The recently introduced gain coupling and multielectrode modulation provide new possibilities for the improvement of that laser. The aim of this dissertation is to develop a comprehensive and versatile numerical tool for the efficient and accurate simulation of those delicate devices and, through rigorous modelling and analysis, to reveal various salient features of gain-coupled DFB lasers.

Based on the standing wave formalism, the coupled mode method and the Green's function analysis are used in this thesis to study gain-coupled DFB lasers. By separating the temporal and spatial dependencies of the modal fields in the lasers, the approach possesses a unique advantage of producing simple and insightful closed form results which help gain physical understanding into the laser operation. With the help of the spatially dependent rate equations, a self-consistent, multimode, full bias range (from below to above threshold) model has been developed for complex-coupled DFB lasers including multielectrode modulation. The detailed analysis of this thesis covers a wide range investigation of gain-coupled DFB laser physics. Using the Bloch wave analysis, the condition of single mode oscillation in gain-coupled DFB lasers has been explained intuitively and the significant effect of unequal section lengths in the gain grating on the single-mode gain margin has

also been revealed for the first time. Based on the spatially dependent multimode rate equations developed in this thesis, the static and dynamic characteristics of the lasing mode and of the side modes of gain-coupled DFB lasers are investigated in detail. The study has also been successfully extended to the analysis of multi-electrode push-pull DFB lasers to include the modal interference effect for the first time. Through the study of the role of the complex coupling coefficient and the various spatial features, an in-depth understanding of the high yield, high power, high speed, high side mode suppression, low threshold, low frequency chirp, and low harmonic distortion in gain-coupled DFB lasers has also been reached.

Condensé en français

Depuis la fabrication par Nakamura *et al.* en 1973 des premiers lasers à rétro-action distribuée (DFB pour distributed-feedback) pompés optiquement et la fabrication en 1974 par Scifres *et al.* des premiers lasers DFB pompés électriquement, ceux-ci ont subit de nombreuses mutations, telles l'introduction d'un déphasage de $\lambda/4$, le réseau *chirpé* et les contacts électriques à largeur modulée, pour augmenter le fonctionnement unimodal. Récemment, les lasers DFB à couplage par gain ont attiré l'attention des chercheurs à cause de leur remarquable performance unimodale. Des travaux tant théoriques qu'expérimentaux ont montré que même un très faible couplage par gain peut augmenter de beaucoup la performance unimodale des lasers DFB à semi-conducteurs. Le couplage par gain a aussi comme avantage de réduire le brûlage de trous spatiaux (SHB) de façon significative dans la cavité laser ce qui rend possible l'utilisation de couches anti-reflet asymétriques dans le but d'augmenter la puissance optique extraite de l'un des miroirs du laser. Pour pouvoir déterminer le design optimal ainsi que pour bien comprendre ces lasers, il faut pouvoir simuler efficacement et avec précision ces nouveaux lasers DFB.

L'objectif de cette thèse est de développer un outil de simulation numérique détaillé, versatile, efficace et précis des lasers DFB à couplage par gain. Par une modélisation et une analyse détaillées, on atteint une compréhension en profondeur de l'émission à grande puissance, de la modulation à haute vitesse, du fort rapport de suppression des modes latéraux (SMSR), du haut rendement unimodal, du faible

courant de seuil, du faible bruit, de la faible dérive en fréquence et de l'oscillation stable du mode principal des lasers DFB à couplage par gain. En considérant plusieurs phénomènes causant des inhomogénéités spatiales dans les lasers DFB à couplage par gain actuels, comme la modulation par électrodes multiples, les conditions asymétriques de réflexion aux facettes de la cavité, l'utilisation d'un réseau de gain, le brûlage de trous spatiaux (SHB), la compression non linéaire du gain et l'émission spontanée, les propriétés des lasers DFB à couplage par gain sont étudiées dans le but de permettre le développement futur et d'améliorer le design de ce type de laser. Afin de conserver l'élégance de l'approche des équations d'évolution et d'en dépasser les limites, cette thèse a aussi pour but d'étendre le formalisme de l'onde stationnaire au régime multimode de même qu'à toute la gamme des conditions d'opération du laser, c'est-à-dire, tant au-dessus qu'au-dessous du seuil.

Cette thèse comprend huit chapitres regroupant un travail analytique et une variété d'études par modélisation numérique du laser à couplage par gain couvrant la performance unimodale, les caractéristiques en régime stationnaire de même qu'en régime dynamique à petit et à grand signal, la distorsion harmonique et la modulation de type *push-pull*. Chaque chapitre contient une introduction et une reproduction complète d'une publication. Dans chacun des chapitres, une emphase particulière est accordée aux développements nouveaux tant au niveau théorique qu'au niveau de la simulation des dispositifs. Tout au long de cette thèse, l'approche des équations d'évolution combinée à l'analyse par fonctions de Green et par la méthode des modes couplés constitue le cadre théorique principal appliqué à l'analyse et la simulation d'une vaste classe de lasers à couplage par gain, incluant les effets liés aux diverses inhomogénéités spatiales dans la cavité laser de même que la modulation par électrodes multiples. En séparant les dépendances spatiales et temporelles des champs modaux dans le laser, l'approche préconisée présente l'avantage unique de conduire à des résultats analytiques simples et révélateurs qui aident à obtenir une

meilleure compréhension physique du fonctionnement du laser à semi-conducteurs. Brièvement, les chapitres de cette thèse sont résumés dans ce qui suit.

Le premier chapitre forme l'introduction de cette thèse. Il débute par une description générale des fondements de ce travail dans le but de démontrer l'importance et la nécessité d'utiliser des lasers à semi-conducteurs de type DFB comme source de rayonnement dans les systèmes de télécommunications par fibre optique. Par la suite, une brève revue des développements technologiques qui ont conduit à l'amélioration de la performance des lasers DFB de même que des progrès récents au niveau de la modélisation et de l'analyse des ces dispositifs de pointe est présentée. En particulier, les différences et les avantages respectifs de l'approche par onde propageante (*travelling wave*) et par onde stationnaire sont clairement soulignés. Finalement, l'objectif de cette thèse, incluant le développement de techniques de modélisation ainsi que l'exploitation des caractéristiques importantes du laser DFB à couplage par gain, est établie.

Le chapitre 2 est principalement constitué d'une publication intitulée "Improvement of Single-Mode Gain Margin in Gain-Coupled DFB Lasers", portant sur l'étude des propriétés des ondes optiques dans les guides à structure périodique. Basée sur l'analyse par onde de Bloch, une explication intuitivement attrayante des mécanismes conduisant à l'oscillation unimodale des lasers DFB à couplage par gain est présentée. On y démontre que le profil d'intensité des modes du laser DFB, du côté de longue et courte longueur d'onde de la bande passante du réseau de Bragg, sont respectivement en phase et en opposition de phase avec le réseau d'indice du laser DFB. Lorsque le réseau de gain est en phase avec une des ondes de Bloch, une oscillation unimodale ayant une large marge de gain est obtenue. Suite à cette observation, il est montré pour la première fois, que des sections du réseau de gain de longueur inégale peuvent avoir un effet significatif sur la suppression des ondes de Bloch en opposition de phase de même que sur les modes d'ordre supérieur dans ces

lasers. Des calculs numériques, reposant sur la méthode des matrices de transfert, montrent qu'un réseau de gain ayant une section courte avec un gain élevé peut augmenter considérablement le rendement unimodal, déterminé en terme de marge de gain, des lasers DGB à couplage par gain. Considérant l'influence du *linewidth enhancement factor* α_M, l'utilisation d'une courte section à gain fort dans le réseau du laser peut augmenter efficacement la marge de gain et améliorer la stabilité modale face au brûlage de trous spatiaux (SHB) au fur et à mesure que le laser est polarisé au-dessus du seuil.

Le chapitre 3 inclut la publication "Self-Consistent Analysis of Side Mode Supression in Gain-Coupled DFB Semiconductor Lasers" qui couvre l'analyse des caractéristiques du laser DFB à couplage par gain en régime stationnaire. Afin d'obtenir une compréhension beaucoup complète des mécanismes de la suppression des modes latéraux dans les lasers DFB à couplage par gain, une analyse multimodale auto-consistante incluant différentes inhomogénéités spatiales dans la cavité DFB, comme la rétroaction distribuée, le couplage par gain dépendant des porteurs, le brûlage de trous spatiaux de même que la compression de gain non linéaire, est développée dans ce chapitre. En introduisant le paramètre de gain modal net dans les équations des modes couplés dans le but d'inclure la contribution de l'émission spontanée, un système d'équations d'évolution multimodales avec dépendance spatiale est obtenu pour la première fois. Une analyse détaillée montre qu'un couplage élevé, par indice et par gain, contribuent à l'amélioration du rapport de suppression des modes latéraux (SMSR) des lasers DFB. Un fort couplage DFB réduit le courant de seuil des lasers et maintient les modes latéraux à des intensités relativement faibles. Comme le couplage par gain réduit significativement l'interaction de l'onde de Bloch en opposition de phase ainsi que celle des modes supérieurs avec le milieu de gain périodique, il en découle un augmentation du taux de amortissement (*decay rate*) des modes latéraux des lasers DFB. Cela confirme aussi que, au-dessus du seuil,

le brûlage de trous spatiaux (SHB) favorise les modes ayant une courte longueur d'onde et donc réduit ou augmente respectivement le SMSR lorsque le couplage par gain est en phase ou en opposition de phase. Pour des intensités optiques élevées, l'analyse auto-consistante révèle que les instabilités dans les lasers DFB à couplage par gain en opposition de phase peuvent détériorer le SMSR alors que l'oscillation stable du mode principal dans les lasers DFB à couplage par gain en phase aide à réduire l'effet de la compression de gain non linéaire sur le SMSR.

Le chapitre 4 porte essentiellement sur l'analyse de la dynamique en régime petit signal des lasers DFB à couplage par gain telle que présentée dans la publication "Relaxation Oscillation Frequency of DFB Lasers with Gain Coupling". La fréquence des oscillations de relaxation est un facteur très important pour la modulation à haute fréquence des lasers DFB à semi-conducteurs. À l'aide d'une analyse par fonctions de Green, la dépendance de la fréquence des oscillations de relaxation dans les lasers DFB à couplage par gain en fonction du coefficient de couplage complexe et de plusieurs autres facteurs est étudiée systématiquement. L'analyse tient compte de la distribution non-uniforme de l'intensité optique, du brûlage de trous spatiaux (SHB), de la saturation du gain et la compression de gain non linéaire. À partir des équations d'évolution, une expressions analytique de la fréquence des oscillations de relaxation a été obtenue. Cette expression montre explicitement que la fréquence des oscillations de relaxation des lasers DFB à semi-conducteurs est déterminée par la distribution spatiale de l'intensité optique, par le gain différentiel effectif local et par la distribution du gain matériel. Cette expression analytique révèle aussi pour la première fois que le *linewidth enhancement factor* α_M joue un rôle significatif dans l'augmentation de la bande passante de modulation des lasers DFB à couplage par gain. L'analyse confirme que cette augmentation de la bande passante est causée par l'interaction entre le réseau de gain et le patron de l'onde stationnaire formé par la distribution de l'intensité optique dans la cavité. Il se

produit une augmentation du gain différentiel effectif local proportionnelle au *linewidth enhancement factor* α_M. En choisissant les réseaux d'indice et de gain du laser DFB en opposition de phase, des oscillations de relaxation d'une plus haute fréquence peuvent être obtenues, particulièrement lorsque le couplage par indice est relativement faible.

Le chapitre 5 contient la publication "Second-Order Harmonic Distortion in AM Response of Gain-Coupled DFB Lasers" qui analyse la distorsion harmonique au deuxième ordre de la réponse en amplitude des lasers DFB à couplage par gain. Cette analyse est importante car une large bande passante de modulation dans les lasers DFB est nécessaire pour les systèmes de télécommunications optiques. De plus, le couplage complexe procure un degré de liberté supplémentaire pour l'amélioration de la distorsion harmonique. En utilisant les équations d'évolution avec dépendance spatiale, ce chapitre présente une étude systématique de la distorsion harmonique au deuxième ordre dans les lasers DFB à couplage par gain. En gardant l'avantage de résultats analytiques, l'étude auto-consistante a révélé de façon explicite l'effet de différentes non-linéarités spatiales sur la distorsion harmonique. En particulier, les effets des oscillations de relaxation et du brûlage de trous spatiaux (SHB) sur de la distorsion harmonique au deuxième ordre apparaissent explicitement dans un résultats analytique. L'analyse illustre clairement que les distorsions harmoniques au deuxième ordre d'origines différentes peuvent avoir des signes différents. Par conséquent, en choisissant une structure a couplage complexe appropriée, une annulation peut se produire et conduire à une faible distorsion harmonique. Les résultats numériques et analytiques se complètent bien. Différentes non-uniformités spatiales, les effets du niveau d'injection et de l'instabilité modale dans les lasers DFB à couplage par gain en opposition de phase sur la distorsion harmonique sont aussi discutés en détail.

Le chapitre 6 est constitué de la publication "Transient Side Mode Suppression

in Gain-Coupled DFB Lasers" qui présente une analyse multimode détaillée de la dynamique en régime grand signal du laser DFB à couplage par gain. Cette analyse est importante car les fluctuations des modes latéraux en régime transitoire peuvent causer une sévère dégradation de la transmission dans les systèmes à longue portée et à débits élevés à cause de la dispersion à 1.55 μm, là où l'absorption est minimale, dans la fibre optique. En approximant les champs modaux par ceux obtenus au seuil, la suppression dynamique des modes latéraux est étudiée dans les lasers DFB à couplage par gain en utilisant les équations d'évolution multimodales avec dépendance spatiale. L'approche préconisée est non seulement relativement simple du point de vue théorique mais présente aussi des avantages importants du point de vue de la modélisation numérique. Les différents résultats analytiques obtenus aident beaucoup à comprendre les effets des différentes inhomogénéités spatiales sur la suppression des modes latéraux dans les lasers DFB à couplage par gain. Il a été démontré pour la première fois que la suppression dynamique des modes latéraux dans les lasers DFB à semi-conducteurs dépend de façon critique du taux de décroissance modal et du gain différentiel dynamique effectif. Le couplage par gain réduit les interactions des modes latéraux avec le milieu de gain périodique, ce qui conduit à des taux de décroissance plus élevés et à un gain différentiel modal en régime dynamique plus faible pour ces modes. Ceci contribue à la suppression des intensités transitoires de ces modes. Cette étude compare aussi les différences causées par l'utilisation d'un couplage par gain en phase ou en opposition de phase sur la suppression dynamique des modes latéraux dans les lasers DFB. En conclusion, il apparaît que le brûlage de trous spatiaux réduit ou augmente respectivement, la suppression dynamique des modes latéraux dans les lasers DFB selon que le couplage par gain est en phase ou en opposition de phase avec le réseau d'indice.

Le chapitre 7 est constitué de la publication "Dynamic Properties of Push-Pull DFB Semiconductor Lasers" qui a étendu avec succès l'analyse par équations d'évo-

lution, à l'étude de la réponse dynamique de modulation des lasers DFB à couplage par gain de type *push-pull* à électrodes multiples. En utilisant un modèle d'interférence à deux modes, l'étude inclut, pour la première fois, la contribution de l'interférence modale dans la réponse de modulation. Différentes non-uniformités spatiales, comme le couplage par gain distribué, le brûlage de trous spatiaux, la compression de gain non linéaire, la modulation *push-pull* et la contribution du mode latéral sont toutes traitées de façon auto-consistante. Les résultats analytiques obtenus d'une analyse petit signal révèlent que la performance à haute fréquence des lasers *push-pull* à semi-conducteurs est caractérisée par la première fréquence de coupure, qui dépend de la puissance, et une fréquence de résonance dépendant de la structure. Il a aussi été démontré analytiquement que la première fréquence de coupure et la fréquence de résonance dépendent respectivement de la différence de gain au seuil et de la différence de fréquence entre le mode laser et le mode latéral antisymétrique le plus proche. Tant les résultats analytiques que numériques présentés dans ce chapitre sont en très bon accord avec une analyse par onde propageante (*travelling wave*) publiée précédemment. Une analyse systématique des différents effets spatiaux indique qu'une très haute fréquence de modulation et une une très faible dérive en fréquence peuvent être obtenues par la modulation directe *push-pull* dans les lasers DFB à couplage par gain.

Le chapitre 8 est la conclusion de cette thèse. On résume d'abord les principales réalisations de ce travail tant au niveau des techniques de modélisation qu'au niveau de l'étude des caractéristiques essentielles des lasers DFB à couplage par gain. Tel qu'esquissé dans les paragraphes précédents, les réalisations et les contributions originales de ce travail sont clairement soulignées. Par la suite, en se basant sur les conclusions de ce travail, des voies pour des études plus approfondies concernant les propriétés encore plus raffinées des lasers DFB à couplage par gain sont suggérées.

En conclusion, cette thèse a permis d'étendre avec succès l'approche des équa-

tions d'évolution à l'analyse des caractéristiques multimodes, en régime stationnaire et dynamique tant au-dessus qu'au dessous du seuil, des lasers DFB à couplage par gain, en incluant aussi les inhomogénéités spatiales. Cette recherche étendue illustre clairement que le couplage par gain améliore plusieurs aspects de la performance des lasers DFB pour les applications exigeantes du domaine des télécommunication par fibre optique. De plus, l'analyse préliminaire des lasers DFB *push-pull* à couplage par gain révèle que la modulation par électrodes multiples offre une nouvelle voie dans la recherche de solutions pour l'exploitation de l'énorme potentiel des lasers DFB à semi-conducteurs. Avec l'apparition de nouvelles applications et le développement de nouvelles techniques de fabrication, des lasers DFB à couplage par gain ayant caractéristiques encore plus performantes vont certainement apparaître et jouer un rôle de plus en plus important dans les systèmes de télécommunications par fibres optiques futurs. Suivant ces progrès, la modélisation et l'analyse des lasers DFB à couplage par gain deviendra encore plus complexe et d'autant plus importante.

TABLE OF CONTENTS

CHAPTER 1

Introduction

1.1 Background of dissertation

The extremely low attenuation and ultra wide bandwidth of the single-mode fibers provide tremendous opportunities for building broadband integrated telecommunication systems. With the unique features of compact size and the ability of direct modulation at high bit rates, semiconductor lasers are the most important light sources in the rapid deployment of such optical fiber communication systems [Agrawal and Dutta, 1993]. Currently, much effort in both research institutes and industries is devoted to the development of single-frequency, high speed, high power, low threshold, low noise, and possibly wavelength tunable lasers.

In conventional Fabry-Perot lasers, the optical feedback in the active medium is provided by the facet reflections at both ends of the laser cavity. The magnitude of those reflections is frequency-independent. It is therefore the same for all the longitudinal modes. The only discrimination among the longitudinal modes in such a laser comes from the gain spectrum itself. However, since the gain spectrum is usually much wider than the longitudinal mode spacing in the cavity, the resulting mode discrimination is rather poor. One possible way of improving the mode selectivity in semiconductor lasers is to use a frequency-dependent feedback mechanism so that the cavity loss can be different for the different longitudinal modes.

Longitudinally distributed feedback gratings produced by the periodic perturbations of the refractive index and/or the gain in the laser cavity itself provide a very neat way of achieving the required feedback in semiconductor lasers. The usefulness of this technique comes from the fact that the scattered coherent lightwaves from the Bragg grating interfere constructively for certain directions when the Bragg phase condition is satisfied. Since the feedback provided by such distributed structures is intrinsically frequency dependent, distributed feedback (DFB) lasers tend to achieve very stable single-mode lasing with a narrow linewidth in broadband gain media. They have therefore attracted considerable attention both experimentally and theoretically [Lee, 1991, Suematsu *et al.*, 1992].

1.2 Historical overview

The first optically pumped DFB semiconductor laser was made by Nakamura *et al.* [Nakamura *et al.*, 1973] in 1973 and the first carrier-injection DFB semiconductor laser was made by Scifres *et al.* [Scifres *et al.*, 1974] in 1974. In 1975, Nakamura *et al.* reported the continuous operation of DFB semiconductor lasers at room temperature [Nakamura *et al.*, 1975]. These lasers were AlGaAs/GaAs lasers emitting at 0.8 μm. Since fiber dispersion is minimum at a wavelength of 1.3 μm and fiber loss is minimum at 1.55 μm, the rapid development of optical communication systems also stimulated the research on InGaAsP/InP DFB lasers. In 1979, Doi *et al.* made the first InGaAsP/InP DFB laser emitting at 1.3 μm [Doi *et al.*, 1979].

The DFB laser theory predicts that there are two equivalent oscillation modes with the same threshold gain in DFB lasers with a uniform grating. The degeneracy can be lifted by the reflection from the facets at both ends of the laser cavity. However, the present cleaving process does not allow to position the facet pre-

cisely, which causes a problem of single-mode operation [Streifer *et al.*, 1975]. In order to obtain a higher single-mode yield, $\lambda/4$-shifted DFB lasers with antireflection/antireflection (AR/AR) facet coatings were proposed in 1976 by Haus and Shank [Haus and Shank, 1976]. Since the corrugation phase needs to be reversed at the center of the laser cavity, the difficulty of producing the $\lambda/4$-shifted gratings delayed the fabrication of such lasers for several years. In 1984, Sekartedjo *et al.* were the first to fabricate $\lambda/4$-shifted DFB lasers with second-order gratings by electron-beam lithography [Sekartedjo *et al.*, 1984] and Utaka *et al.* used first-order gratings fabricated by simultaneous holographic exposure of positive and negative photoresists [Utaka *et al.*, 1984]. The $\lambda/4$-shifted DFB lasers have a high single-mode yield, but they tend to break up into multimode operation when the output power is high. Soda *et al.* explained in 1987 that this phenomenon was caused by spatial hole burning [Soda *et al.*, 1987].

Complex coupling provides an effective alternative for obtaining stable single-mode operation with significantly improved spatial hole burning in DFB lasers. The effect was also discovered first by Kogelnik and Shank in 1972 [Kogelnik and Shank, 1972]. Attempts were made soon after to fabricate gain-coupled DFB lasers by etching the active layer to provide a periodic modulation of its thickness [Nakamura *et al.*, 1974]. Such attempts were not very successful because of the defects introduced during the etching process. Interest in gain-coupled DFB lasers was revived in the late 1980s because of the yield problems associated with index-coupled DFB lasers [Nakano *et al.*, 1989]. Since then, extensive studies have revealed the existence of many properties that make gain-coupled DFB lasers superior to index-coupled DFB lasers [14-23].

1.3 Modelling of DFB lasers

Modelling and analysis are essential to the development of DFB lasers because of their sophisticated structures and interdependent characteristics. Especially, for the gain-coupled DFB lasers, they have been strong driving forces for further progress in design. Traditionally, the conventional rate equations for the photon and carrier densities have been successfully used to model the properties of the Fabry-Perot semiconductor lasers [Agrawal and Dutta, 1993]. However, an intrinsic shortcoming of such an approach is the omission of the account for spatially dependent features such as those found in DFB lasers. Because of the distributed feedback mechanism, the asymmetric facet condition, and the multielectrode nature, the light generation condition and the focusing effects at different locations along the DFB laser cavity can be very different. The photon density distribution inside the DFB cavity is, therefore, no longer uniform. This, in turn, causes a nonuniform distribution in the carrier density, and hence in the refractive index of the corresponding portion of the waveguide. This is the so-called longitudinal spatial hole burning (SHB) effect in DFB semiconductor lasers. It is known to enhance the spontaneous emission rate and to induce nonlinearities in the static and dynamic properties of DFB lasers such as the light-current (L-I) characteristics, the spectral linewidth and the wavelength chirping [Henry, 1986, Tromborg, Olesen and Pan, 1991]. Therefore, it is important to include those spatially dependent features into the laser model. Typically, there are two formalisms so far that have been applied to solve the longitudinal problem, i.e., on one hand, the travelling-wave formalism, which includes the travelling-wave method [Vankwikelberge *et al.*, 1990], the transmission-line method [Lowery, 1990], the power transfer matrix method [Zhang and Carroll, 1992], and the time domain method [Tsang *et al.*, 1994] and, on the other hand, the standing-wave formalism such as the Green's function method [Tromborg, Olesen and Pan, 1991],

the transfer matrix method [Makino, 1993], and the perturbation analysis method [Huang *et al.*, 1995].

Generally, all of the travelling-wave approaches are predominantly numerical. With little modification, they are easily adapted to study arbitrary laser geometries. But, in return, the underlying physical effects may be more difficult to identify. Alternatively, the standing-wave formalism assumes that the temporal and spatial dependencies of the optical field are separable, which implies that the distribution of the lasing modal field is independent of the photon round trip time in the laser cavity and, consequently, the laser dynamics can be described by the amplitudes of DFB modes alone. Such an approach can lead to closed form or semi-analytical results. This way, more insight into the physics of the laser dynamics can be gained. However, the approach will fail when the photon round trip time is close to the time period of the modulation since it assumes the DFB modes are built instantaneously.

In the travelling-wave analysis, the scalar wave equation is transformed into a set of time dependent coupled wave equations for the complex envelopes of the right and left traveling waves. These equations are then solved numerically together with the rate equation for the local carrier density and using the boundary conditions at the end facets. The transmission line method is based on the analogy between a laser cavity and a transmission line in electrical circuit theory. Noise spectra and modulation responses are obtained from the Fourier transforms of time domain simulations. In the power transfer matrix method, the incoherence of spontaneous emission is exploited by transforming the field equations to power equations eliminating the phase information about the spontaneous emission. The mean spontaneous power, derived from the radiative recombination rate, can then be used to drive the power matrices. Time domain methods use the concept of instantaneous frequency to transform the time-dependent scalar travelling wave equations into an F-matrix. By either adding the noise sources or not to the deterministic formulation, the model can calculate

both the dynamic and stochastic properties of DFB lasers.

As initially proposed by Henry [Henry, 1986], the Green's function method assumes that the longitudinal inhomogeneities can be taken into account as distributed excitation sources coupled to the lasing mode. A rate equation for the field amplitude $A(t)$ can be derived. The transfer matrix method extends the standing wave approach to the local normal mode analysis. By matching the modal fields at the index and/or gain grating interfaces, it can be applied to laser structures with strong index and gain perturbations. It can handle the polarization effects and radiation losses in a straightforward manner. Perturbation analysis about the steady-state considers the dynamic fluctuations of carriers and photons in the DFB cavity as perturbations modifying the amplitude of the lasing field. Because of the inherent similarities between the Green's function method and the perturbation analysis, they usually both give the same results.

1.4 Objective of the dissertation

The objective of this dissertation is to develop a comprehensive and versatile numerical tool for an efficient and accurate simulation of gain-coupled DFB semiconductor lasers. Through comprehensive modelling and analysis, an in-depth understanding of the high power, high speed, high side mode suppression, high single-mode yield, low threshold, low noise, low frequency chirp and stable single-mode performance of gain-coupled DFB lasers can be reached. By considering various spatially dependent features of practical gain-coupled DFB lasers, such as multi-electrode modulation, asymmetrical facet condition, distributed complex coupling, spatial hole burning, nonuniform gain compression and spontaneous emission, the properties of gain-coupled DFB semiconductor lasers are investigated for future de-

velopment and improved design. In order to retain the beauty of the rate equation analysis and to overcome its shortcomings, it is also necessary to extend the standing wave formalism into the multimode regime and cover the full laser bias range (from below to above threshold).

Although detailed experimental work is not referred much in this dissertation, most of the work was actually done under close collaboration with the Advanced Laser Design group in Nortel Technology and the papers included in this dissertation were coauthored by the group leader, Dr. Toshihiko Makino. Because of the uncertainties about the large number of parameters in DFB lasers, a direct comparison would not reveal much because because many parameters could be adjusted. It is therefore not the objective of this work. The results obtained in this dissertation are used as effective guidelines for gain-coupled DFB laser design.

1.5 Outline of the dissertation

The bulk of this dissertation contains 6 chapters bringing together a series of 6 papers published in the literature over four years [Chen *et al.*, 1995, Chen *et al.*, 1995, Chen *et al.*, 1996, Chen *et al.*, 1997, Chen *et al.*, 1997, Chen *et al.*, 1997]. Each chapter contains some introductory material and one full length journal paper. They are briefly outlined as follows:

Chapter 2 focuses on the analysis of the mechanism of single-mode oscillation in gain-coupled DFB lasers. Based on the Bloch wave analysis, it is shown that the intensity profiles of DFB modes on the long and short wavelength sides of the Bragg stopband are in phase and in antiphase with the index grating, respectively. Therefore, by making the gain grating to be in phase with one of the Bloch waves, a single-mode oscillation with a large gain margin can be obtained. It is revealed

for the first time that the unequal section length of the gain grating can have a significant effect on the suppression of the antiphase Bloch waves and high order modes in gain-coupled DFB lasers. Numerical calculations by the transfer-matrix method have shown that a gain grating with short high gain section can dramatically improve the single-mode yield in terms of gain margin for gain-coupled DFB lasers.

Chapter 3 covers the analysis of the static characteristics of gain-coupled DFB lasers. It proposes a self-consistent multimode model including various spatial effects for the investigation of the mechanism of side mode suppression in gain-coupled DFB lasers. By introducing the modal net gain into the coupled wave equations so as to include the contribution from spontaneous emission, a set of spatially dependent multimode rate equations is derived. The detailed analysis shows that both high index and gain couplings contribute to improving the side mode suppression ratio $SMSR$ of DFB lasers. Above the lasing threshold, spatial hole burning (SHB) favours the short wavelength DFB modes and hence decreases and increases the $SMSR$ in inphase and antiphase gain-coupled DFB lasers, respectively. At high optical intensity, the self-consistent analysis reveals that instability in antiphase gain-coupled DFB lasers can cause the $SMSR$ to deteriorate and a stable oscillation of lasing mode in inphase gain-coupled DFB lasers helps reduce the nonlinear gain compression effect on the $SMSR$.

Chapter 4 refers to the analysis of small signal dynamics in gain-coupled DFB lasers. Based on the Green's function analysis, the dependency of the relaxation oscillation frequency of gain-coupled DFB lasers on the complex coupling coefficient and various other factors are investigated systematically. With the help of closed form expression of the relaxation oscillation frequency, including various spatial nonuniformities, the analysis reveals for the first time that the linewidth enhancement factor α_M plays a significant role in determining the modulation bandwidth of gain-coupled DFB lasers. By arranging the index and gain gratings of DFB laser

in antiphase, a higher relaxation oscillation frequency can be obtained because the spatial hole burning effect enhances the dynamic modal differential gain.

Chapter 5 analyzes the harmonic distortion in gain-coupled DFB lasers. This is important for the application of analog optical communication systems since the gain-coupled DFB lasers have a wide modulation bandwidth. Besides, the complex coupling provides added flexibility for the improvement of the harmonic distortion in the laser. Applying the spatially dependent rate equations, this chapter is devoted to a systematic study of the second order harmonic distortion in gain-coupled DFB lasers. By retaining the advantage of closed form analysis, the self-consistent study has revealed the effect of various spatial nonlinearities on the harmonic distortion in an explicitly manner. It is shown that the harmonic distortion from different origins can have different signs and, by choosing a proper complex coupling structure, they are able to cancel one another to keep the total harmonic distortion low. Both numerical and analytical results are very relevant for laser design.

Chapter 6 presents a detailed analysis of large signal dynamics in gain-coupled DFB lasers. Based on the approximation of threshold modal fields, dynamic side mode suppression in gain-coupled DFB lasers is studied in an explicit manner by using the spatially dependent multimode rate equations. The obtained closed form results provide a valuable insight into the effects of various spatial features on the side mode suppression in gain-coupled DFB lasers. The analysis indicates that gain coupling reduces the interaction of the side modes with the gain medium and hence yields higher decay rates and a lower dynamic modal differential gain for the side modes, which contributes to the suppression of the transient intensities of the side modes significantly.

Chapter 7 proposes a two-mode interference model for the analysis of the performance of push-pull modulation in gain-coupled DFB lasers. The closed form results obtained from the small signal analysis reveal clearly that the high frequency per-

formance of push-pull DFB lasers is characterized by the first cut-off frequency and the structure dependent resonance frequency, which are also found to depend on the threshold gain difference and the frequency spacing between the lasing mode and its closest antisymmetric side mode, respectively. A systematic analysis of the various spatially dependent effects clearly indicates that direct push-pull modulation of gain-coupled DFB lasers can lead to a very low frequency chirp in high frequency applications.

It is necessary to mention that, although there are only six papers presented in this dissertation, the actual work performed during this study is more than that. It includes several other journal paper and conference presentations [Chen *et al.*, 1996, Chen *et al.*, 1995, Chen *et al.*, 1995, Adams *et al.*, 1996, Chen *et al.*, 1996, Chen *et al.*, 1996, Chen *et al.*, 1996]. Other important aspects of DFB lasers, such as carrier grating effects, mode stability, and carrier transport in multiple quantum well (MQW) lasers were investigated. Furthermore, the experimental characterization of gain spectra for MQW lasers from the measurement of spontaneous emission provided very useful data as well. This additional work was not included in this dissertation because of possible unwarranted concern for cohesiveness and unity in form and content. May the author of this dissertation be forgiven.

CHAPTER 2

Bloch Waves in Gain-Coupled DFB Lasers

In this chapter, Bloch wave analysis is used to address the problem of single-mode oscillation in gain-coupled DFB lasers. Bloch waves are the forward and backward propagating waves in the periodic structures formed by the Bragg gratings of DFB lasers. They are the eigenwaves of the structure and hence do not coupled to each other. An analysis based on the Bloch wave formalism can simplify a great deal the investigation of gain-coupled DFB lasers and provide valuable physical insight. This formalism is used here to analyze the condition of single-mode oscillation in those lasers.

Single frequency emission is one of the essential requirements for the light sources in long-haul and high-bit-rate optical communication systems because of optical fiber dispersion at 1.55 μm. With the distributed structure and fabrication simplicity, gain coupling provides one of the most effective and favorite approach to achieve the goal. However, it is not yet clear what is the mechanism to produce a stable single-mode oscillation in such laser. In order to improve the laser performance, a detailed research into single-mode oscillation in gain-coupled DFB lasers is thus important. This chapter presents the Bloch wave analysis and addresses the issue of the gain margin in gain-coupled DFB lasers.

Published in IEEE J. Quantum Electron., vol. 33, pp. 33-40, 1997

Improvement of Single-Mode Gain Margin in Gain-Coupled DFB Lasers

Jianyao Chen, Alain Champagne, Roman Maciejko, *Senior Member, IEEE*
and Toshihiko Makino, *Senior Member, IEEE*

Abstract

Using the Bloch wave analysis, this paper investigates the effect of the gain grating on the single mode condition in DFB lasers. Various factors affecting the threshold gain of gain-coupled DFB lasers are analyzed in some detail. It is shown for the first time that unequal section lengths in the gain grating can have a significant effect on the single-mode gain margin of gain-coupled DFB lasers, especially when the linewidth enhancement factor α_M is large, because the long and short wavelength Bloch waves are in phase and in antiphase with the index grating of DFB lasers, respectively.

J. Chen, A. Champagne, and R. Maciejko are with the Optoelectronics Laboratory, Department of Engineering Physics, École Polytechnique, P. O. Box 6079, Station "Centre-ville", Montréal, Québec Canada H3C 3A7

T. Makino is with Northern Telecom (Nortel), P. O. Box 3511, Station C, Nepean, Ontario, Canada K1Y 4H7

2.1 Introduction

Stable single-mode lasers with a narrow linewidth are highly desirable in advanced fiber optic systems, in order to prevent pulse broadening caused by dispersion in long-haul transmission. With the build-in frequency selective element, distributed feedback (DFB) semiconductor lasers are the most favorite candidates for this task. The ordinary index grating, however, provides the same feedback strength to the DFB modes on both sides of the Bragg stopband, which induces a modal threshold gain degeneracy and makes the lasing condition sensitive to facet reflections. One solution to this problem has been the introduction of a quarter wavelength phase shift in the uniform index-coupled DFB lasers with AR coatings [1]. However, such an approach suffers from additional drawbacks such as more spatial hole burning caused by the phase shift and a substantial deterioration of the single-mode yield caused by as little as a few percent residual facet reflectivity [2].

An alternative solution to this problem is the introduction of complex coupling, i.e. gain coupling, into DFB lasers [3]. Experimental work showed that even small amounts of gain coupling can significantly improve the single mode yield of the DFB lasers [4, 5]. Gain coupling also reduces spatial hole burning and allows the use of asymmetric facet coatings in order to improve the power extraction efficiency [6, 7]. Using the truncated-well (in-phase) gain-coupled DFB structures, a stable mode operation on the long wavelength side of the Bragg stopband with very high single-mode yield has been reported [8, 9]. In order to gain more physical insight about the mechanism of gain-coupling in DFB lasers, a number of theoretical papers have appeared in the past years [3-13].

So far, most of the research work on the gain-coupled DFB lasers was based on the coupled-wave analysis [3, 4, 6, 10, 12] and the local-normal-wave analysis [5, 7, 8, 9]. Although it is well known that the Bloch waves are the normal modes

of periodic structures [14, 15], very few investigations used the Bloch wave analysis to study the effect of gain coupling in DFB lasers [16]. In this paper, we will show that, using the Bloch wave analysis, a deeper understanding of the gain coupling effect on the single mode selection in DFB lasers can be obtained. It is found that the long and short Bloch waves are respectively in phase and in antiphase with the index grating of DFB lasers. Therefore, using a shorter high gain section and a deep etching in the gain grating can suppress the antiphase Bloch wave as well as the high order side modes effectively. This helps improve the single-mode yield of gain-coupled DFB lasers significantly. Numerical results obtained by the transfer-matrix method illustrate that, by designing the gain grating structure properly, a very high single-mode yield, in terms of gain margin, can be achieved in the truncated-well (in-phase) gain-coupled DFB lasers.

2.2 Bloch waves in DFB lasers

Optical Bloch waves are the natural modes of periodic structures, in the same way as that the guided plane waves are the natural modes of straight waveguides. The forward and backward Bloch waves propagate inside DFB structures independently, without coupling to each other. The investigation of the properties of DFB lasers can therefore be simplified much by the Bloch wave analysis.

To first order of Fourier series expansion, the variations of the effective index $n(z)$ and the modal confinement factor $\Gamma(z)$ along the gain-coupled DFB lasers can be written as:

$$n(z) = n_0 + \gamma \Delta n \cos(2\beta_0 z) \tag{2.1}$$

$$\Gamma(z) = \Gamma_0 \pm \gamma \Delta \Gamma \cos(2\beta_0 z) \tag{2.2}$$

where $\beta_0 = \frac{\pi}{\Lambda}$ is the Bragg wavenumber of the DFB grating. n_0 and Δn denote

the average value of the effective waveguide index and the maximum effective index variation due to the index grating, respectively. Similarly, Γ_0 and $\Delta\Gamma$ are the modal confinement factor and the maximum variation of the gain confinement factor, respectively. The constant γ is the Fourier coefficient determined by the shape of the grating. The sign $\pm$ corresponds to the inphase and the antiphase gain coupling structures, respectively.

Generally, the optical field inside the DFB laser consists of the forward and backward propagating waves:

$$Z_0(z) = Z_R(z)e^{-j\beta_0 z} + Z_L(z)e^{j\beta_0 z} \tag{2.3}$$

According to coupled-wave analysis, at the lasing threshold, the field function $Z_R(z)$ and $Z_L(z)$ can be written in closed form as follows [3, 15]:

$$Z_R(z) = Ae^{-j(\beta_B-\beta_0)z} + B\rho e^{j(\beta_B-\beta_0)z} \tag{2.4}$$

$$Z_L(z) = A\rho e^{-j(\beta_B-\beta_0)z} + Be^{j(\beta_B-\beta_0)z} \tag{2.5}$$

where β_B can be regarded as the propagation constant of the Bloch waves in the DFB structure and is given by:

$$\beta_B - \beta_0 = \sqrt{(\beta-\beta_0)^2 - K^2} \tag{2.6}$$

ρ is the DFB reflection coefficient of Bloch waves given by

$$\rho = \frac{\beta_B - \beta}{K} = -\frac{K}{\beta_B + \beta - 2\beta_0} \tag{2.7}$$

K is known as the coupling coefficient. The two constants A and B in the expressions (2.4) and (2.5) are two quantities determined by appropriate boundary conditions at the laser facets.

Substituting (2.4) and (2.5) into expression (2.3) and rearranging the terms, we obtain

$$Z_0(z) = A\left[1 + \rho e^{j2\beta_0 z}\right] e^{-j\beta_B z} + B\left[1 + \rho e^{-j2\beta_0 z}\right] e^{j\beta_B z} \tag{2.8}$$

The expressions inside the square brackets are periodic functions of z with periodicity Λ, which gives the eigenfunctions of the forward and backward propagating Bloch waves.

Taking the absolute value of $Z_0(z)$ in expression (2.8), we can write the intensity profile of the optical field as:

$$\begin{aligned} |Z_0(z)|^2 &= |A|^2 \left[1+\rho e^{j2\beta_0 z}\right]\left[1+\rho^* e^{-j2\beta_0 z}\right] e^{2Im\{\beta_B\}z} \\ &+ |B|^2 \left[1+\rho e^{-j2\beta_0 z}\right]\left[1+\rho^* e^{j2\beta_0 z}\right] e^{-2Im\{\beta_B\}z} \\ &+ AB^* \left[1+\rho e^{j2\beta_0 z}\right]\left[1+\rho^* e^{j2\beta_0 z}\right] e^{-j2Re\{\beta_B\}z} \\ &+ A^*B \left[1+\rho e^{-j2\beta_0 z}\right]\left[1+\rho^* e^{-j2\beta_0 z}\right] e^{j2Re\{\beta_B\}z} \end{aligned} \tag{2.9}$$

The overlap of intensity profile (2.9) with the gain medium determines the stimulated emission in the DFB laser. Since $Re(\beta_B) >> Im(\beta_B)$, the last two terms in expression (2.9) are highly oscillatory and hence produce a much weaker interaction with the gain medium. If we neglect them from the result, the light intensity profile in terms of Bloch waves can be written as:

$$|Z_0(z)|^2 = |A|^2 I_+(z)\exp\{2Im(\beta_B)z\} + |B|^2 I_-(z)\exp\{-2Im(\beta_B)z\} \tag{2.10}$$

where

$$I_\pm(z) = 1 + |\rho|^2 + 2|\rho| cos(2\beta_0 z \pm \theta_B) \tag{2.11}$$

which gives the intensity profile of the forward and backward propagating Bloch waves. θ_B denotes the phase change from the reflection coefficient ρ. Comparing formulae (2.1) and (2.11), we realize that θ_B gives the phase difference between the intensity profiles of the Bloch waves and the index grating of the DFB laser.

If the boundary conditions at two facets are applied to the optical field expression (2.3), the threshold condition for the lasing modes in the DFB laser can be obtained [15]:

$$\left(\frac{\rho - r_L}{1-\rho r_L}\right)\left(\frac{\rho - r_R}{1-\rho r_R}\right) exp(2j\beta_B L) = 1 \tag{2.12}$$

which shows that, with the use of Bloch waves, the threshold condition of DFB lasers is very similar to that of Fabry-Perot lasers. In the equation, r_R and r_L denote the reflectivities at the right and left facets, respectively.

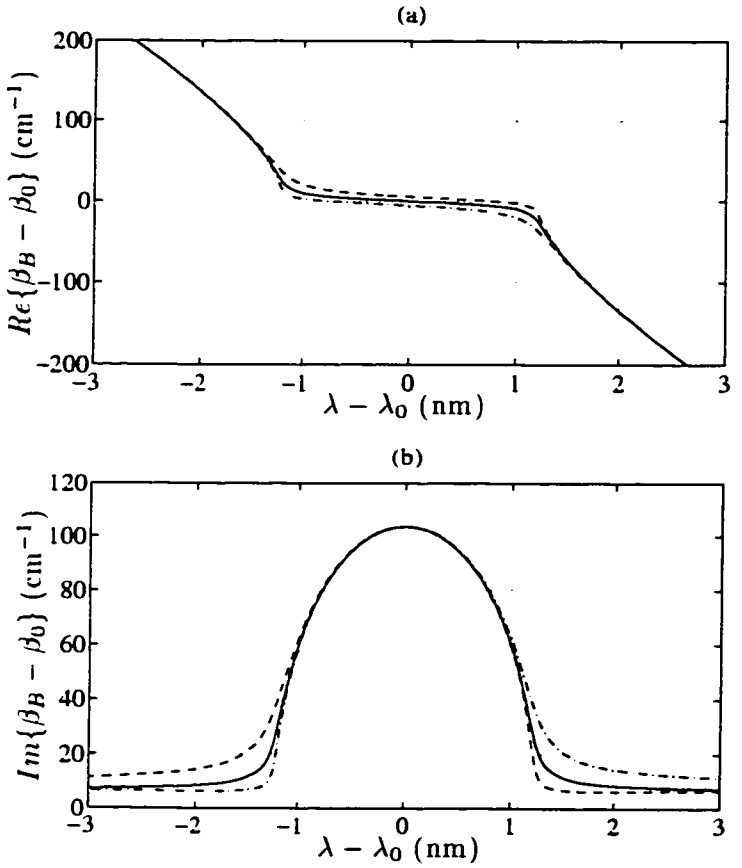

Fig. 1 Dispersion of the Bloch wave propagation constant, where $n_w = 3.23$, $\Delta n = 0.008$, $L = 450\ \mu m$, $\Gamma_+ = 0.05$, $\Gamma_- = 0$ and $\Lambda_+/\Lambda_- = 1$. Solid line: index-coupled; dash-dotted line: inphase gain-coupled; dashed line: antiphase gain-coupled.

Fig. 1 presents the dispersion of the Bloch-wave propagation constant in the index-coupled, inphase gain-coupled and antiphase gain-coupled DFB lasers [1]. In order to illustrate the inphase and antiphase gain coupling effects better, we have

[1]The grating is assumed to be of rectangular shape. Λ_+ and Λ_- give the lengths of the high and the low gain sections in the gain grating, respectively, and $\Lambda_+ + \Lambda_- = \Lambda$. Γ_+ and Γ_- denote the transverse modal power confinement factors of the high and the low gain sections in the gain grating, respectively.

chosen $\alpha_M = 0$ in calculating those curves. It shows that gain coupling breaks the dispersion symmetry about the Bragg wavelength and hence single mode oscillation becomes possible [13]. An inphase gain grating increases the group velocity of the long wavelength Bloch wave at the stopband edge and traps the short wavelength Bloch wave more strongly. Similarly, an antiphase gain grating favors the short wavelength Bloch wave and gives an opposite effect.

Outside the Bragg stopband, the Bloch wave propagation constant β_B changes rapidly. The effect of the facet reflection on the round trip phase condition will not cause a significant change in the lasing wavelength, especially when the $|K|L$ value of the DFB laser is large. Therefore, the threshold condition of gain-coupled DFB lasers can be much less sensitive to facet reflectivity. On the contrary, inside the Bragg stopband, the Bloch propagation constant β_B is nearly constant at the value $\beta_B = \beta_0$. The optical phase change caused by the facet reflection can shift the lasing wavelength of the DFB laser appreciably, which has been found in the case of quarter wavelength shifted index-coupled DFB lasers [2].

Fig. 2 shows the wavelength dependency of the reflection coefficient ρ. We see that, as the optical wavelength increases to cross over the stopband, the phase shift θ_B induced by the DFB reflection changes from π to 2π. At the Bragg wavelength λ_0, $\theta_B = 3\pi/2$. This indicates that the intensity profiles of the long and short wavelength Bloch waves are in phase and in antiphase with the index grating, respectively, according to expression (2.11). The optical field of the long wavelength Bloch wave concentrates in the high index regions in order to satisfy the requirement of periodicity in Λ. For the index-coupled DFB lasers, a longitudinally uniform gain medium provides the same interaction with the Bloch waves on both sides of the stopband. Therefore, a threshold gain degeneracy results. When a gain grating is introduced, a threshold gain difference between the long and the short wavelength Bloch waves can be obtained. Obviously, an inphase gain grating selects the long

wavelength mode and an antiphase gain grating selects the short wavelength mode (see Fig. 3).

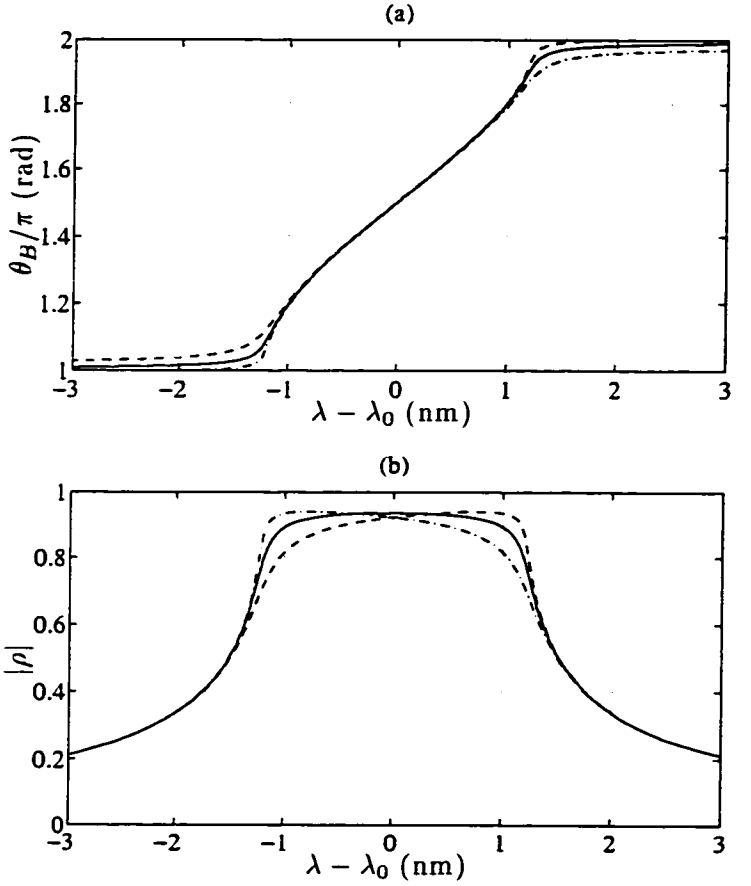

Fig. 2 Phase (a) and amplitude (b) of the DFB reflection coefficient ρ. The parameters used are the same as those in the caption of Fig. 2.1. Solid line: index-coupled; dash-dotted line: inphase gain-coupled; dashed line: antiphase gain-coupled.

Fig. 2(b) shows that the amplitude of the reflection coefficient decreases rapidly as the wavelength shifts away from the stop band, which causes the standing wave ratio of the Bloch wave intensity profiles to decrease significantly. Because the interaction between the Bloch wave and gain medium is proportional to $1 + |\rho|^2$ (see expression (2.11)), higher order modes need a higher gain to reach the lasing threshold. Especially, when the gain grating is introduced in the DFB laser, the overlap

of the intensity profile of the Bloch waves with the gain medium is much reduced for the high order modes. Consequently, the threshold gain difference between the lasing mode and the high order mode will also increase (see Fig. 4).

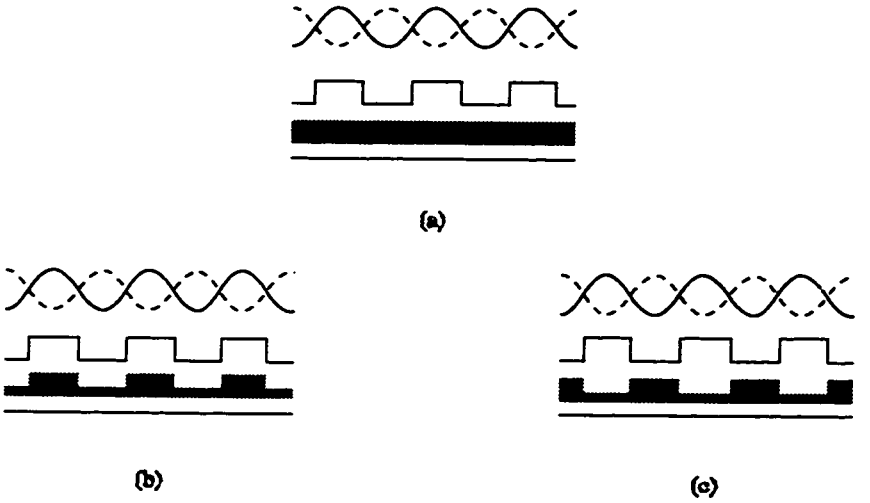

Fig. 3 Illustratiion of the long and short wavelength Bloch waves in DFB lasers. (a) index-coupled; (b) inphase gain-coupled; (c) antiphase gain-coupled. Solid line: long wavelength mode; dashed line: short wavelength mode.

The above inphase and antiphase Bloch wave description of gain coupling effect is similar to the standing wave effect presented in reference [17]. Our Bloch wave analysis also tell us that the significant difference between the quarter wavelength shifted index-coupled and gain-coupled DFB lasers is that the former achieves single-mode oscillation by imposing the phase matching condition to favour a particular mode, while the later provides a higher effective gain for the appropriate Bloch wave. From the point of view of laser fabrication, phase matching is usually much more difficult to achieve. We therefore expect the gain-coupled DFB lasers to provide a higher single-mode yield, which has been confirmed both theoretically and experimentally [4, 5, 7, 8].

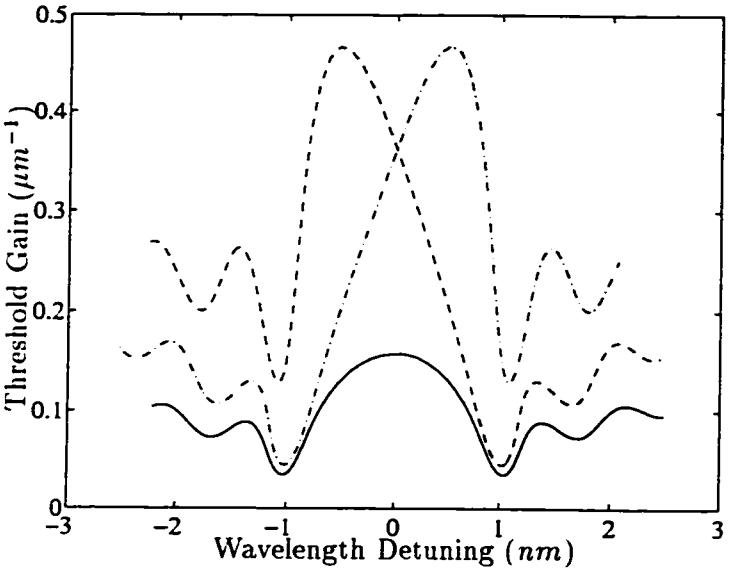

Fig. 4 Threshold gain and wavelength detuning of the longitudinal modes of a DFB lasers with AR/CL facet coatings. Continuous curves are obtained by changing the grating phase at cleaved facet over entire range from 0 to 2π. The parameters used are the same as those in the caption of Fig. 1. Solid line: index-coupled; dash-dotted line: antiphase gain-coupled; dashed line: inphase gain-coupled.

2.3 Single mode condition at threshold

The above Bloch wave analysis indicates that, in DFB lasers, the interaction between the optical field and the gain medium depends on the overlap between the intensity profile of the Bloch wave and the gain regions. By introducing an inphase or antiphase gain grating into DFB lasers, one of the Bloch waves is favoured and, hence, single mode lasing results. Such an approach can produce very stable single mode lasing since there is no critical phase matching condition to satisfy as in the quarter wavelength shifted index-coupled DFB lasers. It is interesting to note that, in gain-coupled DFB lasers, even if a significant part of the gain medium has been etched away (e.g. full-depth-etching) to form the gain grating, the threshold gain of the lasing mode only increases slightly from that of the index-coupled DFB laser

(see Fig. 4). On the contrary, the threshold gain for the Bloch wave on the opposite side of the Bragg stopband increases much more because the intensity profile is in antiphase with the gain grating. Moreover, the threshold gain difference between the fundamental mode and the next higher order mode resulting from gain coupling can also be seen in Fig. 4.

The threshold condition is a crucial parameter for the single-mode yield of DFB lasers. For the gain-coupled DFB lasers, the analysis becomes more complicated because the strength of gain coupling itself is threshold-gain-dependent, especially when the uncertain facet phase is involved. To simplify our study, the following discussion is limited to the AR/CL (antireflection/cleaved) and AR/AR facet configurations only. The laser cavity length is fixed to 450 μm and the Bragg wavelength is set at 1.55 μm. The other parameters are: the waveguide loss equals 20 cm^{-1}, the modal confinement factor $\Gamma_+ = 0.05$ and the modal refractive index $n_w = 3.23$. In order to analyze the effect of unequal section lengths of gain grating, the transfer matrix method is used to carry out the calculations [18]

2.3.1 Section length effect

From the Bloch wave analysis, we realize that, if we reduce the length of the high gain section, the overlap of the intensity profile of the Bloch wave in antiphase with the gain grating will decrease more than that of the inphase Bloch waves. This can increase the threshold gain difference between the inphase and antiphase Bloch waves significantly and lead to a strong suppression of the antiphase Bloch wave (see Fig. 5). The results based on the transfer matrix method clearly show in Fig. 6 that, in the inphase gain-coupled DFB lasers, a short high gain section increases the threshold gain difference between the short wavelength fundamental Bloch mode (-1 mode) and the long wavelength fundamental Bloch mode ($+1$ mode) rapidly. Since the feedback by the index grating is reduced and because of a shorter high

gain section length, a shift in the Bragg stopband towards short wavelengths and a narrowing of the bandgap are visible on the plot. Note that the reduction of the feedback by the index grating due to a smaller duty factor causes the laser threshold gain to increase [19, 20]. This enhances the gain coupling effect of the gain grating with a shorter high-gain section length and improves the single-mode selectivity of the DFB lasers further. On the contrary, a longer high gain section in the gain grating increases the interaction between the -1 mode and the active medium. Consequently, a significantly smaller single-mode margin results. For the antiphase gain-coupled DFB laser, Fig. 7 shows that, in a similar way, a shorter high gain section in the gain grating weakens the interaction between the long wavelength Bloch wave ($+1$ mode) and gain medium and hence increases its threshold gain significantly.

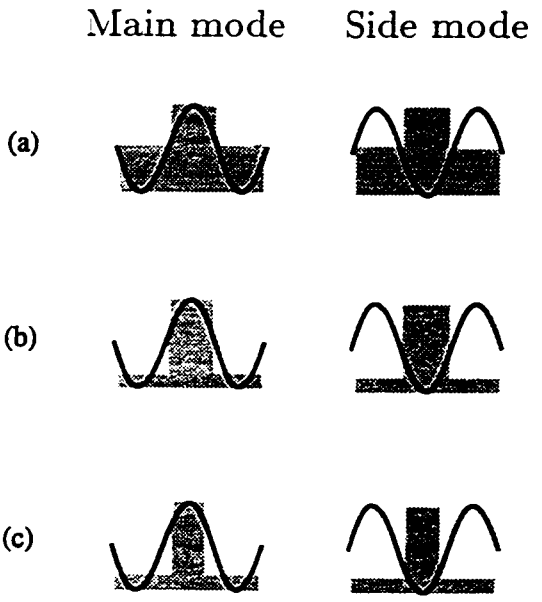

Fig. 5 Illustration of gain grating shape effect on the interaction between the Bloch waves and gain medium. Deeper etching (b) and shorter high gain section (c) reduced overlap between the intensity profile of antiphase Bloch wave with the gain regions.

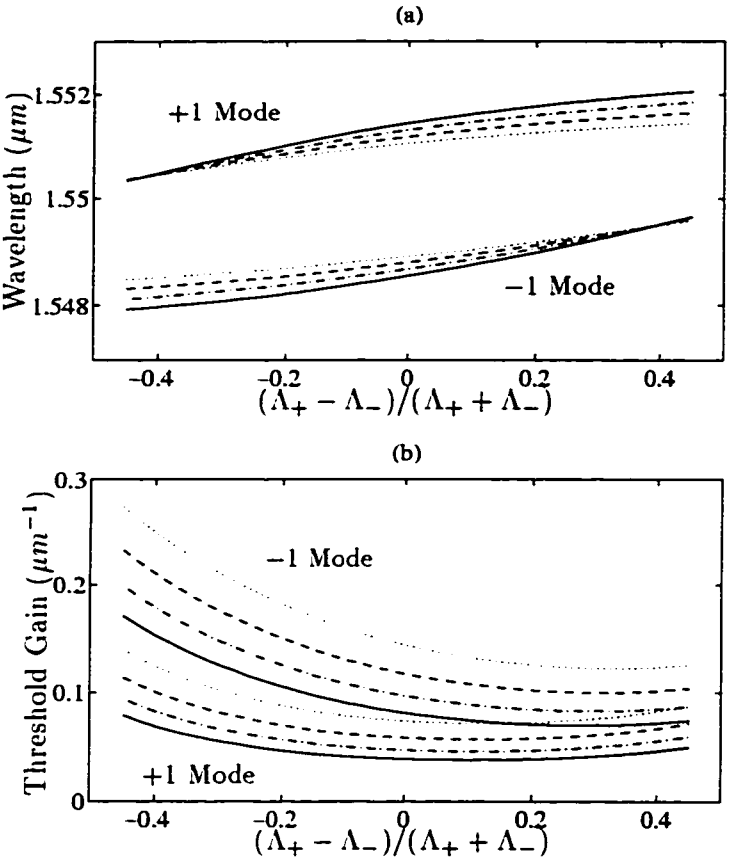

Fig. 6 Resonance wavelength and threshold gain of the long and short wavelength fundamental modes in the inphase gain-coupled DFB lasers with AR/AR facet coatings, where $\Gamma_-/\Gamma_+ = 0.2$. Solid line: $\Delta n = 0.008$; dash-dotted line: $\Delta n = 0.007$; dashed line: $\Delta n = 0.006$; dotted line: $\Delta n = 0.005$.

Facet reflections influence the modal threshold gain of DFB lasers strongly. They also affect the predominance of the lasing mode in DFB lasers and, therefore, raise a yield problem because of the uncontrollable grating phase at the cleaved facet. Although the threshold gains of the +1 mode and the −1 mode change differently as the facet phase varies from 0 to 2π, the results of Fig. 8 show that using a shorter high gain section generally increases the threshold gain difference in the AR/CL-coated DFB laser. The results of Fig. 8 were obtained from the average of 50 calculations with different grating phases at the cleaved facet. As we can see

from the plot, their general behaviour is very similar to that of the AR/AR-coated DFB lasers. Because of the extra feedback by the facet reflections, the average threshold gains of the AR/CL-coated DFB lasers are also lower than those of the AR/AR-coated ones. A large threshold gain difference or a single-mode gain margin enhances the immunity of the DFB mode oscillation to cleaved facet reflections. The related improvement in the single-mode yield is also shown in Fig. 8(b).

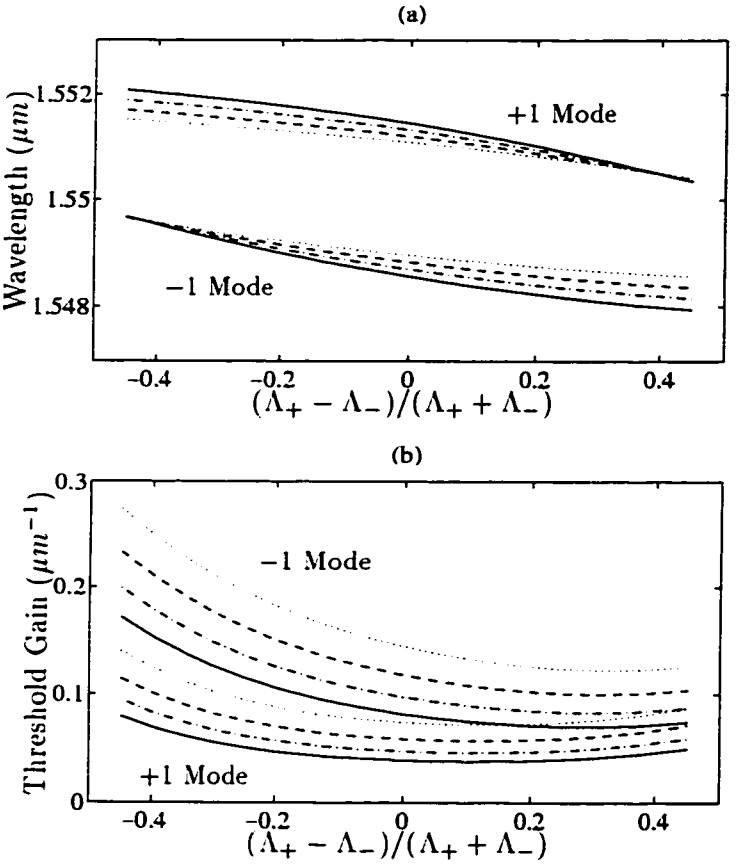

Fig. 7 Resonance wavelength and threshold gain of the long and short wavelength fundamental modes in the antiphase gain-coupled DFB lasers with AR/AR facet coatings, where $\Gamma_-/\Gamma_+ = 0.2$. Solid line: $\Delta n = 0.008$; dash-dotted line: $\Delta n = 0.007$; dashed line: $\Delta n = 0.006$; dotted line: $\Delta n = 0.005$.

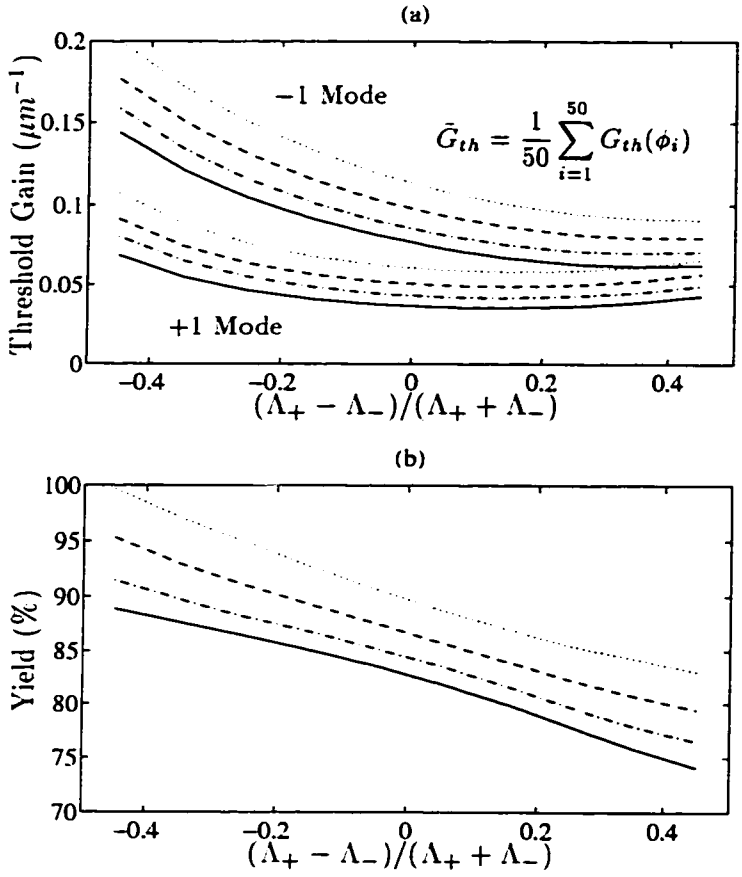

Fig. 8 (a) Average threshold gain of the long and short wavelength fundamental modes and (b) the corresponding single-mode yield of the inphase gain-coupled DFB lasers with AR/CL facet coatings, where $\Gamma_-/\Gamma_+ = 0.2$. Solid line: $\Delta n = 0.008$; dash-dotted line: $\Delta n = 0.007$; dashed line: $\Delta n = 0.006$; dotted line: $\Delta n = 0.005$.

2.3.2 Etching depth effect

The transfer-matrix analysis leading to Fig. 9 shows that the effect of a shorter high gain section in the gain grating is more pronounced when the gain grating is etched deeper in the gain-coupled DFB laser. Because the gain grating is in phase with the lasing mode and in antiphase with the side mode, a deep etching reduces the overlap of the intensity of the antiphase Bloch wave with the gain medium.

Hence, it also suppresses the interaction of side mode with the gain grating (see Fig. 5). For the same reason, a shorter high gain section reduces the intensity overlap of the side mode with the gain medium more when the etching depth is deeper. Fig. 9 shows that, close to a complete etching, the threshold gain difference between the long and short wavelength Bloch waves changes rapidly as the section length of the gain grating is varied. On the contrary, when the etching depth is shallow, the effect becomes much more reduced.

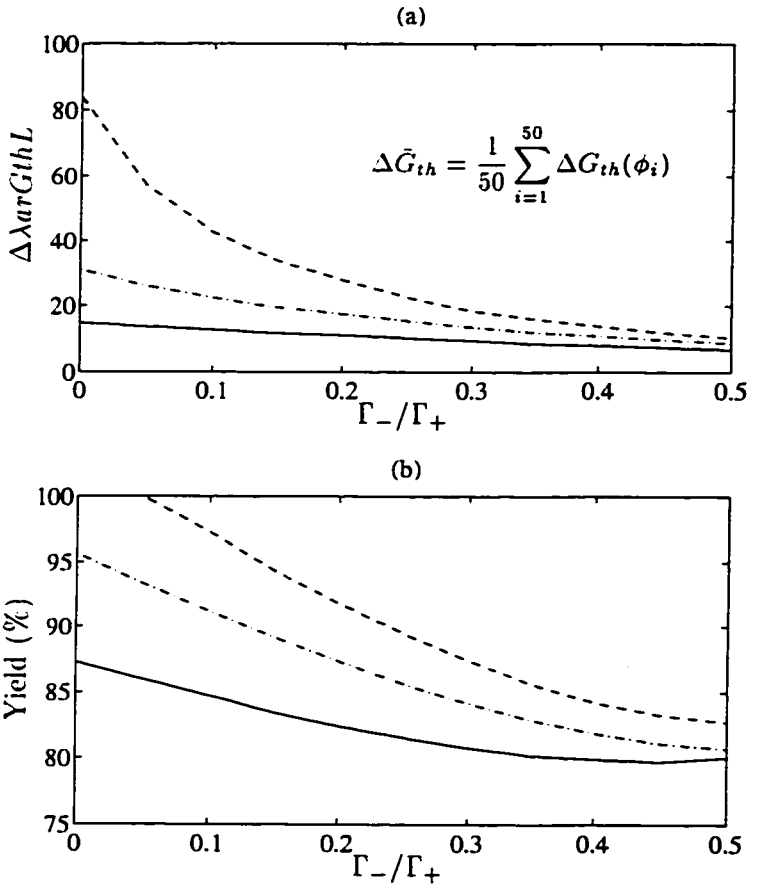

Fig. 9 (a) Threshold gain difference between the long and short wavelength fundamental modes and (b) the corresponding single-mode yield in gain-coupled DFB lasers with AR/CL facet coatings, where $\Delta n = 0.005\Gamma_-/\Gamma_+$. Solid line: $(\Lambda_+ - \Lambda_-)/(\Lambda_+ + \Lambda_-) = 0.3$; dash-dotted line: $(\Lambda_+ - \Lambda_-)/(\Lambda_+ + \Lambda_-) = 0.0$; dashed line $(\Lambda_+ - \Lambda_-)/(\Lambda_+ + \Lambda_-) = -0.3$.

It should be pointed out that, in the calculation of Fig. 9, the index grating also changes as we etch the gain grating deeper. In many cases, e.g. for the truncated-well (inphase) gain-coupled DFB laser [5, 9], the gain and index gratings are formed together by the same etching process. Thus, a deeply etched gain grating, although it is made to increase gain coupling, will also induce a larger index difference and increase the strength of the index coupling. Since the strength of the gain coupling depends on the threshold gain of the DFB laser, a stronger feedback from the index grating can reduce the gain coupling effect on the single-mode margin (see Figs. 6 and 7 also). However, our calculation reveals that, for a normal gain-coupled DFB laser (e.g. with $|\kappa|L < 8$), the strength of the gain coupling always increases faster than that of the index coupling with etching depth. Therefore, a deep etch of the gain grating is always preferable to enhance the gain coupling effect as well as the short high gain section effect.

2.3.3 Linewidth enhancement factor effect

In the previous discussion, we have assumed a zero material linewidth enhancement factor, i.e. $\alpha_M = 0$, in order to compare the effects of inphase and antiphase gain couplings. In reality, the material linewidth enhancement factor α_M is not equal to zero in semiconductor lasers. The nonzero α_M-factor brings an additional interdependency between the real and imaginary parts of the complex coupling coefficient of gain-coupled DFB lasers [21]. In inphase gain-coupled DFB lasers, a nonzero α_M-factor brings about an index coupling strength reduction as the gain increases. This leads to a further enhancement of the modal discrimination in gain-coupled DFB laser. Because the side mode needs a higher gain to reach its threshold, the α_M-related index reduction effect can be more pronounced. Hence, a large material linewidth enhancement factor α_M helps increase the single-mode gain margin in the inphase gain-coupled DFB lasers. When the high gain section length in the gain

grating is reduced, the decrease of the index coupling strength induced by the α_M-factor is even more pronounced and a significantly higher single-mode gain margin results (see Fig. 10). We also notice a kink on the curve for a high α_M value in Fig 10(a). This is because a large α_M-factor reduces the grating index so much as to produce an antiphase gain coupling (the effective grating index difference becomes negative) for the short wavelength Bloch mode. On the contrary, in the antiphase gain-coupled DFB laser, a nonzero α_M-factor enhances the index coupling strength and hencc reduces the gain coupling effect on the single-mode selection (see Fig. 10(b)). Nevertheless, the short high gain section still appears advantageous for a higher single-mode gain margin. It is also important to notice that such an α_M-factor effect does not change the threshold gain of the lasing mode much even when the high gain section in the gain grating is reduced. Such a property reveals that using a shorter high gain section in the gain grating can be very effective for suppressing the side mode in the inphase gain-coupled DFB laser.

2.4 Conclusion and discussion

Using the Bloch wave analysis, we have investigated the gain coupling effect in DFB lasers on the single mode condition in some detail. The mechanism of the single-mode selection by inphase and antiphase gain coupling has been explained. It has been shown that the long and short wavelength Bloch waves are in phase and in antiphase with the index grating of the DFB lasers, respectively. By making the gain grating in phase with one of the Bloch waves, a single mode oscillation with a large threshold gain margin can be obtained. Furthermore, we have also shown for the first time that the section length of the gain grating has a significant effect on the suppression of the antiphase Bloch waves as well as on the higher order

side modes in gain-coupled DFB lasers. Numerical calculations by the transfer-matrix method have demonstrated that, including the effect of a nonzero material linewidth enhancement factor α_M, shorter high gain sections in the gain grating can dramatically increase the single-mode gain margin of inphase gain-coupled DFB lasers and hence improve their single-mode yield.

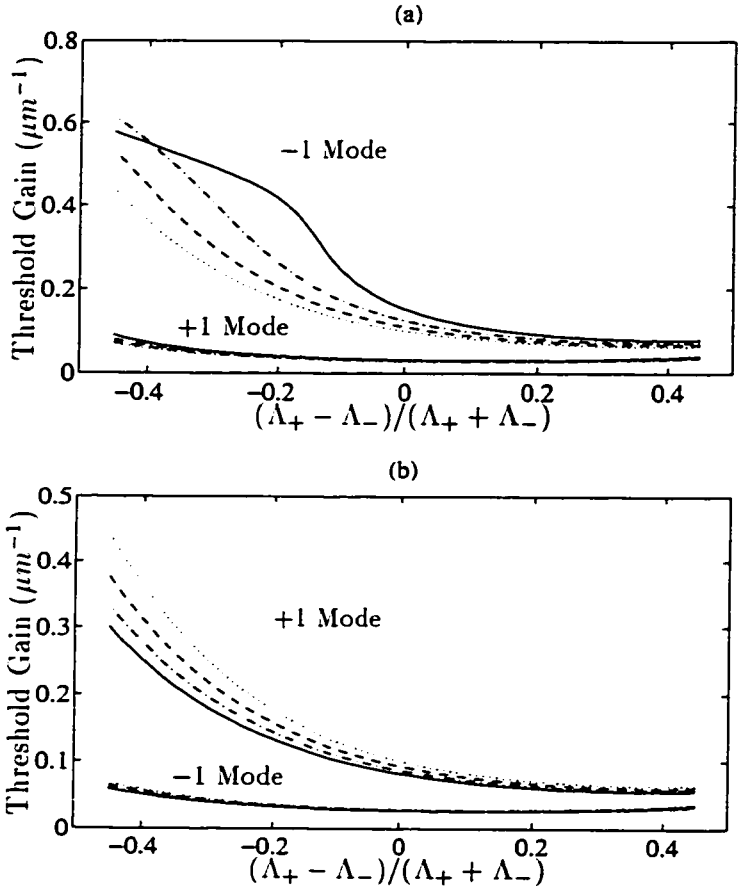

Fig. 10 Threshold gain of the long and short wavelength fundamental modes in the inphase (a) and antiphase (b) gain-coupled DFB lasers, where $\Delta n = 0.005$ and $\Gamma_-/\Gamma_+ = 0$. Solid line: $\alpha_M = 3$; dash-dotted line: $\alpha_M = 2$; dashed line: $\alpha_M = 1$; dashed line $\alpha_M = 0$.

Although the above analysis is limited to the threshold gain study only, we believe that the Bloch wave analysis is also helpful in gaining some physical insight into gain-coupled DFB lasers even above threshold. For example, the Bloch wave

analysis has indicated that the intensities of the long and short Bloch waves are confined into the high and low index sections of the DFB grating, respectively. This shows that the lasing mode in the antiphase gain-coupled DFB lasers will not be as stable as that in the inphase gain-coupled DFB lasers, above threshold [22]. The index change induced by the spatial hole burning effect can modify the ratio of the index difference on both sides of the grating section. At a high enough bias current, this will eventually destroy the lasing mode stability in the antiphase gain-coupled DFB lasers since the index perturbation will pull the optical field into the high index region. Following this argument, it is also not difficult to show that a shorter high gain section can be helpful for the improvement of the lasing mode stability in antiphase gain-coupled DFB lasers [23].

REFERENCES

[1] H. A. Haus and C. V. Shank, "Antisymmetric taper of distributed feedback lasers", IEEE J. Quantum Electron., Vol. 12, pp. 532–539, 1976.

[2] J. Kinoshita and K. Matsumoto , "Yield analysis of SML DFB lasers with axially-flattened internal field", IEEE J. Quantum Electron., Vol. 25, pp. 1324–1332, 1989.

[3] H. Kogelnik and C. V. Shank , "Coupled-wave theory of distributed feedback lasers", J. Appl. Phys., Vol. 43, pp. 2327–2335, 1972.

[4] Y. Nakano , Y. Luo , and K. Tada , "Facet reflection independent, single longitudinal mode oscillation in a GaAlAs/GaAs distributed feedback laser equipped with a gain-coupling mechanism", Appl. Phys. Lett., Vol. 55, pp. 1606–1608, 1989.

[5] G. P. Li , T. Makino , R. Moore , N. Puetz , K. Leong , and H. Lu , "Partly gain-coupled 1.55 μm strained-layer multi-quantum-well DFB lasers' IEEE J. Quantum Electron., Vol. 29, pp. 1736–1742, 1993.

[6] K. David , G. Morthier , P. Vankwikelberge , and R. G. Baets , "Gain-coupled DFB lasers versus index-coupled and phase-shifted DFB lasers: a comparison based on spatial hole burning corrected yield", IEEE J. Quantum Electron., Vol. 27, pp. 1714–1723, 1991.

[7] Y. Nakano , Y. Uchida , and K. Tada , "Highly efficient single longitudinal-mode oscillation capability of gain-coupled distributed feedback semiconductor lasers - advantage of asymmetric facet coating", IEEE Photon Tech. Lett., Vol. 4, pp. 308–311, 1992.

[8] G. P. Li and T. Makino , "Single-mode yield analysis of partly gain-coupled multiquantum-well DFB lasers", IEEE Photon. Tech. Lett., Vol. 5, pp. 1282–1284, 1993.

[9] D. Adams and T. Makino , "Mechanism for enhanced gain-periodicity in truncated-well gain-coupled DFB lasers", Electron. Lett, Vol. 31, pp. 975–977, 1995.

[10] E. Kapon , A. Hardy , and A. Katzir , "The effect of complex coupling coefficients on distributed feedback lasers", IEEE J. Quantum Electron., Vol. 18, pp. 66–71, 1984.

[11] J. Hamasaki and T. Iwashima , "A single-wavelength DFB structure with a synchronized gain profile", IEEE J. Quantum Electron., Vol. 24, pp. 1864–1872, 1988.

[12] D. A. Cardimona, M. P. Sharma, V. Kovanis and A. Gavrielides, "Dephased index and gain coupling in distributed feedback lasers", IEEE J. Quantum Electron., Vol. 31, pp. 60–66, 1995.

[13] T. Makino , "Mechanism for high single-mode stability of gain-coupled DFB lasers with periodically etched quantum wells", Electron. Lett., Vol. 31, pp. 1579–1581, 1995.

[14] S. Wang , "Principles of distributed feedback and distributed Bragg- reflector lasers", IEEE J. Quantum Electron., Vol. 10, pp. 413–427, 1974.

[15] G. P. Agrawal and N. K. Dutta, *Semiconductor Lasers*, Chapter 7, Van Nostrand Reinhold, New York, 1993.

[16] T. Makino , "Side-mode suppression mechanism of gain-coupled DFB lasers with periodically etched quantum wells", IEEE Photon. Technol. Lett., Vol. 8, pp. 602–604 , 1996.

[17] K. David, J. Buus, and R. Baets, "Basic analysis of AR-coated, partly gain-coupled DFB lasers: the standing wave effect", IEEE J. Quantum Electron., Vol. 28, pp. 427–433, 1992.

[18] T. Makino , "Threshold condition of DFB semiconductor lasers by the local-normal-mode transfer-matrix method: correspondence to the coupled-wave method", IEEE J. Lightwave Technol., Vol. 12, pp. 2092–2099, 1994.

[19] K. David, J. Buus, G. Morthier, and R. Baets, "Coupling coefficients in gain-coupled lasers: inherent compromise between coupling strength and loss" IEEE Photon. Technol. Lett., Vol. 3, pp. 439–441, 1991.

[20] H. L. Cao, Y. Luo, Y. Nakano, M. Dobashi, and H. Hosomatsu, "Optimization of grating duty factor in gain-coupled DFB lasers with absorptive grating-analysis and fabrication", IEEE Photon. Technol. Lett., Vol. 4, pp. 1099–1102, 1992.

[21] J. Chen, R. Maciejko, A. Champagne and T. Makino, "Relaxation oscillation frequency of DFB lasers with gain coupling", IEEE J. Quantum Electron., Vol. 31, pp. 1443–1450, 1995.

[22] A. J. Lowery, B. Jonsson, H. Olesen, and D. Novak, "Mode instabilities in complex-coupled DFB semiconductor lasers", Electron. Lett., Vol. 31. pp. 40–41, 1995.

[23] B. Jonsson, A. J. Lowery, H. Olesen, and B. Tromborg, "Instabilities and nonlinear L-I characteristics in complex-coupled DFB lasers with antiphase gain and index gratings", IEEE J. Quantum Electron., Vol. 32, pp. 839–850, 1996.

CHAPTER 3

Static Characteristics of Gain-Coupled DFB Lasers

Static characteristics provide information about the laser performance under continuous-wave (CW) operation. Generally, the light-current (L-I) curve and the longitudinal mode spectrum are the two basic indicators of performance. The L-I curve shows how the output power varies with the injection current and the longitudinal mode spectrum indicates how the power is distributed among the various modes at a given injection current. To measure the spectral purity in DFB lasers, a side mode suppression ratio ($SMSR$) is defined as the power ratio between the main and side modes.

In DFB lasers, the various spatial features of the cavity have a strong influence on the modal field distribution and hence affect the laser static characteristics. Above threshold, because of the nonuniformly distributed photon emission, spatial hole burning and nonlinear gain compression appear in the DFB cavity which inevitably affects the laser performance. Moreover, the power-dependent feedback and the interference between the periodically varied gain and the standing wave pattern of the light fields are at the source of several new effects in gain-coupled DFB lasers. Therefore, a self-consistent analysis of $SMSR$ including the L-I curves and the mode spectrum is essential for those lasers.

Submitted to IEEE J. Quantum Electron.

Self-Consistent Analysis of Side Mode Suppression in Gain-Coupled DFB Semiconductor Lasers

Jianyao Chen, Roman Maciejko, *Senior Member, IEEE*
and Toshihiko Makino, *Senior Member, IEEE*

Abstract

Based on a set of spatially dependent multimode rate equations derived from Maxwell's equations, a self-consistent analysis of gain-coupled DFB lasers is developed. By introducing the modal net gain into the coupled wave equations, we also obtain a closed form formula of the side mode suppression ratio ($SMSR$) for DFB lasers. It is shown that, associated with the distributed feedback, the longitudinal spatial hole burning and the nonlinear gain compression effects, gain coupling produces significant effects on the side mode suppression ratio.

J. Chen, and R. Maciejko are with the Optoelectronics Laboratory, Department of Engineering Physics, École Polytechnique, P. O. Box 6079, Station "Centre-ville", Montréal, Québec Canada H3C 3A7

T. Makino is with Northern Telecom (Nortel), P. O. Box 3511, Station C, Nepean, Ontario, Canada K1Y 4H7

3.1 Introduction

A high side-mode suppression ratio ($SMSR$) in single-mode DFB lasers is essential for high modulation frequency applications in optical telecommunication systems. A low $SMSR$ can lead to a high intensity noise in the laser output and broaden the spectral linewidth, which can introduce a severe dispersion penalty in the system. Although the $\lambda/4$ phase-shifted DFB lasers have received much interest in the past for their predominantly single-mode operation, it has been shown that spatial hole burning caused by the longitudinal nonuniformity of the photon distribution in the cavity can reduce the $SMSR$ for high optical intensities [1]. Several methods have been proposed to eliminate spatial hole burning, such as the use of nonuniform longitudinal carrier injection [2], multiple phase-shift structures [3], corrugation-pitch-modulated (CPM) structures which consist of two different grating periods along the cavity [4], varying coupling coefficients along the cavity [5], and distributed phase-shift structures with S-bent waveguides [6]. Those configurations, however, add significant complexity to the laser structure and hence to the laser design and fabrication.

The use of gain coupling in DFB lasers has been shown to be effective for the single-mode selection [7]. With an inphase or antiphase uniform gain grating, one of the Bloch modes can be favoured with a large single-mode gain margin [8]. Recent work has shown that gain-coupled DFB lasers have better properties, such as low spatial hole burning, high single-mode yield, immunity to external reflection, high power and high speed performance [9, 10, 11, 12]. Much attention has also been devoted to the enhancement of the $SMSR$ in gain-coupled DFB lasers [13, 14]. In contrast to other types of DFB lasers, the strength of the optical feedback from the complex coupling structure is power-dependent in gain-coupled DFB lasers. The interaction between the periodically varying gain medium and the standing wave

pattern of the DFB modal fields can also result in an enhancement of the spontaneous emission and a substaintial side-mode suppression. For a design with a high $SMSR$, a systematic analysis of the $SMSR$ in gain-coupled DFB lasers, including spatial hole burning and the other various spatial effects is important.

An accurate study of the $SMSR$ in DFB lasers requires a self-consistent multimode model. Vankwikelberge *et al.* used the travelling wave equations in order to obtain the multimode optical fields [15]. The contribution of spontaneous emission is included by introducing the local rates of the emission into the coupled wave equations. Pan *et al.* developed a procedure based on the Green's function method, which expands the Wronskian of the scalar wave equation about its root in the complex frequency plane [16]. This paper presents a self-consistent analysis of gain-coupled DFB lasers using the spatially dependent multimode rate equations. We include various spatial effects, such as distributed complex coupling, spatial hole burning as well as nonlinear gain compression into the model and analyze the effects on the side mode suppression. With the use of a modal decay rate γ_i in the coupled wave equations, we also obtain a closed form result for the $SMSR$ in DFB lasers. It is shown that the complex coupling mechanism produces a very high $SMSR$.

3.2 Multimode rate equations

The optical fields inside semiconductor lasers satisfy the Maxwell's equations [17]:

$$\nabla_t \times \boldsymbol{E} + \mu_0 \frac{\partial \boldsymbol{H}}{\partial t} = -\frac{\partial}{\partial z} \boldsymbol{i}_z \times \boldsymbol{E} \tag{3.1}$$

$$\nabla_t \times \boldsymbol{H} - \frac{\partial (\varepsilon \boldsymbol{E})}{\partial t} = -\frac{\partial}{\partial z} \boldsymbol{i}_z \times \boldsymbol{H} + \boldsymbol{J}_{sp} \tag{3.2}$$

where $\boldsymbol{E}$ and $\boldsymbol{H}$ are the electric and magnetic field vectors. $\boldsymbol{J}_{sp}$ stands for the current density causing the spontaneous emission events which are completely irregular in

space and time. According to the fluctuation-dissipation theorem [18], the Fourier decomposition of $\boldsymbol{J}_{sp}$ satisfies the correlation relation:

$$< \boldsymbol{J}_{sp}(z,\omega), \boldsymbol{J}_{sp}(z',\omega') >= 2\hbar\omega^2 n_{sp}(z) Im\{\varepsilon(z,\omega)\}\delta(z-z') \tag{3.3}$$

where n_{sp} is the population inversion factor. ε is the dielectric constant of the laser waveguide. Here, it varies periodically along the longitudinal direction. Using a spatial Fourier expansion, we can express it as:

$$\varepsilon(z) = \tilde{\varepsilon}(\omega, N, S)\left[1 + 2\sum_n c_n \cos(2\beta_n z + \theta)\right] \tag{3.4}$$

where $\beta_n = \frac{n\pi}{\Lambda}$ is the Bragg wavenumber and the integer n is the order of the Bragg grating. $\tilde{\varepsilon}(\omega, N, S)$ gives the slowly varying part of the dielectric constant induced by the longitudinal spatial hole burning and nonlinear gain compression. N and S denote the distributions of carrier and photon densities.

For simplicity, we assume that the DFB laser has been designed to support a single transverse mode, which is often the case in practice. Under the standing wave approximation, the temporal and spatial dependencies of the optical fields are separable. We can expand the electric and magnetic fields in terms of the eigenmode of the pumped laser cavity as follows:

$$\boldsymbol{E}(x,y,z,t) = \sum_i \left\{Z_i^+(z)e^{-j\beta_n z}\boldsymbol{e}_i^+(x,y,z) + Z_i^-(z)e^{j\beta_n z}\boldsymbol{e}_i^-(x,y,z)\right\} A_i(t)e^{j\omega_i t} \tag{3.5}$$

$$\boldsymbol{H}(x,y,z,t) = \sum_i \left\{Z_i^+(z)e^{-j\beta_n z}\boldsymbol{h}_i^+(x,y,z) + Z_i^-(z)e^{j\beta_n z}\boldsymbol{h}_i^-(x,y,z)\right\} A_i(t)e^{j\omega_i t} \tag{3.6}$$

where $\pm$ indicates the forward and backward propagating waves, respectively. $A_i(t)$ gives the time-dependent amplitude of mode i. $\boldsymbol{e}_i^{\pm}(x,y,z)$ and $\boldsymbol{h}_i^{\pm}(x,y,z)$ represent the transverse distributions of the guided fields. They satisfy the Maxwell's equations:

$$\nabla_t \times \boldsymbol{e}_i^{\pm}(x,y,z) + j\omega_i\mu_0\boldsymbol{h}_i^{\pm}(x,y,z) = \pm j\beta_i(z)\boldsymbol{i}_z \times \boldsymbol{e}_i^{\pm}(x,y,z) \tag{3.7}$$

$$\nabla_t \times \boldsymbol{h}_i^{\pm}(x,y,z) - j\omega_i\tilde{\varepsilon}_i(z)\boldsymbol{e}_i^{\pm}(x,y,z) = \pm j\beta_i(z)\boldsymbol{i}_z \times \boldsymbol{h}_i^{\pm}(x,y,z) \tag{3.8}$$

where $\beta_i(z)$ is the local modal propagation constant along the laser waveguide. $\bar{\varepsilon}_i(z) = \bar{\varepsilon}[\omega_i, \bar{N}(z), \bar{S}(z)]$ gives the value of dielectric constant at steady state. The subscript i indicates that the optical mode oscillates at the frequency ω_i.

Although, in equations (3.7) and (3.8), the transverse distributions of the modal fields $\boldsymbol{e}_i$ and $\boldsymbol{h}_i$ are in principle z-dependent because of spatial hole burning and nonlinear gain compression in the DFB cavity, their overlap with the active regions does not change much because of the weakly guiding nature of the laser waveguide. Therefore, those slight variations are ignored. Since the frequency spacing between the DFB modes is so narrow, the differences in the field distributions by modal frequency are also ignored. With those approximations, substituting (3.5) and (3.6) into the Maxwell's equations (3.1) and (3.2) and using (3.7) and (3.8), we obtain the following set of travelling wave equations from collecting the terms with the same harmonic dependency:

$$-\sum_i e^{j\omega_i t}\Big\{VZ_i^+\frac{\partial}{\partial t} + U\frac{\partial Z_i^+}{\partial z} + j[(\beta_i-\beta_n)U + D_i(t)]Z_i^+ + jc_n e^{-j\theta}[K_i + D_i(t)]Z_i^-\Big\}A_i(t) = J_{sp}^+ \quad (3.9)$$

$$-\sum_i e^{j\omega_i t}\Big\{VZ_i^-\frac{\partial}{\partial t} - U\frac{\partial Z_i^-}{\partial z} + j[(\beta_i-\beta_n)U + D_i(t)]Z_i^- + jc_n e^{j\theta}[K_i + D_i(t)]Z_i^+\Big\}A_i(t) = J_{sp}^- \quad (3.10)$$

where

$$U = \iint_A (\boldsymbol{e}_t \times \boldsymbol{h}_t)\cdot \boldsymbol{i}_z da \quad (3.11)$$

$$V = \iint_A \frac{\partial \omega\varepsilon}{\partial\omega}\boldsymbol{e}_t\cdot\boldsymbol{e}_t da \quad (3.12)$$

$$D_i = \iint_A [\bar{\varepsilon}(\omega_i) - \bar{\varepsilon}(\omega_i)]\boldsymbol{e}_t\cdot\boldsymbol{e}_t da \quad (3.13)$$

$$K_i = \omega_i \iint_A \bar{\varepsilon}(\omega_i)\boldsymbol{e}_t\cdot\boldsymbol{e}_t da \quad (3.14)$$

$$J_{sp}^{\pm} = \frac{1}{2\pi}\int_0^\infty \left[\iint_A \boldsymbol{e}_t\cdot\boldsymbol{J}_{sp}(\beta,t)ds\right] e^{-j(\beta\pm\beta_n)z}d\beta \quad (3.15)$$

$\boldsymbol{J}_{sp}(\beta,t)$ is the spatial Fourier transform of $\boldsymbol{J}_{sp}(z,t)$. In deriving equations (3.9)

and (3.10), we have also used the conditions $\boldsymbol{e}^{\pm} = \boldsymbol{e}_t \pm \boldsymbol{e}_z$ and $\boldsymbol{h}^{\pm} = \pm\boldsymbol{h}_t + \boldsymbol{h}_z$ for the modal fields.

At steady state, $N(z,t) = \bar{N}(z)$, $S(z,t) = \bar{S}(z)$, and $D_i(t) = 0$. In order to take into account the contribution from spontaneous emission to the individual modes, it is convenient, in the spirit of the bookkeeping approach of rate equations, to introduce a $j\gamma_i V$ term in the coupled wave equations for the eigenmodes in the pumped DFB laser as:

$$\frac{dZ_i^+}{dz} + j[\beta_i(z) + j\gamma_i V - \beta_n]Z_i^+ = -jc_n e^{-j\theta} K_i(z) U^{-1} Z_i^- \tag{3.16}$$

$$-\frac{dZ_i^-}{dz} + j[\beta_i(z) + j\gamma_i V - \beta_n]Z_i^- = -jc_n e^{j\theta} K_i(z) U^{-1} Z_i^+ \tag{3.17}$$

Then, γ_j yields the amplitude decay rate of mode j in the corresponding rate equation, as shown now: inserting equations (3.16) and (3.17) into equations (3.9) and (3.10) and applying orthogonality (3.40), a set of multimode rate equations for the modal amplitudes can be obtained as follows:

$$\frac{dA_j}{dt} + \gamma_j A_j(t) = -j \sum_i e^{j(\omega_i - \omega_j)t} G_{ij}(t) A_i(t) + F_j(t) \tag{3.18}$$

where $G_{ij}(t)$ represents the coupling coefficient due to the longitudinal gain variation induced by the spatial hole burning and nonlinear gain compression effects. It can be written as:

$$G_{ij}(t) = \frac{\int_L D_i(z,t) \left[Z_i^+ Z_j^- + Z_i^- Z_j^+ + c_n \left(Z_i^- Z_j^- e^{-j\theta} + Z_i^+ Z_j^+ e^{j\theta} \right) \right] dz}{2V \int_L Z_j^+ Z_j^- dz} \tag{3.19}$$

The last term in equation (3.18),

$$F_j(t) = -\frac{\int_L \left[J_{sp}^+ Z_j^- + J_{sp}^- Z_j^+ \right] dz}{2V \int_L Z_j^+ Z_j^- dz} e^{-j\omega_j t} \tag{3.20}$$

gives the Langevin function for the amplitude noise. If the photon number in mode j is defined as $I_j(t) = \frac{1}{\hbar\omega_j} A_j(t) A_j^*(t)$ [1], it is straightforward to show with (3.3) and

[1] This actually implies that $\int_L [|Z_j^+|^2 + |Z_j^-|^2] dz = 1$

(3.15) that

$$< F_j(t)A_j^*(t) >= \frac{R_{sp}^j}{2} \tag{3.21}$$

where

$$R_{sp}^j = \frac{\int_L \omega_j n_{sp} W \left[Im\{\bar{\varepsilon}_j\} \left(|Z_j^+|^2 + |Z_j^-|^2 \right) + 2Im\{c_n \bar{\varepsilon}_j\} Re\left(Z_j^- Z_j^{+*} e^{-j\theta} \right) \right] dz}{\left| 2V \int_L Z_j^+ Z_j^- dz \right|^2} \tag{3.22}$$

gives the rate of spontaneous emission into mode j and

$$W = \iint_A |e_t|^2 da \tag{3.23}$$

Expression (3.22) gives a closed form for R_{sp}^j in terms of the coupled wave functions. This shows explicitly the effect of gain coupling on the spontaneous emission rate. Compared with the result of Henry [19] and Tromborg [20] using the Green's function approach, we see that they are similar except for the spatially oscillatory terms, which contribute little to the integral.

Equations (3.16), (3.17) and (3.18) are the basis for our analysis of the cavity modes in DFB lasers. Before applying them to the multimode analysis, we underline some limitations introduced by the derivation of the rate equations (3.18). First, the material has been assumed to have an instantaneous response, which allows us to multiply the dielectric constant by the complex field amplitudes directly instead of using a convolution. This condition is valid as long as the variations of field amplitudes are much slower than the optical frequencies. Second, the standing wave approximation requires that the photon round trip time in the DFB cavity ($\sim$ 1 ps) is much shorter than the laser response caused by modulation. In normal DFB lasers (with $\sim$ 100 μm cavity length), this can be justified up to $\sim$ 100 GHz. Third, rigorously speaking, the longitudinal modes in DFB lasers are not perfectly orthogonal to each other. This could introduce some effect on the static, dynamic and

even stochastic properties of DFB laser [21]. However, a detailed investigation of this point is beyond the scope of this paper.

3.3 Self-consistent solutions

A complete model also includes the spatially dependent carrier rate equation:

$$\frac{\partial N}{\partial t} = J(z,t) - R[N(z,t)] - G[N(z,t), S(z,t)]S(z,t) \tag{3.24}$$

where $J(z,t)$ is the pumping rate and $R(z,N)$ gives the carrier recombination rate:

$$R(z,N) = AN(z,t) + BN^2(z,t) + CN^3(z,t) \tag{3.25}$$

where A, B and C correspond to the non-radiative, radiative and Auger recombination coefficients, respectively. $G(z,N,S)$ is the net rate of stimulated emission. $S(z,t)$ denotes the photon density distribution. The carrier dynamics in the transverse plane are not included.

At the steady state, $J(z,t) = \bar{J}(z)$ and modulation of the dielectric constant vanishes or $D_i(z,t) = 0$. Solutions are obtained by setting $d/dt = 0$ and eliminating the noise terms in (3.18) and (3.24). Based on (3.21), we get:

$$\bar{I}_i = R^i_{sp}/(2\gamma_i) \tag{3.26}$$

$$\bar{J}(z) = R[\bar{N}(z)] + G[\bar{N}(z), \bar{S}(z)] \sum_i |Z_i(z)|^2 \bar{I}_i \tag{3.27}$$

Equation (3.26) determines the stationary value of the photon number in mode i, which is very similar to that obtained by the conventional rate equations [22].

The laser output power from the right and left facets is calculated from:

$$\bar{P}^i_L = v_g \hbar\omega_i (1 - |r_L|^2)|Z^-_i(0)|^2 \bar{I}_i \tag{3.28}$$

$$\bar{P}^i_R = v_g \hbar\omega_i (1 - |r_R|^2)|Z^+_i(L)|^2 \bar{I}_i \tag{3.29}$$

where v_g is the light group velocity, r_L and r_R are the facet reflectivities at left and right ends, respectively. We obtain the $SMSR$ for the corresponding facets as:

$$SMSR_L = \frac{\bar{P}_L^m}{\bar{P}_L^s} = \frac{|Z_m^-(0)|}{|Z_s^-(0)|} SMSR_{ph} \tag{3.30}$$

$$SMSR_R = \frac{\bar{P}_R^m}{\bar{P}_R^s} = \frac{|Z_m^+(L)|}{|Z_s^+(L)|} SMSR_{ph} \tag{3.31}$$

where the superscript and subscript m and s denote the main mode and side mode, respectively.

$$SMSR_{ph} = \frac{\gamma_s \omega_m R_{sp}^m}{\gamma_m \omega_s R_{sp}^s} \tag{3.32}$$

is the ratio of the photon numbers between two modes. This shows that, when $r_L \neq r_R$, the values of $SMSR_R$ and $SMSR_L$ can be different due to the different longitudinal distributions of the modal fields [16].

The self-consistent analysis for a given injection requires the solution of equations (3.26) and (3.27) together with (3.16) and (3.17) simultaneously. Above threshold, the carrier distribution $\bar{N}(z)$ inside the DFB cavity becomes nonuniform due to the spatial hole burning and nonlinear gain compression. Closed form results from the coupled wave equations are no longer available. In order to obtain the self-consistent solutions, we use the F-matrix method [23] to calculate the modal field distributions, dividing the DFB cavity into many small subsections. Within each subsection, the carrier density is assumed to be uniform and the coupled wave equations are solved analytically. Matching the modal fields $Z_i^+(z)$ and $Z_i^-(z)$ at each interface between subsections, we determine the distributions from one end of the laser to the other. The modal resonances occur when the boundary conditions at the facets are satisfied:

$$Z_i^+(0) = r_L Z_i^-(0) \tag{3.33}$$

$$Z_i^-(L) = r_R Z_i^+(L) \tag{3.34}$$

To achieve that, a proper set of γ_i and ω_i values need to be searched for a given bias $\bar{J}(z)$. In our numerical procedure, this is done by inserting a set of initial guess

values for γ_i and ω_i into the F-matrix decomposition of equations (3.16) and (3.17). We then match the modal fields at the first facet for each mode and calculate the modal fields $Z_i^+(z)$ and $Z_i^-(z)$ as well as the distribution of carrier density $\bar{N}(z)$ by solving the F-matrix together with the carrier rate equation (3.24) in the following subsections. When the solutions reach the other end of the laser, the boundary conditions are checked. If they are not satisfied by all modes, a new set of guess values is used and the iteration continues until all the modes are obtained.

The system formed by equations (3.16), (3.17) and (3.24) is highly nonlinear. That makes the initial guess values for γ_i and ω_i critical to the solutions. However, far below threshold, the distribution of carriers $N(z)$ is uniform in the cavity because the photon number in all eigenmodes is nearly zero. Therefore, we can choose the same value for the initial guess for all γ_i since they are all far away from their thresholds. Moreover, the uniform carrier distribution makes the description of the laser emission spectrum easy [24]: the emission peaks are used to locate the modal resonance frequency ω_i. After the solutions for the first bias value are obtained, the injection is increased in small steps and the process is solved iteratively. This way, the light-current (L-I) curves for each mode over a large bias range can be obtained.

3.4 Numerical results

In this paper, only lasers with first-order gratings are simulated. The key parameters are listed in Table I. Fig. 1 presents the results for an antiphase gain-coupled DFB laser. It is shown clearly that antiphase gain coupling selects the lasing mode on the short wavelength side of the Bragg stopband and the side mode powers are clamped when the bias is set above threshold. Because the inphase gain coupling reduces the $|K|L$ value of the grating below threshold, a broadening of the Bragg

stopband can be seen as the gain increases. Above threshold, the decay rate γ of the lasing mode decreases steeply, which causes the photon number of the lasing mode and hence the laser output power to increase. Since the feedback from the index grating is enhanced by spatial hole burning, the spontaneous emission rate R_{sp} of the lasing mode decreases slightly above threshold in the antiphase gain-coupled DFB laser. Although the contribution of the spontaneous emission depends on the overlap between the modal fields with the gain medium (see (3.22)), the results show that, above threshold, the spontaneous emission rates are all clamped at similar power levels, which leads us to infer that the $SMSR$ in DFB lasers is mainly determined by the ratio of modal decay rate γ between the main mode and the highest side mode. One should also notice that, although higher decay rates limit the photon number in side modes, some higher order side modes may output more power than the lower order ones because their modal fields are more concentrated at both ends of DFB laser cavity. Because of the gain coupling effect on the mode selection [8], the strongest side mode in gain-coupled DFB lasers, often appears on the same side of the stopband next to the lasing mode, in contrast to index-coupled DFB lasers, where it is often the fundamental mode on the other side of the stopband.

Both analytical formulae and our numerical results indicate that the modal decay rate γ is an important parameter for the determination of the cavity mode behaviour in DFB lasers. Since the side mode suppression is determined by the ratio of the decay rate between main mode and side mode, a large difference between γ_m and γ_s is desirable. Based on the coupled wave equations (3.16) and (3.17), we find that this is determined by several features of gain-coupled DFB lasers, i.e. the distributed feedback, the gain coupling effect and the spatial hole burning as well as the nonlinear gain compression effects[2].

[2]As given in Table I, we choose the facet reflectivity $r_R = r_L = 0$ here to simplify the analysis and we do not consider the grating phase shift effect in this paper.

Table I Physical parameters used in the model

Bragg wavelength	λ_B	1.55 μm
waveguide width	w	1.5 μm
thickness of active layer	d	0.1 μm
cavity length	L	350 μm
group index of refraction	n_g	3.7
effective waveguide index of refraction	n_w	3.23
end-facet reflectivity	r_L, r_R	0
waveguide loss	α_0	20 cm^{-1}
transverse modal confinement factor	Γ_0	0.1
differential gain	g_d	6×10^{-16} cm^2
carrier density at transparency	N_0	1.5×10^{18} cm^{-3}
nonradiative recombination coefficient	A	1×10^{-9} s^{-1}
radiative recombination coefficient	B	1×10^{-10} $cm^3 s^{-1}$
Auger recombination coefficient	C	1.3×10^{-28} $cm^6 s^{-1}$
spontaneous emission factor	n_{sp}	3
linewidth enhancement factor	α_M	3

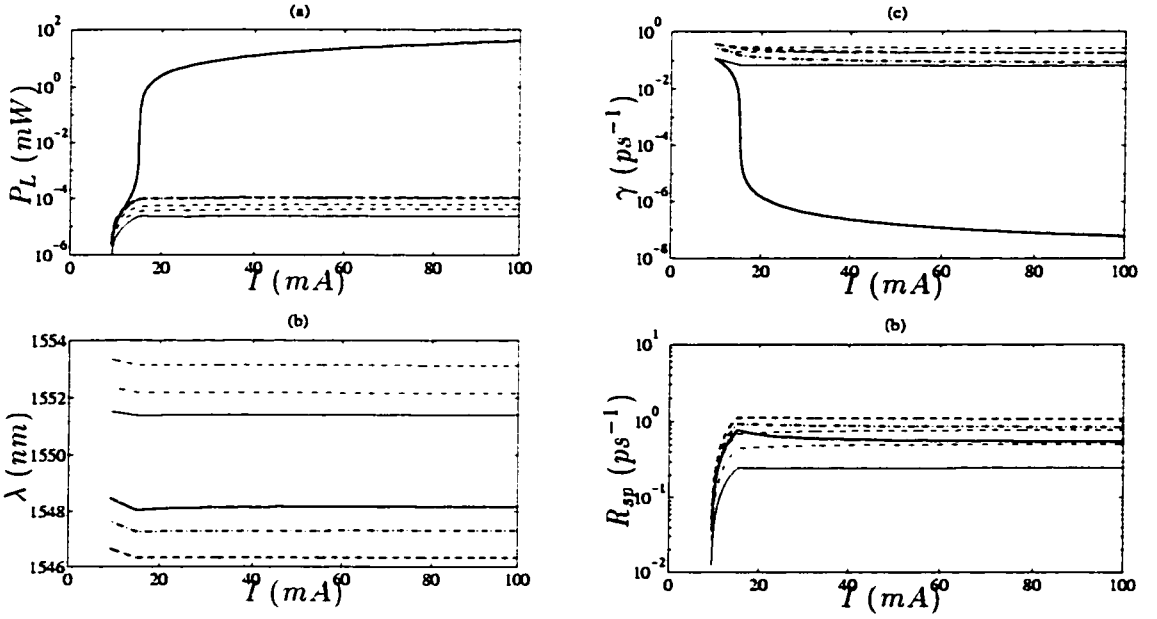

Fig. 1 Modal power (a), wavelength (b), decay rate (c) and spontaneous emission rate (d) evolution with bias current for an antiphase gain-coupled DFB laser with $|K|L = 4$. Solid line: first order mode; dash-dotted line: second order mode; dashed line: third order mode. Thicker lines: short wavelength mode; thiner lines: long wavelength mode.

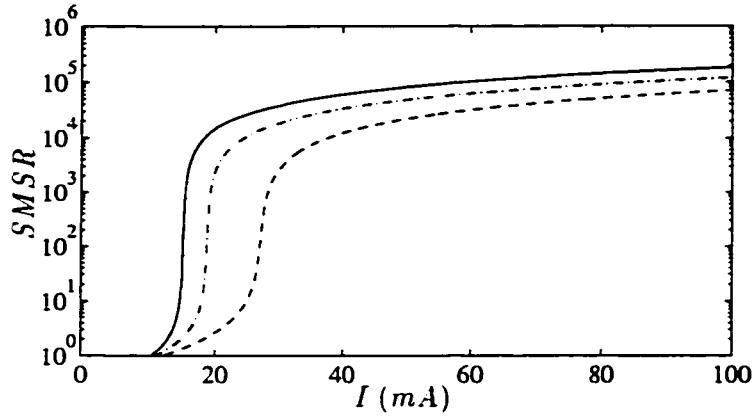

Fig. 2 Dependency of side mode suppression ratio on the coupling strength of inphase gain-coupled DFB lasers. Solid line: $|K|L = 4$; dash-dotted line: $|K|L = 3$; dashed line: $|K|L = 2$.

3.4.1 Distributed feedback effect

It is well known that the distributed feedback provides a strong mode selection mechanism in DFB lasers. Fig. 2 depicts the dependency of the $SMSR$ on $|K|L$ in inphase gain-coupled DFB lasers. It shows that a higher $|K|L$ gives a higher $SMSR$. A high $|K|L$ corresponds to a low threshold gain, which implies that, above threshold, the spontaneous emission as well as the side mode powers are clamped at relatively lower levels. Therefore, in agreement with energy conservation, under the same injection conditions, the lasing mode with a higher $|K|L$ will carry more photons and hence a higher $SMSR$ value. Fig. 3 shows the same trend for the antiphase gain-coupled DFB lasers. Because of a nonzero linewidth enhancement factor α_M, the antiphase gain coupling enhances the grating feedback as gain increases. Hence, below and above threshold, antiphase gain coupling configurations produce a relatively lower and higher $SMSR$ than its inphase counterparts, respectively. This indicates that, with the same $|K|L$, an antiphase gain-coupled DFB laser has a higher $SMSR$ than its inphase counterpart. More details about this will be found in the analysis of the spatial hole burning effect. Flanigan and Carroll

obtain a higher $SMSR$ value in inphase gain-coupled DFB lasers using a dynamic time domain model [25]. This discrepancy calls for a further detailed investigation.

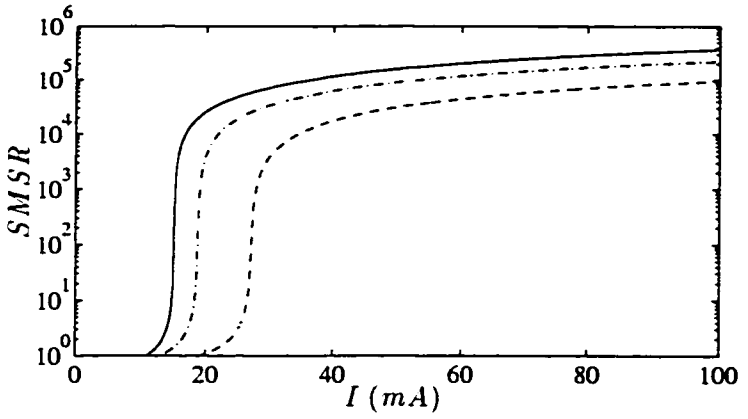

Fig. 3 Dependency of side mode suppression ratio on the coupling strength of antiphase gain-coupled DFB lasers. Solid line: $|K|L = 4$; dash-dotted line: $|K|L = 3$; dashed line: $|K|L = 2$.

3.4.2 Gain coupling effect

With the possibility of being either in phase and in antiphase with the index grating, the gain grating can favour the Bloch modes on the long and short wavelength sides of the Bragg stopband respectively, which induces another mechanism for the suppression of side modes in DFB lasers [8]. The gain coupling effect can be enhanced by increasing the modulation depth of the gain grating. As shown in Figs. 4 and 5, with the same $|K|L$, the suppression of the short or the long wavelength side modes in inphase and antiphase gain-coupled DFB lasers, respectively, increases as the modulation depth $\Delta d/d$ of the gain grating increases. For comparison, we also present the results for index-coupled DFB lasers on the same plots. In contrast to the $|K|L$ effect, the spontaneous emission in gain-coupled DFB lasers does not decrease much as the threshold current decreases because of the interaction between the gain grating and the standing wave pattern of the modal fields. Nevertheless,

gain coupling still produces higher decay rates for side modes generally and increases the $SMSR$. Since the gain coupling effect is presented even below threshold, we infer that it can be helpful for the transient side mode suppression as well.

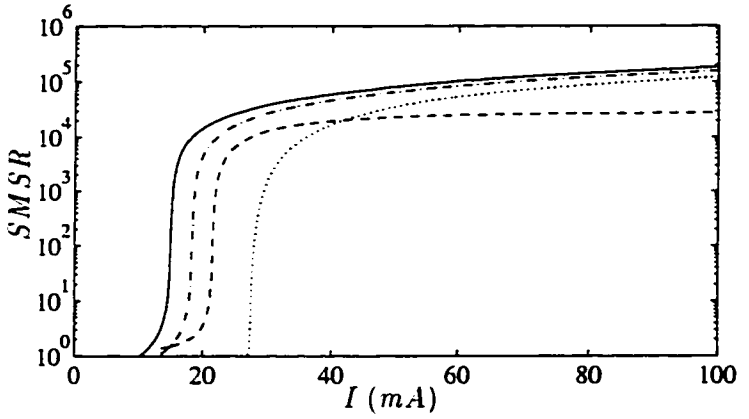

Fig. 4 Dependency of the $SMSR$ on the modulation depth of the gain grating in inphase gain-coupled DFB lasers with $|K|L = 4$. Solid line: $\Delta d/d = 1$; dash-dotted line: $\Delta d/d = 0.75$; dashed line: $\Delta d/d = 0.5$. Dotted line: $\Delta d/d = 0$ (index-coupled).

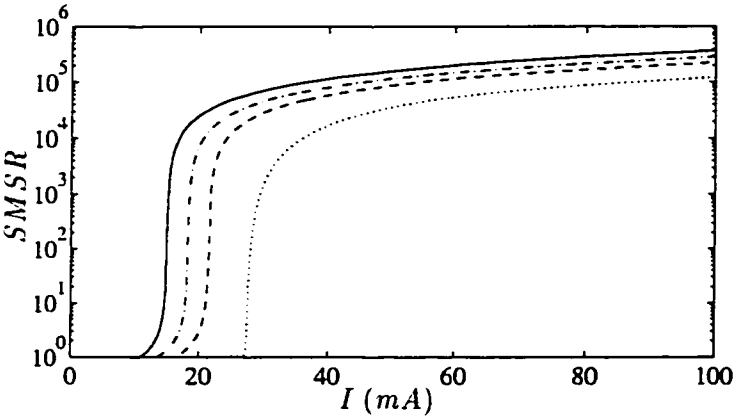

Fig. 5 Dependency of the $SMSR$ on the modulation depth of the gain grating in antiphase gain-coupled DFB lasers with $|K|L = 4$. Solid line: $\Delta d/d = 1$; dash-dotted line: $\Delta d/d = 0.75$; dashed line: $\Delta d/d = 0.5$; dotted line: $\Delta d/d = 0$ (index-coupled).

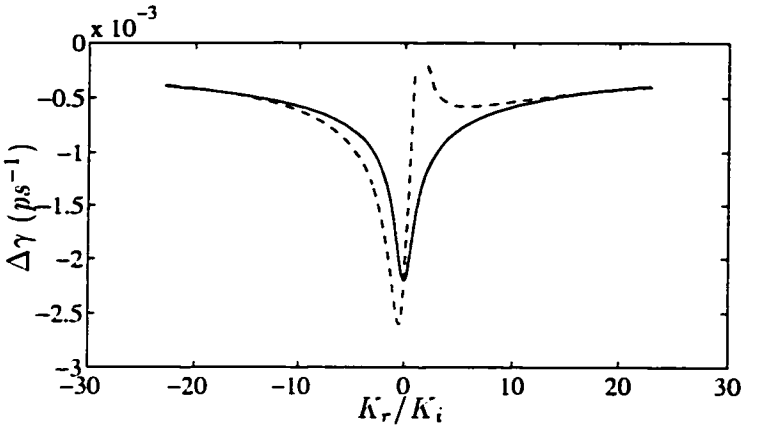

Fig. 6 Dependency of the decay rate of the lasing mode on the complex coupling coefficient $K = K_r + jK_i$ in gain-coupled DFB lasers at $I = I_{th} + 10\ mA$, where $\Delta\gamma = \gamma - \gamma_{th}$. Solid line: $\alpha_M = 0$; Dash-dotted line: $\alpha_M = 3$.

3.4.3 Spatial hole burning effect

We see in Fig. 4 that, when the gain coupling is weak, the $SMSR$ can even decrease at high bias current in inphase gain-coupled DFB lasers. This indicates that spatial hole burning also plays a role in side mode suppression. Generally, because of a nonzero linewidth enhancement factor, the spatial hole burning effect induces a nonuniform index change in DFB laser cavity, which disturbs the round trip conditions for the cavity modes and induces another mechanism for suppressing side modes. Using a perturbation technique, we calculate the changes of the modal decay rates in gain-coupled DFB lasers with different values of the material linewidth enhancement factor α_M (see Appendix B). Comparing the results of Fig. 6, we see that spatial hole burning suppresses the mode on the long wavelength side of the Bragg stopband and favours the mode on the short wavelength side. Therefore, in inphase and antiphase gain-coupled DFB lasers, the $SMSR$ value respectively decreases and increases because of this effect. Physically, this can be understood by

the fact that, in inphase gain-coupled DFB lasers, spatial hole burning reduces the feedback strength of the index grating and hence a higher net gain $2\gamma V$ is required, which leads to a higher decay rate for the lasing mode. On the contrary, an antiphase structure can enhance the feedback strength of the index grating, which allows the photons to be stored in the lasing mode with a longer lifetime.

3.4.4 Nonlinear gain compression effect

Nonlinear gain compression induces another type of nonuniformity of the index of refraction in DFB laser cavities. In gain-coupled DFB lasers, gain compression not only reduces the optical gain, but also decreases the optical feedback. In conjunction with spatial hole burning, nonlinear gain compression can produce a marked effect on the side mode suppression. In inphase gain-coupled DFB lasers, the lasing mode is stable and dominant in the cavity. The induced change normally concentrates where the intensity of lasing mode is high. In turn, this also makes gain compression affect the lasing mode most (and not influence the side mode behaviour much). Our calculation in Fig. 7(a) shows that gain compression reduces the power of the lasing mode slightly and results in a small decrease of the $SMSR$. However, in antiphase gain-coupled DFB lasers, nonlinear gain compression can have an effect on the stability of the lasing mode [26]. Our self-consistent analysis shows that a high gain compression reduces the critical power for the instability of the lasing mode. At that power, the lasing mode breaks up into two asymmetric modes with two different powers at the output facets in spite of a symmetric cavity. The occurrence of such an instability also causes the side mode power to increase (see Fig. 7 (b)). Consequently, the value of the $SMSR$ decreases as the bias current increases.

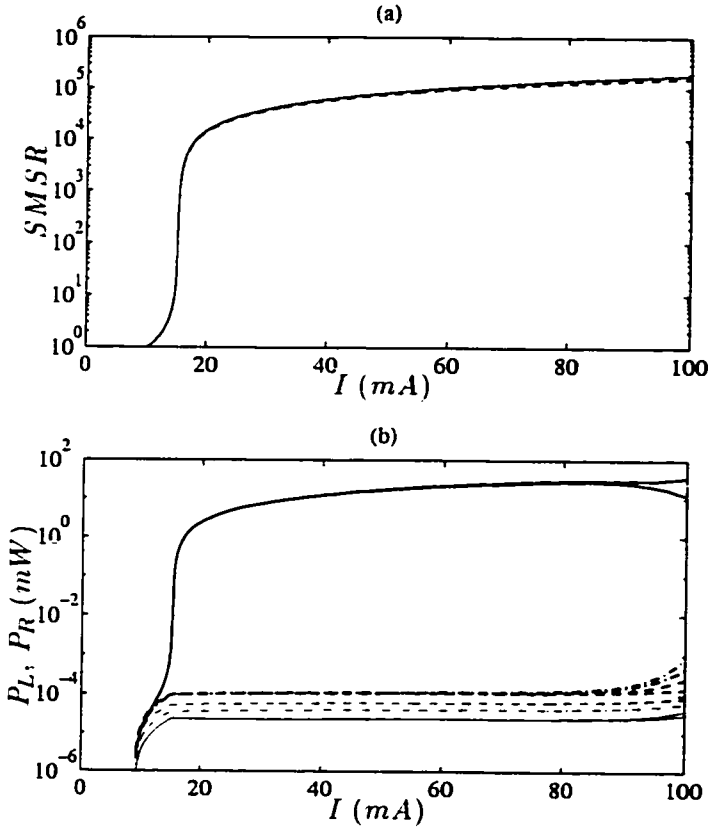

Fig. 7 (a) Gain compression effect on $SMSR$ in inphase gain-coupled DFB lasers with $|K|L = 4$. Solid line: $\varepsilon_N = 0$; dashed line: $\varepsilon_N = 5 \times 10^{-17}\ cm^3$. (b) Modal power evolution with bias current in an antiphase gain-coupled DFB laser with $|K|L = 4$ and $\varepsilon_N = 5 \times 10^{-17}\ cm^3$. Solid line: first order modes; dash-dotted line: second order modes; dashed line: third order modes. Thicker lines: long wavelength modes; thiner lines: short wavelength modes.

3.5 Conclusion

Using the spatially dependent multimode rate equations, a self-consistent multimode analysis of gain-coupled DFB lasers has been developed. The model has included various spatial nonuniformities of DFB lasers, such as the distributed feedback, the carrier dependent gain coupling and nonuniform spatial hole burning. Introducing the modal net gain into the coupled wave equations, we were able to

solve the carrier and photon rate equations together with the modal optical fields in a self-consistent manner. The approach generalizes the conventional rate equation analysis and yields various results including the spatial features in a closed form. Although the scope of this paper is limited to steady state analysis, the formalism can be extended to time dependent solutions.

Our detailed analysis of gain-coupled DFB lasers demonstrates that both high index coupling and high gain coupling contribute to improving $SMSR$ of DFB lasers. A stronger DFB coupling reduces the laser threshold and keeps the side mode powers at relatively lower levels. Since the gain coupling significantly reduces the interaction of the antiphase Bloch modes as well as the high order side modes with the periodically varied gain medium, it increases the decay rates of side modes. Combined with the frequency-dependent grating feedback effect, gain coupling produces a very high $SMSR$ in DFB lasers. The self-consistent analysis also reveals that spatial hole burning favours the short wavelength Bloch modes and hence decreases and increases the side mode suppression in inphase and antiphase gain-coupled DFB lasers, respectively. Moreover, the instability in antiphase gain-coupled DFB lasers can cause the side mode suppression to deteriorate. In contrast, inphase gain coupling gives a very stable lasing mode in the DFB laser, which helps reduce the nonlinear gain compression effect on the $SMSR$.

APPENDIX

A. Orthogonality of DFB modes in the pumped cavity

In the pumped DFB cavity, because of the spatial hole burning and the nonlinear gain compression, the carrier density distribution is not longitudinally uniform, which causes the material gain as well as the index of refraction to become

z-dependent and makes the modal propagation constant $\beta_i(z)$ and the frequency-dependent grating coupling coefficient $K_i(z)$ vary in the cavity. Within the effective index approximation [27], to first order, we have:

$$\beta_i(z) = k_i n_0 + j\frac{\Gamma_0}{2}\Big\{(1+j\alpha_M)g[\bar{N}(z),\bar{S}(z)] - \alpha_L\Big\} \tag{3.35}$$

$$c_n K_i(z) U^{-1} = k_i n_0 c_r \pm j\frac{\Gamma_0}{2}\Big\{(1+j\alpha_M)g[\bar{N}(z),\bar{S}(z)] - \alpha_L\Big\}c_g \tag{3.36}$$

where k_i is the modal wavenumber in free space. n_0 and Γ_0 give the average value of the effective waveguide index and of the transverse modal confinement factor over the gain cross section, respectively. α_M is the material linewidth enhancement factor and α_L represents the loss in the active region. c_r and c_g give the Fourier coefficients for the index and gain gratings, respectively. The sign $\pm$ in the coupling coefficient corresponds to the inphase and antiphase gain couplings, respectively.

If we multiply equation (3.16) of mode i and equation (3.17) of mode j with Z_j^- and Z_i^+, respectively, the following equation can be obtained by subtraction

$$\begin{aligned}\left\{\frac{d}{dz} + j[\beta_i(z) - \beta_j(z) + j(\gamma_i - \gamma_j)V]\right\} Z_i^+ Z_j^- \\ = -jc_n[K_i(z)Z_i^- Z_j^- e^{-j\theta} - K_j(z)Z_i^+ Z_j^+ e^{j\theta}]U^{-1}\end{aligned} \tag{3.37}$$

By interchanging the indexes i and j in (3.37) and subtracting both equations, we get

$$\begin{aligned}\frac{d}{dz}[Z_i^+ Z_j^- - Z_j^+ Z_i^-] &= -j[(k_i - k_j)n_0 + j(\gamma_i - \gamma_j)V][Z_i^+ Z_j^- + Z_j^+ Z_i^-] \\ &\quad -jc_r(k_i - k_j)n_0[Z_i^- Z_j^- e^{-j\theta} + Z_i^+ Z_j^+ e^{j\theta}]\end{aligned} \tag{3.38}$$

Since $c_r << 1$, we can neglect the second term on the right hand side of the equation (3.38). Applying longitudinal integration over equation (3.38) and using the boundary conditions (3.33) and (3.34), we get the following relation

$$j[(k_i - k_j)n_0 + j(\gamma_i - \gamma_j)V]\int_L [Z_i^+ Z_j^- + Z_j^+ Z_i^-]dz = 0 \tag{3.39}$$

Since $(k_i - k_j)n_0 + j(\gamma_i - \gamma_j)V \neq 0$ when $i \neq j$, we have

$$\int_L [Z_i^+ Z_j^- + Z_j^+ Z_i^-]dz = 0 \qquad i \neq j \tag{3.40}$$

B. Perturbation analysis of spatial hole burning

If we denote the modal fields at biases I_a and I_b by $Z_a^{\pm}(z)$ and $Z_b^{\pm}(z)$, respectively, then, following the same procedure as in Appendix A, i.e. substituting $Z_i^{\pm}$ and $Z_j^{\pm}$ by $Z_a^{\pm}$ and $Z_b^{\pm}$, respectively, we obtain:

$$\left\{\frac{d}{dz} + j[\beta_a(z) - \beta_b(z) + j(\gamma_a - \gamma_b)V]\right\} Z_a^+ Z_b^- = -jc_n[K_a(z)Z_a^- Z_b^- e^{-j\theta} - K_b(z)Z_a^+ Z_b^+ e^{j\theta}]U^{-1} \tag{3.41}$$

$$\left\{\frac{d}{dz} + j[\beta_b(z) - \beta_a(z) + j(\gamma_b - \gamma_a)V]\right\} Z_b^+ Z_a^- = -jc_n[K_b(z)Z_b^- Z_a^- e^{-j\theta} - K_a(z)Z_b^+ Z_a^+ e^{j\theta}]U^{-1} \tag{3.42}$$

where $\beta_a(z)$, $c_n K_a(z)U^{-1}$ and $\beta_b(z)$, $c_n K_b(z)U^{-1}$ denote the propagation constants and coupling coefficients at biases I_a and I_b, respectively. Subtracting equation (3.42) from (3.41) and using (3.35) and (3.36) together with the boundary conditions at both end facets (3.33) and (3.34), we obtain:

$$\gamma_a - \gamma_b = -Re\left\{\frac{\Gamma_0}{2V}\int_L (1 + j\alpha_M)[g_a(z) - g_b(z)]C(z)dz\right\} \tag{3.43}$$

$$k_a - k_b = Im\left\{\frac{\Gamma_0}{2n_0}\int_L (1 + j\alpha_M)[g_a(z) - g_b(z)]C(z)dz\right\} \tag{3.44}$$

where

$$C(z) = \left[2Z^+Z^- + c_g\left(Z^-Z^-e^{-j\theta} + Z^+Z^+e^{j\theta}\right)\right]\left[2\int_L Z^+Z^-dz\right]^{-1} \tag{3.45}$$

and $Z_a^{\pm}(z) = Z_b^{\pm}(z) = Z^{\pm}(z)$ is assumed for the small difference between biases I_a and I_b.

REFERENCES

[1] H. Soda, Y. Kotaki, H. Sudo, H. Ishikawa, S. Yamakoshi, and H. Imai, "Stability in single longitudinal mode operation in GaInAsP/InP phase adjusted DFBlasers", IEEE J. Quantum Electron., Vol. 23, pp. 804–814, 1987.

[2] M. Usami and S. Akiba, "Suppression of longitudinal spatial hole burning effect in $\lambda/4$-shifted DFB lasers by nonuniform current distributions", IEEE J. Quantum Electron., Vol. 25, pp. 1245–1253, 1989.

[3] G. P. Agrawal, J. E. Geusic, and P. J. Anthony, "Distributed feedback lasers with multiple phase-shift regions", Appl. Phys. Lett., Vol. 53, pp. 178–179, 1988.

[4] M. Okai, "Spectral characteristics of distributed feedback semiconductor lasers and their improvements by corrugation-pitch-modulated structure", J. Appl. Phys., Vol. 75, pp. 1–29, 1994.

[5] G. Morthier, K. David, P. Vanwilkelberge, and R. Beats, "A new DFB laser diode with reduced spatial hole burning", IEEE Photon. Technol. Lett., Vol. 2, pp. 388–390, 1990.

[6] J. Salzman, H. Olesen, A. Moller-Larsen, O. Albrektsen, J. Hanberg, J. Norregaard, B. Jonsson, and B. Tromborg, "Distributed feedback lasers with an S-bent waveguide for high-power single-mode operation", IEEE J. Selected Topics in Quantum Electron., Vol. 1, pp. 346–355, 1995.

[7] H. Kogelnik and C. V. Shank , "Coupled-wave theory of distributed feedback lasers", J. Appl. Phys., Vol. 43, pp. 2327–2335, 1972.

[8] J. Chen, A. Champagne, R. Maciejko, and T. Makino, "Improvement of single-mode gain margin in gain-coupled DFB lasers", submitted to IEEE J. Quantum Electron..

[9] G. P. Li, T. Makino, R. Moore, N. Puetz, K. Leong, and H. Lu, "Partly gain-coupled 1.55 μm strained-layer multi-quantum-well DFB lasers", IEEE J. Quantum Electron., Vol. 29, pp. 1736–1742, 1993.

[10] W. T. Tsang, M. C. Wu, Y. K. Chen, F. S. Choa, R. A. Logan, S. N. G. Chu, A. M.Sergent, P. Magill, K. C. Reichman, and C. A. Burrus, "Long-wavelength InGaAsP/InP multiquantum well distributed feedback and distributed Bragg reflector lasers grown by chemical beam epitaxy", IEEE J. Quantum Electron., Vol. 30, pp. 1370–1380, 1994.

[11] H. Lu, C. Blaauw, B. Benyon, G. P. Li, and T. Makino, "High-power and high-speed performance of $1.3 - \mu m$ strained MQW gain-coupled DFB lasers", IEEE J. Selected Topics in Quantum Electron., Vol. 1, pp. 375–381, 1995.

[12] H. Lu, T. Makino, and G. P. Li, "Dynamic properties of partly gain-coupled $1.55 - \mu m$ DFB lasers", IEEE J. Quantum Electron., Vol. 31, pp. 1443–1450, 1995.

[13] T. Makino , "Mechanism for high single-mode stability of gain-coupled DFB lasers with periodically etched quantum wells", Electron. Lett., Vol. 31, pp. 1579–1581, 1995.

[14] T. Makino , "Side-mode suppression mechanism of gain-coupled DFB lasers with periodically etched quantum wells", IEEE Photon. Technol. Lett., Vol. 8, pp. 602–604 , 1996.

[15] P. Vankwikelberge, G. Mothier, and R. Beats, "CLADISS-a longitudinal multimode model for the analysis of the static, dynamic, and stochastic behavior of diode lasers with distributed feedback", IEEE J. Quantum Electron., Vol. 26, pp. 1728–1741, 1990.

[16] X. Pan, B. Tromborg, and H. Olessen, "Complex pole expansion approach to multimode DFB laser modelling", IEE Proc. Optoelectron., Vol. 141, pp. 271–264, 1994.

[17] H. Wenzel and H. J. Wunsche , "An equation for the amplitudes of the modes in semiconductor lasers", IEEE J. Quantum Electron., Vol. 30, pp. 2073–2080, 1994.

[18] L. D. Landau and E. M. Lifshitz, *Statistical Physics*, Pergamon Press, Oxford, 1980.

[19] C. H. Henry, "Theory of spontaneous emission noise in open resonators and its application to lasers and optical amplifiers", J. Lightwave Technol., Vol. 4, pp. 288–297, 1986.

[20] B. Tromborg, H. Olesen, and X. Pan, "Theory of linewidth for multielectrode Laser diodes with spatially distributed noise sources", IEEE J. Quantum Electron., Vol. 27, pp. 178–192, 1991.

[21] P. Szczepanski and A. Kujawski, "Non-orthogonality of the longitudinal eigenmodes of a distributed feedback laser", Opt. Commun., Vol. 87, pp. 259–262, 1992.

[22] G. P. Agrawal and N. K. Dutta, *Semiconductor Lasers*. Van Nostrand Reinhold, New York, 1993.

[23] M. Yamada and K. Sakuda, "Analysis of almost-periodic distributed feedback slab waveguides via fundamental matrix approach", Appl. Opt., Vol. 26, pp. 3474–3478, 1987.

[24] T. Makino, "Transfer-matrix formulation of spontaneous emission noise of semiconductor lasers", IEEE J. Lightwave Technol., Vol. 9, pp. 84–91, 1991.

[25] B. J. Flanigan and J. E. Carroll, "Mode selection in complex-coupled semiconductor DFB lasers", Electron. Lett., Vol. 31, pp. 977–979, 1995.

[26] A. J. Lowery, B. Jonsson, H. Olesen, and D. Novak, "Mode instabilities in complex-coupled DFB semiconductor lasers", Electron. Lett., Vol. 31. pp. 40–41, 1995.

[27] T. Makino, "Effective-index matrix analysis of distributed feedback semiconductor lasers", IEEE J. Quantum Electron., Vol. 28, pp. 434–440, 1992.

CHAPTER 4

Small Signal Dynamics in Gain-Coupled DFB Lasers

One of the important advantages of semiconductor lasers is that they can be modulated directly by the injection current. A wide modulation bandwidth is of primary interest in the laser applications for in high-bit-rate and long-haul communications systems.

The relaxation oscillation frequency determines the laser modulation bandwidth and hence plays an important role in the laser dynamic characteristics. Due to the nature of carrier recombination and photon generation, various nonuniformities affect the relaxation oscillation frequency. For gain-coupled DFB lasers, the interference between the gain grating and the standing wave pattern of lasing light and the nonuniform optical feedback resulting from spatial hole burning produce a particular enhancement effect on the relaxation oscillation frequency. Small signal analysis of the rate equations provides a basic understanding of the laser modulation characteristics. For gain-coupled DFB lasers, such an analysis also needs to include the various structural and functional inhomogeneities in the cavity. The spatially dependent photon rate equations developed by the Green's function analysis therefore provide an effective tool for this purpose. This chapter presents a thorough investigation of the gain coupling effect on the laser modulation bandwidth.

Published in IEEE J. Quantum Electron., vol. 31, pp. 1955-1963, 1995

Relaxation Oscillation Frequency of DFB Lasers with Gain Coupling

Jianyao Chen, Roman Maciejko, *Senior Member, IEEE*, Alain Champagne and Toshihiko Makino, *Senior Member, IEEE*

Abstract

Using the spatially-dependent rate equations based on the Green's function analysis, we investigate the dependency of the relaxation oscillation frequency on the complex coupling coefficient and other parameters of gain-coupled DFB lasers by simultaneously considering spatial-hole-burning, gain saturation and gain compression. An explicit expression for the relaxation oscillation frequency for DFB lasers including the longitudinal spatial effects has been obtained. It is found that antiphase gain-coupling significantly enhances the local effective differential gain in the gain-coupled DFB laser and hence increases the relaxation oscillation frequency. We have also shown for the first time that the modal linewidth enhancement factor α_M plays an important role in determining the relaxation oscillation frequency of gain-coupled DFB lasers, especially when the built-in index coupling is weak.

J. Chen, R. Maciejko, and A. Champagne are with the Optoelectronics Laboratory, Department of Engineering Physics, École Polytechnique, P. O. Box 6079, Station "Centre-ville", Montréal, Québec Canada H3C 3A7

T. Makino is with Northern Telecom (Nortel), P. O. Box 3511, Station C, Nepean, Ontario, Canada K1Y 4H7

4.1 Introduction

High-speed semiconductor lasers with a single-longitudinal-mode operation are desirable for high-bit-rate and long-haul fiber optical communication systems. In the past decade, much progress has been made by developing the distributed-feedback (DFB) laser and distributed Bragg reflector (DBR) laser. With the frequency-dependent feedback mechanism, such lasers are capable of stable single mode operation with a narrow linewidth under direct high-speed modulation. Most of the commonly used DFB lasers in practical systems employ an index corrugation for the single mode selection and light feedback in the cavity. Recent research has indicated that a DFB laser with a periodic gain corrugation, i.e. the gain-coupled DFB laser, has many superior characteristics over the conventional index-coupled DFB laser, such as higher single-mode yield, less dependency on facet reflectivity and lower wavelength chirp [1, 2]. With the extra flexibility provided by the complex coupling structure, the possibility of improving device performance by properly arranging index and gain gratings in gain-coupled DFB lasers is being pursued [3, 4, 5, 6].

The relaxation oscillation frequency plays an important role in determining the high frequency response of semiconductor lasers. For practical DFB lasers, spatial nonuniformities such as light intensity distribution, spatial hole burning and gain compression affect the interaction between carriers and photons and influence significantly the modulation speed and relaxation oscillation frequency of DFB semiconductor lasers. A more detailed analysis of those effects is therefore required.

In gain-coupled DFB lasers, the optical feedback by the complex coupling structure changes with the carrier density. Moreover, the periodic variation of the material gain can constructively interfere with the standing-wave pattern of the lasing field in the cavity. The spatial effects can have a much more profound influence on their dynamic performance. It has been reported that antiphase coupling can

significantly enhance the relaxation oscillation frequency of gain-coupled DFB lasers [4, 5]. Using the spatially-dependent rate equations based on the Green's function approach, this paper presents a systematic investigation of the relaxation oscillation frequency for the gain-coupled DFB laser. Here, we limit our analysis to first-order, small-signal analysis for single-mode DFB lasers. The spatial effects of nonuniform light intensity distribution, spatial hole burning, gain saturation and gain compression are all included. An explicit expression for the relaxation oscillation frequency Ω_R including those spatial features is also derived. We have shown for the first time that the linewidth enhancement factor α_M has significant effects in determining the relaxation oscillation frequency of gain-coupled DFB lasers. The antiphase coupling structure effectively increases the local effective differential gain and hence broadens their intensity modulation bandwidth.

4.2 Spatially-dependent rate equation analysis

Fig. 1 illustrates a typical partly gain-coupled buried DFB semiconductor laser with a grating corrugation in the active layer. The transverse nonuniformities of the carrier and photon densities in the active region are neglected. Using the Green's function method (see Appendix) and the effective index approximation [7, 8], a set of rate equations for the total number of photons P in the lasing mode and the carrier density N can be obtained, assuming above-threshold single mode operation:

$$\frac{dP}{dt} = P(t)\int_L [G_N(z)\Delta N(z,t) + G_S(z)\Delta S(z,t)]\,dz + R_{sp} \tag{4.1}$$

$$\frac{\partial N}{\partial t} = J(z,t) - R(N,z) - v_g\Gamma g(N,z)S(z,t) \tag{4.2}$$

where $\Delta N(z,t)$ and $\Delta S(z,t)$ are the local deviations of the carrier and photon densities from the threshold values, N_{th} and $S_{th}(z)$. $J(z,t)$ is the pumping rate,

$R(N,z)$ gives the spontaneous recombination rate per unit volume. $S(z,t)$ denotes the photon density.

The rate equations (4.1, 4.2), together with the Green's function analysis presented in the Appendix, define our basis for the spatially-dependent dynamic model of DFB semiconductor lasers. As a first indication of some of the physics, the influence of the DFB structure on the modulation characteristics can be explored by performing the small signal analysis of those equations. For this purpose, we introduce the following expansions:

$$J(z,t) = J_0(z) + J_1(z)e^{j\Omega t} \tag{4.3}$$

$$N(z,t) = N_0(z) + N_1(z)e^{j\Omega t} \tag{4.4}$$

$$P(t) = P_0 + P_1 e^{j\Omega t} \tag{4.5}$$

and assume $J_0(z) >> J_1(z)$, $N_0(z) >> N_1(z)$, and $P_0 >> P_1$. Here, Ω is the laser intensity modulation frequency. $J_0(z)$, $N_0(z)$ and P_0 represent the stationary solutions which can be obtained self-consistently by setting all the time derivatives in Eqs. (4.1, 4.2) to zero. $J_1(z)$, $N_1(z)$ and P_1 correspond to the driving current and the resulting small signal carrier distribution and photon number, respectively. Substituting expressions (4.3-4.5) into the rate equations (4.1, 4.2) and expanding the $R(N)$ and $g(N,z)$ terms linearly about $N_0(z)$, an explicit solution for the response to intensity modulation can be obtained as:

$$\frac{P_1}{P_0} = \frac{\int_L \frac{G_N(z)J_1(z)dz}{j\Omega + \Gamma_N(z)}dz}{j\Omega + \Gamma_P + \int_L \frac{S_0(z)G(z)G_N(z)}{j\Omega + \Gamma_N(z)}dz} \tag{4.6}$$

where

$$\Gamma_P = \frac{R_{sp}}{P_0} - \int_L G_S(z)S_0(z)dz \tag{4.7}$$

$$\Gamma_N(z) = \frac{\partial R}{\partial N} + \frac{\partial G}{\partial N}S_0(z) \tag{4.8}$$

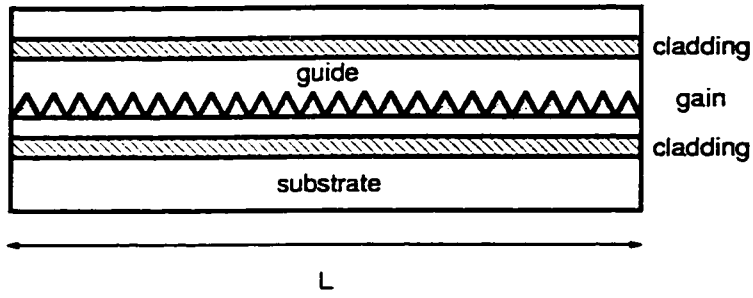

Fig. 1 Partly gain-coupled DFB laser structure with a periodic variation in thickness in the active layer [1].

are defined as the photon damping rate and local carrier damping rate, respectively. $G(N,z) = v_g g(N,z)\Gamma$ is the net rate of stimulated emission. $S_0(z)$ denotes the stationary photon distribution in the laser cavity according to expression (4.20) (see Appendix A). With this result, the dependency of the intensity modulation (AM) characteristics of the DFB laser on the longitudinal spatial hole burning and grating structure can be investigated systematically.

In DFB semiconductor lasers, the relaxation oscillation resonance occurs at a very high frequency. The study of the intensity modulation efficiency at high frequency can be made under the conditions $\Omega >> \Gamma_P$ and $\Omega >> \Gamma_N(z)$. In that case, expression (4.6) can be further reduced to:

$$\frac{P_1}{P_0} = \frac{\int_L G_N(z) J_1(z) dz}{\Omega_R^2 - \Omega^2} \tag{4.9}$$

where Ω_R is identified as the relaxation oscillation frequency of the DFB laser and can be written as follows:

$$\Omega_R = \sqrt{\int_L S_0(z) G(z) G_N(z) dz} \tag{4.10}$$

Expression (4.10) generalizes the conventional expression for the relaxation oscillation frequency which relates Ω_R to the total number of photons in the lasing mode,

the material gain and the differential gain [9, 10]. A result similar to the formula (4.10) has been obtained by the transfer matrix method in reference [11] (see formula (39) in reference [11]). The new formula shows that, in DFB lasers, the relaxation oscillation frequency Ω_R depends on the photon distribution $S_0(z)$, the gain $G(N, z)$ and the local effective differential gain $G_N(z)$, which are all spatially distributed and coupling-coefficient dependent. This property indicates that the intensity modulation bandwidth of DFB lasers has a strong dependency on the index and gain grating structures.

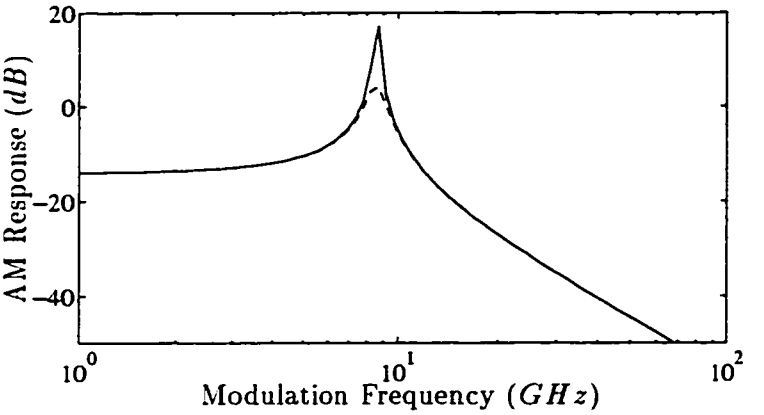

Fig. 2 Intensity modulation response of the gain-coupled DFB laser, where $\gamma = 2/\pi$, $|K|L = 1.2$ with $K_r < 0$ and $J = J_{th} + 2.5 \times 10^{27}$ cm^{-3} s^{-1} ($I = I_{th} + 15$ mA). Gain compression and spontaneous emission are not included. Other calculation parameters are listed in Table I. Solid line: produced from Eq. (4.9); dashed line: produced from Eq. (4.6).

Fig. 2 presents a comparison of the intensity modulation response for a gain-coupled DFB laser using formulae (4.6) and (4.9), respectively. A close agreement between the two curves demonstrates that both results give the relaxation oscillation resonance peak at the same place. This verifies that formula (4.10) can be used to determine the relaxation oscillation frequency of DFB lasers. With this result, we will discuss the improvement of the relaxation oscillation frequency in gain-coupled DFB lasers in the next section.

Table I Physical parameters used in the model

Bragg wavelength	λ_B	1.55 μm
group index of refraction	n_g	3.7
effective waveguide index of refraction	n_w	3.25
end-facet reflectivity	R_m	0
modal confinement factor	Γ	0
waveguide loss	α_0	20 cm^{-1}
differential gain	g_d	6×10^{-16} cm^2
logarithmic gain coefficient	g_c	1500 cm^{-1}
carrier density at transparency	N_0	1.5×10^{18} cm^{-3}
nonradiative recombination coefficient	A	1×10^{-9} s^{-1}
radiative recombination coefficient	B	1×10^{-10} cm^3s^{-1}
Auger recombination coefficient	C	1.3×10^{-28} cm^6s^{-1}

4.3 Gain-coupled DFB laser

In gain-coupled DFB lasers, the optical feedback is provided not only by the index grating, but also by the gain grating. Consider the first-order component in the Fourier series expansion of the index of refraction, the gain and the loss with a longitudinal dependency:

$$n(z) = n_0 + 2\gamma\Delta n \cos(2\beta_0 z + \theta_N) \tag{4.11}$$

$$g(z) = g_0(N)\,[1 + 2\gamma \cos(2\beta_0 z + \theta_G)] \tag{4.12}$$

$$\alpha(z) = \alpha_0 + 2\gamma\Delta\alpha \cos(2\beta_0 z + \theta_G) \tag{4.13}$$

where n_0 is the effective waveguide index. The constant coefficient γ is determined by the shape of the grating. θ_N and θ_G denote the reference phases for the index grating and gain grating, respectively. For instance, when the phase difference $\theta_N - \theta_G$ is 0 or π, we have either an inphase or antiphase grating. $g_0(N)$ represents the slowly varying part of the material gain. Δn and $\Delta\alpha$ denote the effective index and loss differences between active and passive regions.

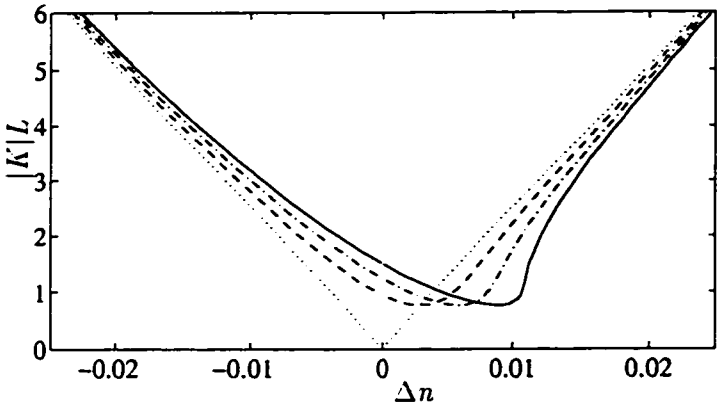

Fig. 3 Normalized coupling strength in the gain-coupled DFB laser with $\gamma = 1/2$. Solid line: $\alpha_M = 3$; dash-dotted line: $\alpha_M = 2$; dashed line: $\alpha_M = 1$; dotted line: index-coupled DFB laser, i.e. $K = k_0 \Delta n$. The curves in the regions where $\Delta n < 0$ and $\Delta n > 0$ correspond to the antiphase and inphase index and gain grating arrangements, respectively.

4.3.1 Complex coupling coefficient

Substituting the expressions (4.11-4.13) into the coupled-wave equations of Green's function analysis, the complex coupling coefficient of the gain-coupled DFB laser can be written as [12]:

$$K = K_r + jK_i = \left\{ \pm k_0 \Delta n + j\frac{\Gamma}{2}\left[(1 + j\alpha_M)g_0 - \Delta\alpha\right] \right\} \gamma \qquad (4.14)$$

where k_0 is the wave number in the vacuum. The signs + and − represent the inphase and antiphase configurations of the index and the gain gratings, respectively[1]. The real K_r and imaginary K_i parts of the coupling coefficient K measure the strength of the optical feedback provided by the index and gain gratings, respectively. Expression (4.14) indicates that, in gain-coupled DFB lasers, the real and imaginary parts of the coupling coefficient K are related to each other through the modal α_M-parameter. With the inphase and antiphase grating configurations, the normalized

[1]In this paper, we use + and − signs in formula (4.14) to represent the cases of inphase and antiphase (index and gain) grating, respectively. Moreover, we refer to the cases $K_r > 0$ and $K_r < 0$ as inphase and antiphase coupling, respectively.

coupling strength $|K|L$ can be negatively and positively enhanced, respectively. As depicted in Fig. 3, the coupling strength of the inphase grating is reduced (below the dotted line) due to the decrease of the grating index by the modal gain increase. Fig. 3 demonstrates that such a gain-induced coupling change is proportional to the value of linewidth enhancement factor α_M. The effect is more pronounced when the built-in index coupling is weak. Especially, when the built-in index coupling is weak enough, the gain-induced index change in the inphase gain-coupled DFB laser can even completely cancel out the index grating effect. In that case, the DFB laser becomes purely gain-coupled and lases exactly at the Bragg wavelength.

4.3.2 Threshold effects

Using the stationary solution of the carrier rate equations (4.1) and (4.2), a useful alternative expression to formula (4.10) can be written in terms of the drive current as:

$$\Omega_R = \sqrt{\int_L \left[J(z) - J_{th} - \frac{\partial R}{\partial N} \Delta N(z) \right] G_N(z) dz} \tag{4.15}$$

Expression (4.15) tells us that the relaxation oscillation frequency of the DFB laser is determined by the local effective differential gain $G_N(z)$, the threshold laser pumping rate J_{th} and the spatial hole burning in the laser. It also shows that spatial hole burning reduces the relaxation oscillation frequency of the DFB laser. A nonuniformly distributed injected current to counter the effects of spatial hole burning could be beneficial to obtain a higher relaxation oscillation frequency.

Because the threshold current of gain-coupled DFB lasers is determined by the normalized coupling strength $|K|L$ (see Fig. 4), such a gain-induced index decrease causes the laser to have a higher threshold current. On the contrary, an antiphase grating configuration gives an opposite contribution to the index change which amplifies the index grating effect and enhances the optical feedback (above the dotted

line). Hence, the laser threshold current can be reduced. According to the formula (4.15), such an effect on the lasing threshold will cause the relaxation oscillation frequency for the inphase and antiphase gain-coupled DFB laser to decrease and increase, respectively.

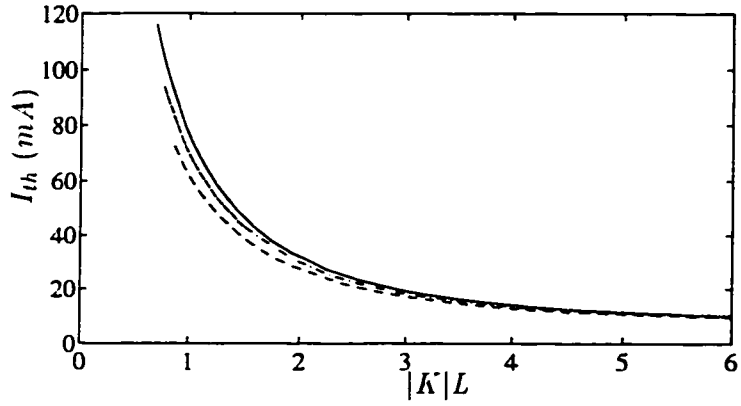

Fig. 4 Dependence of threshold current of gain-coupled DFB laser on the normalized coupling strength $|K|L$. The curves for the inphase coupling are coincided with those for the antiphase coupling. Solid line: $\gamma = 4/\pi^4$; dash-dotted line: $\gamma = 1/2$; dashed line: $\gamma = 2/\pi$.

A stronger coupling strength $|K|L$ reduces the threshold and generally produces a higher optical power, for the gain-coupled DFB lasers. Because the α_M-related index change in the gain-coupled DFB laser, the optical power increase in the antiphase gain-coupled DFB laser by the injected current enhances the coupling strength, which can result in a positive power feedback. This implies that the output of antiphase gain-coupled DFB laser is able to rise and fall relatively faster or have a higher relaxation oscillation frequency.

4.3.3 Standing wave effects

In gain-coupled DFB lasers, the spatially-distributed gain grating can interact with the standing wave pattern. This introduces a modification of the effective gain

and local effective differential gain expressions:

$$\frac{\partial g}{\partial N}C_2 Z_0^2(z) = \frac{\partial g_0}{\partial N}C_2\left[2Z_R Z_L + \gamma(Z_R^2 e^{j\theta_G} + Z_L^2 e^{-j\theta_G})\right] = \frac{\partial g_0}{\partial N}A(z) \quad (4.16)$$

$$g(N,z)|Z_0(z)|^2 = g_0(N)\left[|Z_R|^2 + |Z_L|^2 + 2\gamma Re(Z_R Z_L^* e^{j\theta_G})\right] = g_0(N)B(z) \quad (4.17)$$

where the rapidly oscillating terms have been neglected and θ_G gives the possible phase shift for the gain grating. Equations (4.16) and (4.17) show that the enhancements are proportional to the grating constant γ. Therefore, a gain grating with a larger Fourier coefficient γ, the rectangular-shaped grating for instance, will induce a stronger standing wave interaction and enhance the effective gain and local effective differential gain. Consequently, a higher relaxation oscillation frequency can be achieved. With a linear gain dependency on the carrier density

$$g_0(N) = \frac{\bar{g}_d[N(z) - N_0]}{1 + \varepsilon_N \Gamma[1 + 2\gamma\cos(2\beta_0 z + \theta_G)]S_0(z)} \quad (4.18)$$

where $\bar{g}_d$ denotes the average material differential gain, ε_N the gain compression coefficient and N_0 the carrier density for transparency, Fig. 5 presents the dependency of the relaxation oscillation frequency on the complex coupling coefficient in three gain-coupled DFB lasers with different grating shapes. Indeed, the rectangularly shaped gain grating gives the highest contribution to the relaxation oscillation frequency. Moreover, it shows that the antiphase coupling ($K_r < 0$) generally gives a higher relaxation oscillation frequency. The strongest enhancement of the relaxation oscillation frequency occurs around $|K|L = 1$. The symmetric projection on the complex KL plane reveals that the inphase and antiphase gain-coupled DFB lasers with the same coupling strength $|K|L$ gives the same value of $|K_r/K_i|$.

It is worth mentioning that the gain gratings considered in this paper are all full-depth-etched gratings which gives a larger Fourier coefficient γ, but reduces the average material differential gain $\bar{g}_d$ of the DFB laser by half. In order to obtain a higher resonance frequency, a higher average material differential gain $\bar{g}_d$ and a

larger grating structure constant γ are both desirable. A compromise will, therefore, produce an optimized etching depth of the gain grating in order to obtain an even higher relaxation oscillation frequency in the antiphase gain-coupled DFB laser.

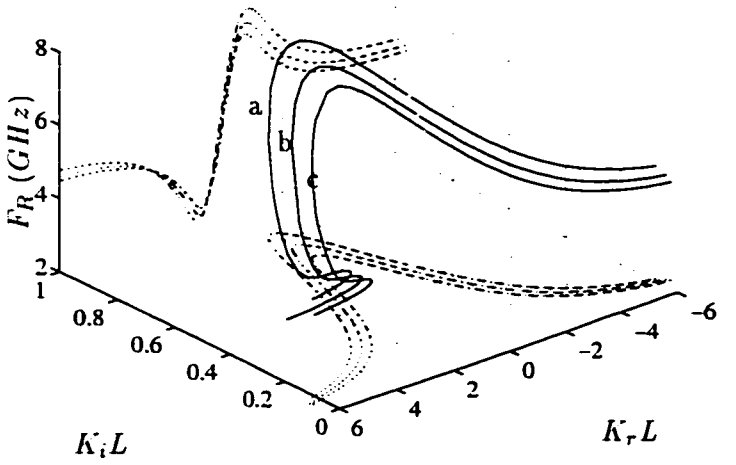

Fig. 5 Relaxation oscillation frequency $F_R = \Omega_R/2\pi$ of the gain-coupled DFB laser with linear gain material for $J = J_{th} + 2.5 \times 10^{27}$ $cm^{-3}s^{-1}$ ($I = I_{th} + 15$ mA). $L = 250$ μm and $\alpha_M = 3$. Gain compression is not included. Dashed lines are the projections of the solid lines on the corresponding planes. Curve (a): $\gamma = 2/\pi$ (rectangular shape); curve (b): $\gamma = 1/2$ (sinusoidal shape) and curve (c): $\gamma = 4/\pi^2$ (triangular shape).

4.3.4 Local effective differential gain

A detailed study indicates that the higher relaxation oscillation frequency in the antiphase gain-coupled DFB laser is caused by a stronger enhancement of the local effective differential gain. In particular, when the built-in index coupling is weak, the threshold current of the gain-coupled DFB laser becomes relatively high. The imaginary part of the complex coupling coefficient K and that of the Green's function $Z_0(z)$ can be comparable to their real parts. Then, the local effective differential gain $G_N(z)$ (see Appendix and (4.16)) and the relaxation oscillation

frequency can be enhanced through the factor $1 + j\alpha_M$. If the imaginary part of $A(z)$ in (4.16) is negative, a positive enhancement, proportional to the modal line width enhancement factor α_M, can contribute to the effective differential gain $G_N(z)$ and hence the relaxation oscillation frequency Ω_R.

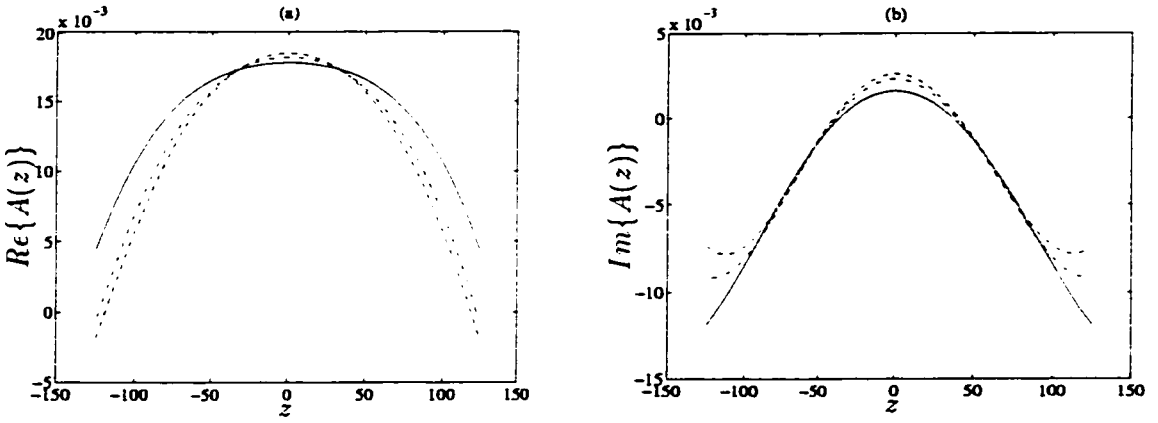

Fig. 6 Distribution of the function $A(z)$ in antiphase ($K_r/K_i < 0$) gain-coupled DFB laser, where $\alpha_M = 3$ and $\gamma = 1/2$. Solid line: $|K|L = 1$; dot-dashed line: $|K|L = 1.3$; dashed line: $|K|L = 1.5$; dotted line: $|K|L = 2$.

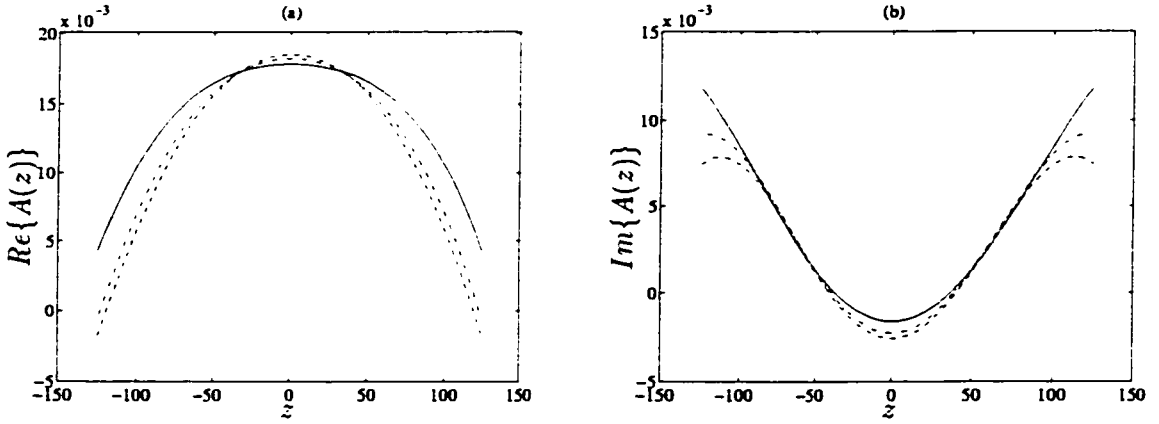

Fig. 7 Distribution of the function $A(z)$ in inphase ($K_r/K_i > 0$) gain-coupled DFB laser, where $\alpha_M = 3$ and $\gamma = 1/2$. Solid line: $|K|L = 1$; dot-dashed line: $|K|L = 1.3$; dashed line: $|K|L = 1.5$; dotted line: $|K|L = 2$.

Figs. 6 and 7 depict the fact that inphase and antiphase gain-couplings produce the same distributions for the real part of the function $A(z)$, but opposite distri-

butions for the imaginary part of $A(z)$. This difference makes the antiphase gain coupled DFB lasers have a much higher effective differential gain $G_N(z)$. However, as the built-in grating index difference Δn increases, the imaginary parts of the coupling coefficient K as well as that of the Green's function $Z_0(z)$ decrease rapidly such that the enhancement of the effective differential gain $G_N(z)$ and that of the relaxation oscillation frequency Ω_R approaches zero. Since such an enhancement is proportional to the α_M -parameter, Fig. 8 shows that a more significant effect can be observed in the gain-coupled DFB laser with a larger α_M value. Although a small α_M-parameter is usually desirable for semiconductor lasers in order to reduce the lasing linewidth, it has been reported that antiphase gain-coupling also reduces the effective linewidth enhancement factor α_{eff} of the gain-coupled DFB laser [3].

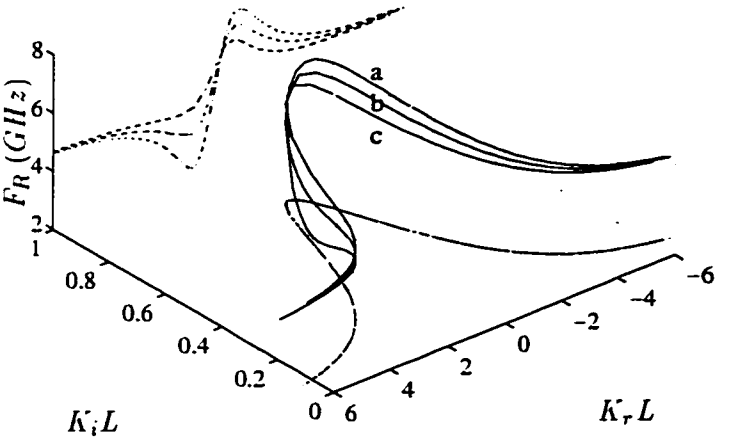

Fig. 8 Relaxation oscillation frequency $F_R = \Omega_R/2\pi$ of the gain-coupled DFB laser with a linear gain material at $J = J_{th} + 2.5 \times 10^{27}$ $cm^{-3}s^{-1}$ pumping rate level (i.e., $I = I_{th} + 15$ mA) where $\gamma = 1/2$ and $L = 250$ μm Gain compression is not included. Curve (a): $\alpha_M = 3$; curve (b): $\alpha_M = 2$; curve (c): $\alpha_M = 1$. Dashed lines are the projections of the solid lines on the corresponding planes.

4.3.5 Spatial hole burning

The study of the spatial hole burning also adds support to the trend of an increased relaxation oscillation frequency in the antiphase gain-coupled DFB laser. Eq. (4.17) indicates that the periodically varying modal gain can correlate with the standing wave pattern of the lasing light in the cavity. This shows that the spatial hole burning in the gain-coupled DFB laser does not only depend on the envelope of the lasing light intensity $|Z_R|^2+|Z_L|^2$, but also the interference with the gain grating (see Eq. (4.2)). As analyzed by Kudo in reference [3], the inphase and antiphase gain-couplings give a different optical feedback. As a consequence, carriers and photons interact differently in the inphase and antiphase gain-coupled DFB lasers. Figs. 9 and 10 depict that, although inphase and antiphase gain couplings with the same coupling strength $|K|L$ give the same distribution for the function $B(z)$ in expression (4.17), the resulting carrier distributions in the cavity for the antiphase gain-coupled DFB laser generally deviate much less from the threshold values. This implies that the laser can be driven more easily at high speed.

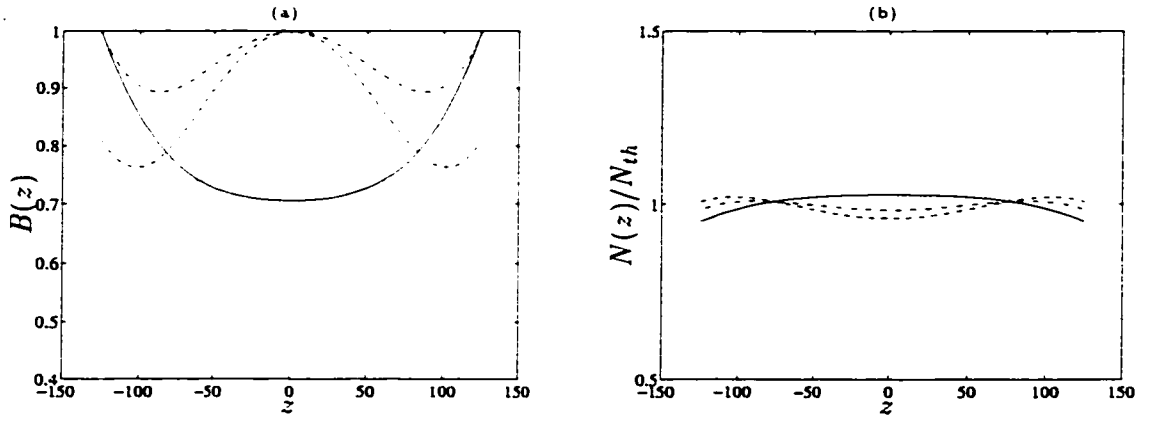

Fig. 9 (a) Distribution of the function B(z) in the antiphase ($K_r < 0$) gain-coupled DFB laser for various coupling coefficients. (b) Corresponding carrier distribution in the laser cavity, where $\alpha_M = 3$, $\gamma = 1/2$. Solid line: $|K|L = 1$; dot-dashed line: $|K|L = 1.3$; dashed line: $|K|L = 1.5$; dotted line: $|K|L = 2$.

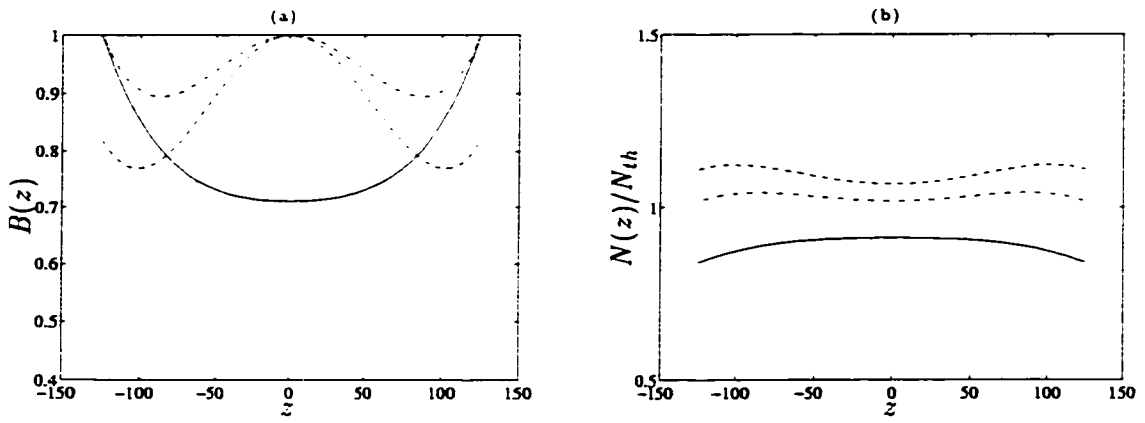

Fig. 10 (a) Distribution of the function B(z) in the inphase ($K_r > 0$) gain-coupled DFB laser for various coupling coefficients. (b) Corresponding carrier distribution in the laser cavity, where $\alpha_M = 3$, $\gamma = 1/2$. Solid line: $|K|L = 1$; dot-dashed line: $|K|L = 1.3$; dashed line: $|K|L = 1.5$; dotted line: $|K|L = 2$.

4.3.6 Gain compression effect

Gain compression influences the dynamic performance of semiconductor lasers very much [13]. In gain-coupled DFB lasers, the gain compression not only decreases the optical gain, but also reduces the optical feedback of the DFB grating. Moreover, similarly to the periodically varying material gain, the longitudinally distributed gain compression can interact with the standing wave pattern of the lasing light also. The effect of nonlinear gain compression on the relaxation oscillation frequency of gain-coupled DFB lasers can be more profound. Previously, Figs. 9 and 10 have shown that the inphase and antiphase gain-coupled DFB lasers with the same coupling strength $|K|L$ give the same distribution of function $B(z)$. According to the formulae (4.18) and (4.20), for the same coupling strength $|K|L$, the laser with a higher photon level P_0 will suffer more gain compression. The results of Fig. 11-(a) show that, except for the region $|K_r/K_i| < 1.4$ (which corresponds to $|K|L < 1.2$), antiphase coupling generally produces a higher photon level P_0. Hence, gain compression effects on the relaxation oscillation frequency are stronger

in the antiphase gain-coupled DFB lasers. Nevertheless, Fig. 11-(b) shows that antiphase coupling still gives a higher relaxation oscillation frequency for the gain-coupled DFB laser due to the enhanced local effective differential gain. Therefore, we assume that antiphase coupling in gain-coupled DFB lasers contributes the more to the enhancement of the relaxation oscillation frequency.

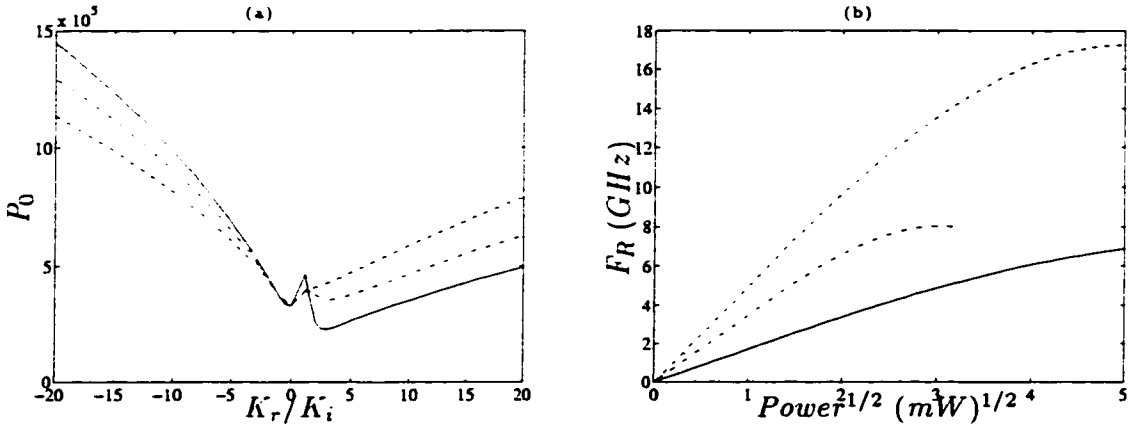

Fig. 11 (a) Total photon number of the lasing mode P_0 in the gain-coupled DFB laser with logarithmic gain material, where $\gamma = 2/\pi$ and $L = 600$ μm. Solid line: $\alpha_M = 3$; dot-dashed line: $\alpha_M = 2$; dashed line: $\alpha_M = 1$. (b) Gain compression effect on the relaxation oscillation frequency of gain-coupled DFB lasers with logarithmic gain material, where $\alpha_M = 3$, $\gamma = 2/\pi$, $L = 600$ μm and $\varepsilon_N = 5 \times 10^{-17}$ cm^{-3}. Solid line: $|K|L = 1$ with $K_r > 0$; dot-dashed line: $|K|L = 2$ with $K_r > 0$; dashed line: $|K|L = 1$ with $K_r < 0$; dotted line: $|K|L = 2$ with $K_r < 0$.

4.3.7 Gain saturation effect

In the above analysis, only a simple linear gain expression (4.18) was considered. Linear gain dependency on carrier density is still used in most existing DFB laser semiconductor modelling work. According to such a gain model, the material differential gain is constant which makes the local effective differential gain independent of the carrier density. Recent work on strained multiple quantum well (MQW)

lasers indicates that material gain in those materials can saturate rapidly at high carrier density levels [14]. This gain saturation effect is characteristic of quantum well lasers as compared to bulk semiconductor lasers and is essentially caused by the step-like density of states in the quantum well active layer [15]. Using strained MQW material in gain-coupled DFB lasers may result in a different effect on the local effective differential gain. Hence, the dependency of the relaxation oscillation frequency on the complex coupling coefficient may be changed.

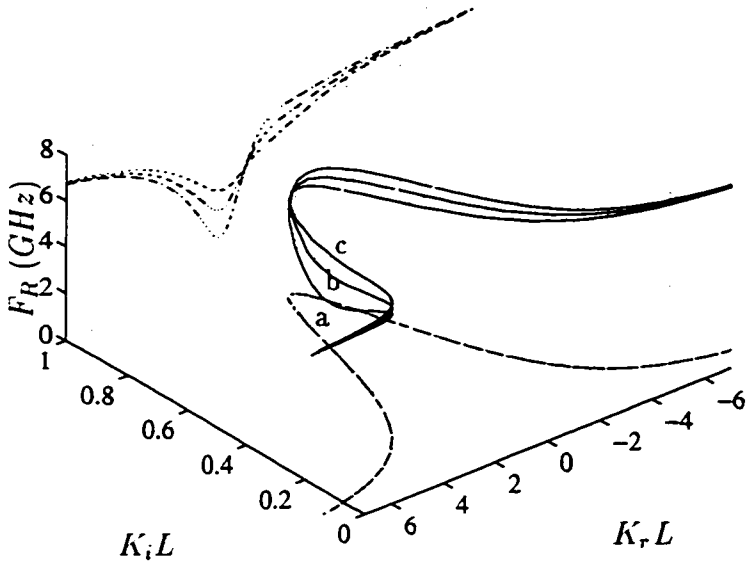

Fig. 12 Relaxation oscillation frequency $F_R = \Omega_R/2\pi$ of a gain-coupled DFB laser with logarithmic gain material at $J = J_{th} + 3.33 \times 10^{27}$ cm^{-3}s^{-1} pumping rate level (i.e. $I = I_{th} + 20$ mA), where $\gamma = \pi/2$ and $L = 250$ μm. The gain compression effect is not included. Curve (a): $\alpha_M = 3$; curve (b): $\alpha_M = 2$; curve (c): $\alpha_M = 1$. Dashed lines are the projections of the solid lines on the correspond ing planes.

In order to consider the gain saturation effect, a more realistic material gain dependency on carrier density is assumed:

$$g_0(N) = \frac{\bar{g}_c ln[N(z)/N_0]}{1 + \varepsilon_N \Gamma[1 + 2\gamma cos(2\beta_0 z + \theta_G)]S_0(z)} \tag{4.19}$$

where $\bar{g}_c$ is the average gain coefficient. Such a logarithmic gain model has been used previously and verified experimentally and theoretically [15, 16]. In this model, the

material differential gain dg/dN is determined by $g_c/N(z)$ which is dependent of carrier density.

The results in Fig. 12 show that, with the logarithmic gain material, the enhancement of relaxation oscillation frequency in the region around $|K|L = 1$ by the antiphase-coupling is absent as opposed to Fig. 8. Instead, a higher relaxation oscillation frequency occurs at a larger K_rL where the material differential gain dg/dN is higher. Moreover, the α_M-parameter dependency in the low K_rL region is also partly suppressed because of the lower material differential gain.

4.3.8 Cavity length effect

In the gain-coupled DFB laser with strained MQW material, operation at a lower carrier density is preferred in order to take advantage of the quantum size effects and utilize the higher differential gain. Our previous analysis has indicated that the maximum enhancement of local effective differential gain by antiphase coupling is obtained in the region around $|K|L = 1$ where the imaginary part of the complex coupling coefficient K is comparable to its real part. To obtain the same coupling strength $|K|L$, the gain-coupled DFB laser with a shorter cavity length requires a relatively larger coupling coefficient $|K|$. In other words, gain and carrier density are higher in the gain-coupled DFB laser with a shorter cavity length, which makes the gain saturation effects become more pronounced. Therefore, the local effective differential gain enhanced by antiphase coupling is suppressed by the low material differential gain. In order to reduce gain saturation in the gain-coupled DFB laser, choosing a longer cavity length appears to be advantageous. A long cavity can make the carrier density in the laser become lower and, at the same time, allow the use of a weaker index grating coupling in order to maintain the coupling strength $|K|L$ around 1. With such a choice, a higher material differential gain can be obtained in the gain-coupled DFB laser with a large imaginary part of coupling coefficient

K_i. With a combination of the contributions from the antiphase coupling and the high material differential gain, Fig. 13 shows that a higher relaxation oscillation frequency can be reached by a long cavity antiphase gain-coupled DFB laser with strained MQW material.

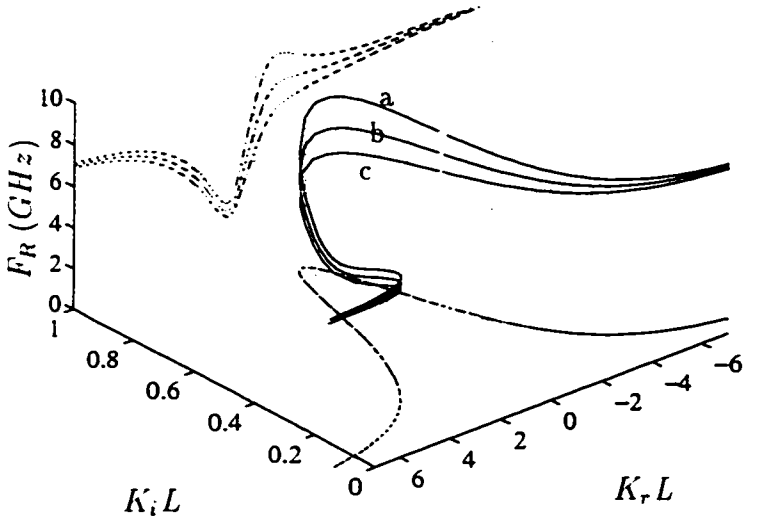

Fig. 13 Relaxation oscillation frequency $F_R = \Omega_R/2\pi$ of the gain-coupled DFB laser with a logarithmic gain material at $J = J_{th} + 3.5 \times 10^{27}\ \mathrm{cm^{-3}s^{-1}}$ pumping rate level, where $\alpha_M = 3$ and $\gamma = \pi/2$. The gain compression effect is not included. Dashed lines are the projections of the solid lines on the corresponding planes. Curve (a): $L = 600\ \mu$m; curve (b): $L = 350\ \mu$m; curve (c): $L = 250\ \mu$m.

Increasing device length has been shown to be a means of compensating for the gain saturation effect on the relaxation oscillation frequency. For nonlinear gain compression, length dependency is also important. To separate out the gain saturation effects , we consider a linear gain material in the calculations of Fig. 14-(a). The results show that gain compression influences the relaxation oscillation frequency more in the long cavity gain-coupled DFB laser because more optical feedback is changed. This gives a length dependency opposite to that of the gain saturation effect on the relaxation oscillation frequency in gain-coupled DFB lasers. As a consequence, when both gain saturation and gain compression effects are included simultaneously, an

optimum cavity length can be found for the highest relaxation oscillation frequency in antiphase gain-coupled DFB lasers (see Fig. 14-(b)).

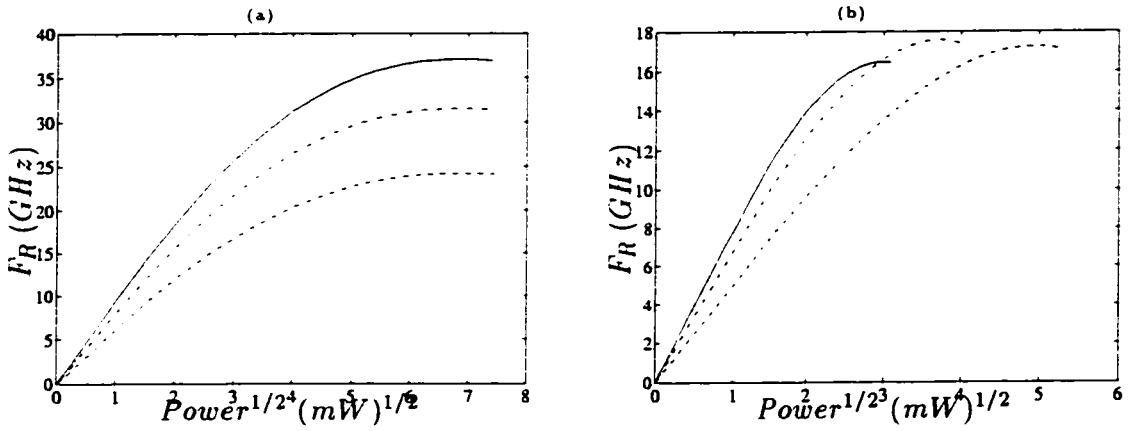

Fig. 14 (a) Length dependency of the gain compression effect on the relaxation oscillation frequency $F_R = \Omega_R/2\pi$ in antiphase gain-coupled DFB laser with a linear gain material, where $|K|L = 1$, $\alpha_M = 2$, $\varepsilon_N = 5 \times 10^{-17}$ cm^{-3} and $\gamma = 2/\pi$. (b) Length dependency of the gain compression effect on the relaxation oscillation frequency $F_R = \Omega_R/2\pi$ in antiphase gain-coupled DFB laser with logarithmic gain material, where $|K|L = 1$, $\alpha_M = 3$, $\varepsilon_N = 5 \times 10^{-17}$ cm^{-3} and $\gamma = 2/\pi$. Solid line: $L = 250$ μm; dot-dashed line: $L = 350$ μm; dashed line: $L = 600$ μm.

4.4 Conclusion

Using the spatially dependent rate equations based on the Green's function analysis, we have presented a systematic investigation on the relaxation oscillation frequency of gain-coupled DFB lasers. This analysis has taken into account the light intensity distribution, spatial hole burning, gain saturation and gain compression effects. An explicit expression of the relaxation oscillation frequency for DFB laser including those spatial features has also been derived. Our results have generalized the conventional analysis and shown that the relaxation oscillation frequency

of gain-coupled DFB laser is determined by the photon distribution, the local effective differential gain and the distributed material gain. As a consequence, the longitudinal spatial features have a great influence on the modulation bandwidth of gain-coupled DFB lasers. Detailed studies reveal that antiphase gain-coupling not only reduces the lasing threshold current and carrier density deviation from the threshold value, but also enhances the coupling strength as well as the local effective differential gain. All those properties contribute positively to enhance the relaxation oscillation frequency of the gain-coupled DFB laser.

We have found that the significant enhancement on the relaxation oscillation frequency of antiphase gain-coupled DFB laser is due to the interaction between the gain grating and the standing wave pattern of the photon distribution in the cavity. Such a property is unique to the gain-coupled DFB lasers and depends on the value of modal linewidth enhancement factor α_M strongly. With the antiphase coupling structure in the gain-coupled DFB laser, an enhancement proportional to the material α_M-parameter can affect the local effective differential gain and hence the relaxation oscillation frequency Ω_R.

The effects of gain saturation and gain compression on the relaxation oscillation frequency have also been studied. In strained MQW gain-coupled DFB lasers, the enhancement of local effective differential gain by the antiphase coupling may be suppressed by the carrier-density-dependent material differential gain. To overcome that problem, choosing a long cavity length to bring down the overall carrier density level in the gain-coupled DFB laser seems preferred. With a trade-off, an optimum cavity length can be found in the case of an antiphase gain-coupled DFB laser with strained MQW material in order to obtain the highest relaxation oscillation frequency.

APPENDIX

A. The Green's Function Formalism

Within the approximation of first-order perturbation, we neglect the influences of carrier nonuniformity on the optical field distribution. If the change of shape of the photon distribution above threshold is ignored, we can express the photon distribution as:

$$S(z,t) = C_1|Z_0(z)|^2 P(t) \tag{4.20}$$

where C_1 is a normalization constant (see below). The spatial weight functions $G_X(z)$ $(X = N, S)$ can be regarded as the local effective modal differential gains with respect to the changes in carrier and photon densities, respectively. They can be written in the following form [7]:

$$G_X(z) = v_g \Gamma Re\left[C_2(1 + j\alpha_M)Z_0^2(z)\frac{\partial g}{\partial X}\right] \tag{4.21}$$

where C_2 is an integration constant related to the Green's function (see below). Γ is the transverse modal confinement factor. α_M is the modal linewidth enhancement factor, which is defined by the ratio of the changes of the real and imaginary parts of the modal index. $g(N,z)$ corresponds to the distributed material gain of the DFB laser. The spontaneous emission rate coupled into the lasing mode is given by [7]:

$$R_{sp} = C_1^{-1}|C_2|^2 n_{sp} v_g \Gamma \int_L g(N,z)|Z_0(z)|^2 dz \tag{4.22}$$

where v_g is the group velocity and n_{sp} is the spontaneous emission factor.

The function $Z_0(z)$ in the above formulae is the Green's function which is related to the optical field distribution along the laser cavity. It usually consists of right and left travelling waves $Z_R(z)$ and $Z_L(z)$ as follows:

$$Z_0(z) = Z_R(z)e^{-j\beta_0 z} + Z_L(z)e^{j\beta_0 z} \tag{4.23}$$

where $\beta_0 = \frac{\pi}{\Lambda}$ is the Bragg wavenumber of the distributed feedback grating. There is a number of ways of constructing the Green's function. One simple and physically meaningful approach is by solving the coupled-wave equations [12]. A dispersion relation for the lasing mode can then be derived. Because of the complex coupling coefficient of the gain-coupled DFB laser, the eigenvalues of the dispersion equation are usually complex. They can be obtained numerically using a nonlinear optimization algorithm to search for the local minima in the complex plane.

B. Normalization Constants

Two normalization constants C_1 and C_2 are frequently used in the Green's function analysis:

$$C_1^{-1} = A_c \int_L |Z_0(z)|^2 dz \tag{4.24}$$

$$C_2^{-1} = \int_L Z_0^2(z) dz \tag{4.25}$$

where A_c denotes the transverse cross-section area of the active region and C_2 is complex. If we neglect the rapidly oscillating terms in the integrations, they can also be expressed as follows:

$$C_1^{-1} = A_c \int_L \left[|Z_R(z)|^2 + |Z_L(z)|^2 \right] dz \tag{4.26}$$

$$C_2^{-1} = 2 \int_L Z_R(z) Z_L(z) dz \tag{4.27}$$

REFERENCES

[1] G. P. Li, T. Makino, R. Moore, N. Puetz, K. Leong and H. Lu, "Partly gain-coupled 1.55μm strain-layer multi-quantum-well DFB lasers", *IEEE J. Quantum Electron.*, Vol. 29, pp. 1736–1742, 1993.

[2] W. T. Tsang, F. S Choa, M. C. Wu, Y. K. Chen, R. A. Logan, S. N. G. Chu and A. M. Sergent, "Semiconductor distributed feedback laser with quantum well or superlattice gratings for index or gain-coupled optical feedback", *Appl. Phys. Lett.*, Vol. 60, pp . 2580-2582, 1992.

[3] K. Kudo, S. Arai and J. I. Shim, "Linewidth reduction of DSM lasers due to effects of composite cavity and distributed reflectors", *IEEE J. Quantum Electron.*, Vol. QE-29, pp. 1769–1781, 1993.

[4] L. M. Zhang, J. E. Carroll and C. Tsang, "Dynamic response of the gain-coupled DFB laser", *IEEE J. Quantum Electron.*, Vol. QE-29, pp. 1722–1727, 1993.

[5] L. M. Zhang and J. E. Carroll, "Enhanced AM and FM modulation response of complex coupled DFB lasers", *IEEE Photon. Techno Lett.*, Vol. 5, pp. 506–508, 1993.

[6] D. Novak and A. J. Lowery, "Up to 15 dB improvement in second harmonic distortion in complex-coupled DFB semiconductor lasers", *Electron. Lett.*, Vol. 29, pp. 1954–1956, 1993.

[7] B. Tromborg, H. Olesen and X. Pan, "Theory of linewidth for multielectrode laser diodes with spatial distributed noise sources", *IEEE J. Quantum Electron.*, Vol. QE-27, pp. 178–192, 1991.

[8] T. Makino, "Effective-index matrix analysis of distributed feedback semiconductor lasers", *IEEE J. Quantum Electron.*, Vol. QE-28, pp. 434–440, 1992.

[9] G. P. Agrawal and N. K. Dutta, *Long-Wavelength Semiconductor Lasers.* Van Nostrand Reinhold, New York, pp. 246, 1986.

[10] K. Uomi, T. Tsuchiya, H. Nakano, M. Aoki, M. Suzuki and N. Chinone, "High-speed and ultralow-chirp 1.55μm multi-quantum well $\lambda/4$-shifted DFB lasers", *IEEE J. Quantum Electron.*, Vol. QE-27, pp. 408–414, 1992.

[11] T. Makino, H. Lu and G. P. Li, "Transfer-matrix dynamic model of partly gain-coupled 1.55μm DFB lasers with a strained-layer MQW active grating", *IEEE J. Quantum Electron.*, Vol. QE-30, Nov., 1994.

[12] H. Kogelnik and C. V. Shank, "Coupled-wave theory of distributed feedback lasers", *J. Appl. Phys.*, Vol. 43, pp. 2327–2335, 1972.

[13] G. P. Agrawal, "Modulation bandwidth of high-power single-mode semiconductor lasers: effect of intraband gain saturation", *Appl. Phys. Lett.*, Vol. 57, pp. 1–3, 1990.

[14] C. H. Lin and Y. H. Lo, "Empirical formulas for design and optimization of 1.55μm InGaAs/InGaAsP strained-quantum well lasers", *IEEE Photon. Technol. Lett.*, Vol. 5, pp. 288–290, 1993.

[15] T. Makino, "Analytical formulas for the optical gain of quantum well lasers", Submitted to IEEE J. Quantum Electron..

[16] J. Hong, W. P. Huang and T. Makino, "Effect of linear gain saturation on small-signal dynamics of MQW DFB lasers", *IEEE Photon. Technol. Lett.*, Vol. 5, pp. 1373–1376, 1993.

CHAPTER 5

Harmonic Distortion in Gain-Coupled DFB Lasers

With their multigigahertz bandwidth capability, gain-coupled DFB lasers are particularly interesting as light sources in analog optical communications systems. For such applications, the characteristics of the nonlinear harmonic and intermodulation distortions are fundamental quantities of concern. Since spatial hole burning and nonlinear gain compression effects are power-dependent, spatial nonuniformities in DFB lasers can have strong effects on the laser harmonic distortion. Therefore, a systematic investigation of their interdependencies is necessary.

Complex coupling in gain-coupled DFB lasers provides additional possibilities for the improvement of laser harmonic distortion. Moreover, inphase and antiphase gain couplings provide different conditions for the carrier and photon interaction within the laser. With the carrier-dependent feedback mechanism, gain-coupled DFB lasers have many unique features. In order to study the various underlying physical phenomena, it is required to use spatially dependent rate equations. The purpose of this chapter is, therefore, to reach an in-depth understanding of the gain-coupling effect on harmonic distortion in DFB lasers.

Published in Intl. J. Optoelectron., vol. 10, pp. 139-149, 1995

Second-Order Harmonic Distortion in AM Response of Gain-Coupled DFB Lasers

Jianyao Chen, Roman Maciejko, and Toshihiko Makino

Abstract

Expressions for the second-order harmonic distortion in distributed feedback (DFB) semiconductor lasers are derived, in closed form, from the spatially-dependent rate equations based on the Green's function analysis. Salient features of the DFB lasers such as the longitudinal spatial hole burning, distributed spontaneous emission and nonlinear gain compression are all included into the formulation rigorously. By performing an extended small signal analysis, the effects of those nonlinearities and relaxation oscillation in DFB lasers are analyzed in an explicit way. Numerical results on the gain-coupled DFB lasers show that spatial hole burning, nonlinear gain compression and relaxation oscillation can influence the second-order harmonic (SH) distortion significantly.

J. Chen, and R. Maciejko are with the Optoelectronics Laboratory, Department of Engineering Physics, École Polytechnique, P. O. Box 6079, Station "Centre-ville", Montréal, Québec Canada H3C 3A7

T. Makino is with Northern Telecom (Nortel), P. O. Box 3511, Station C, Nepean, Ontario, Canada K1Y 4H7

5.1 Introduction

The dynamic single-mode distributed feedback (DFB) semiconductor laser is presently one of the most important light sources for the optical communications. Over the past few years, there has been much interest in using DFB lasers in analog 'subcarrier' modulation of light wave transmission system because of their multi-gigahertz bandwidth capabilities [1]. For such applications, the laser light intensity is required to be a linear function of the drive current. The characteristics of nonlinearly generated harmonic and intermodulation distortions obviously become quantities of concern. Traditionally, the conventional rate equations were applied to predict the characteristics of harmonic distortion in semiconductor lasers. With such an approach, simple yet insightful analytical expressions can be obtained to help identifying the origin of nonlinearities and assess their impact [2, 3]. In a DFB laser, however, the longitudinal characteristics such as the complex coupling coefficients, the grating phase shift, the facet reflectivity and the optical field nonuniformity have significant effects on the laser properties. Such a spatially-independent rate equation treatment becomes, therefore, inadequate. To overcome those problems, a number of rigorous studies have been undertaken, which includes G. Morthier et al.'s travelling wave analysis of second-harmonic (SH) distortion in $\lambda/4$ phase-shifted index-coupled DFB lasers [4], D. Novak and A. J. Lowery's transmission-line modeling of harmonic distortion in the gain-coupled DFB lasers [5], and T. Okuda et al.'s transfer matrix method for the intermodulation distortion in the index-coupled DFB laser [6]. In those papers, detailed calculations of the harmonic distortion in the AM response of DFB lasers were carried out and various significant nonlinear effects were discovered. However, since the methods were predominantly numerical, the identification of the various underlying physical effects on the harmonic distortion was less obvious.

The Green's function method, as initially proposed by Henry to study spon-

taneous emission noise in an open resonator laser [7], is an effective and accurate approach for the inclusion of longitudinal inhomogeneities in DFB semiconductor lasers. Using the Green's function, the longitudinal inhomogeneities are taken into account as distributed excitation sources coupled into the lasing mode. With such an approach, the characteristics of the laser can be expressed analytically in terms of the Wronskian determinant and its functional derivatives. Because of its analytical features, this technique has been successfully applied to analyze the dynamical and noise properties of various DFB laser structures [8, 9]. Combined with an efficient transfer matrix method, the Green's function approach can also be extended to treat the DFB lasers with a large index corrugation and is capable of handling lateral waveguiding simultaneously [10, 11]. The spatially dependent spontaneous emission noise, nonlinear gain compression and longitudinal spatial hole burning effects are all treated in this approach.

The gain-coupled DFB lasers have many attractive properties such as high side-mode suppression ratio and high modulation speed [12, 13]. The application of in-phase and antiphase gain couplings also add more flexibility to laser design [5, 14, 15]. In such DFB lasers, however, the optical feedback from the complex coupling structure can change with the carrier density which is nonuniform longitudinally above the lasing threshold. Moreover, the periodically varied modal gain can also interact with the standing wave pattern of the lasing field in the cavity. The spatial effects in the gain-coupled DFB lasers have a more profound influence on their dynamic properties. Applying the Green's function method, this paper presents a systematical analysis of the second-harmonic distortion in gain-coupled DFB semiconductor lasers. Several spatially-dependent nonlinear effects such as longitudinal spatial hole burning, local carrier damping rate, gain compression and spontaneous emission are consequently included into the model. By performing the extended small signal analysis, simple, yet insightful, expressions are obtained and the second harmonic

distortions at low and high frequencies are discussed in an explicit manner. Furthermore, the effects of inphase and antiphase gain couplings are also discussed in detail.

5.2 Rate equations

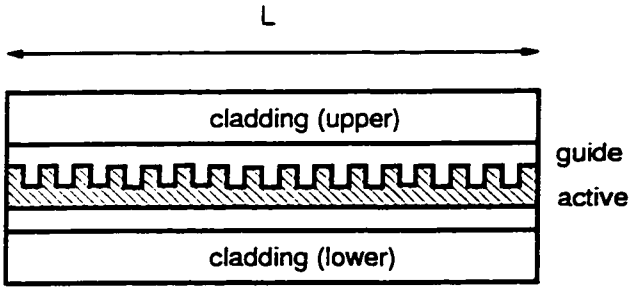

Fig. 1 Typical DFB laser structure.

Fig. 1 depicts a typical DFB laser in which the grating corrugation may be arbitrary and the injected current may be nonuniformly distributed. This can be generalized to include the cases of index or gain coupled gratings and with or without phase-shifted structures in the cavity. To simplify the analysis, we assume that the light waves propagate along the z axis and that the laser operates in the single-mode condition. The scalar wave equation for the optical field inside the DFB cavity can be written as

$$\frac{d^2E_\omega(z)}{dz^2} + k^2(z)E_\omega(z) = f_\omega(z) \tag{5.1}$$

where $k(z)$ is the complex wavenumber including the periodic variation of the Bragg grating. $f_\omega(z)$ gives the basic Langevin force representing the spontaneous emission.

According to the Green's function analysis, the solution of the wave equation (5.1) can be written in the following form [7, 8]

$$E_\omega(z) = \frac{1}{W}\int_L g(z,z')f_\omega(z')dz' \tag{5.2}$$

where $W(\omega, N, S)$ is the Wronskian of the solutions of the homogeneous wave equation (i.e. equation (5.1) with $f_\omega(z) = 0$), which is independent of z but may be considered as a complex functional of the wavenumber $k(z)$. $g(z, z')$ is a Green's function for the DFB structure.

The operating point of DFB laser corresponds to a zero point of the Wronskian, i.e., $W(\omega_0, N_0(z), S_0(z)) = 0$. In order to consider the influence of the perturbation from the dynamic modulation on the carrier and the photon densities, we expand the Wronskian to the first order around the stationary solution. From this, a set of rate equations determining the total number of photons P in the lasing mode and the phase fluctuation of the lasing light Φ can be obtained as [8]

$$\frac{dP}{dt} = P(t)\int_L [G_{Nr}(z)\Delta N(z,t) + G_{Sr}(z)\Delta S(z,t)]\,dz + R_{sp} \tag{5.3}$$

$$\frac{d\Phi}{dt} = \frac{1}{2}\int_L [G_{Ni}(z)\Delta N(z,t) + G_{Si}(z)\Delta S(z,t)]\,dz \tag{5.4}$$

where $\Delta N(z,t)$ and $\Delta S(z,t)$ are the local deviations of the carrier and photon densities from the steady-state values, $N_0(z)$ and $S_0(z)$. The spatial weight functions $G_N(z)$ and $G_S(z)$ can be regarded as the local effective modal differential gain with respect to changes in carrier and photon densities. They are usually complex and can be determined from

$$G_X(z) = -j2\frac{\delta W}{\delta k(z)}\frac{\partial k(z)}{\partial X}\left[\frac{\partial W}{\partial \omega}\right]^{-1} = (1 + j\alpha_M)\frac{Z_0^2(z)\dfrac{\partial G}{\partial X}}{\displaystyle\int_L Z_0^2(z)dz} \qquad X = N, S \tag{5.5}$$

where α_M denotes the material linewidth enhancement factor. The subscripts r and i used in the equations (5.3) and (5.4) represent the real and imaginary parts, respectively. $G(z, N) = v_g\Gamma(z)g(z, N)$ is the net rate of stimulated emission. In order to include nonlinear gain-compression in DFB lasers, we use the following gain expression:

$$g_0(z, N) = g_d[N(z) - N_t]\{1 - \varepsilon_N\Gamma_0[1 + 2\gamma\cos(2\beta_0 z + \theta_G)]S(z)\} \tag{5.6}$$

where g_d, N_t and ε_N are the differential gain, the carrier density at transparency and the coefficient of gain compression. Finally, the term R_{sp} gives the spontaneous emission rate coupled into the lasing mode and can be written as [7, 8]

$$R_{sp} = n_{sp} \frac{\int_L |Z_0(z)|^2 dz \int_L G(z,N)|Z_0(z)|^2 dz}{\left| \int_L Z_0^2(z) dz \right|^2} \tag{5.7}$$

where n_{sp} is the population inversion factor. The function $Z_0(z)$ is the solution of the longitudinal scalar wave equation for the DFB laser.

In order to complete the dynamical modelling of the DFB semiconductor laser, one also needs to include the spatially dependent carrier rate equation as follows:

$$\frac{\partial N}{\partial t} = J(z,t) - R(z,N) - G(z,N)S(z,t) \tag{5.8}$$

where $J(z,t)$ is the laser pumping rate, $R(z,N)$ is the spontaneous carrier recombination rate which can be given in the usually way as

$$R(z,N) = AN(z,t) + BN^2(z,t) + CN^3(z,t) \tag{5.9}$$

where A, B and C correspond to nonradiative, radiative and Auger recombination coefficients, respectively. As a consequence of the Green's function method [9], the photon density distribution $S(z,t)$ can be written as

$$S(z,t) = \frac{|Z_0(z)|^2}{A_c \int_L |Z_0(z)|^2 dz} P(t) \tag{5.10}$$

where A_c denotes the transverse cross-sectional area of the active region.

The above equations are the basis of our formalism for the dynamic analysis of the DFB laser properties. The analytical and spatially dependent form allows us to study the effects of longitudinal spatial hole burning, distributed gain compression and spontaneous emission in DFB lasers in an illustrative and consistent manner. However, one should bear in mind that such a Green's function approach actually

assumes that the temporal and spatial dependency of the optical field is separable as indicated in equation (5.10). That implies that the distribution of the lasing modal field is independent of the photon round trip time in the DFB laser cavity and that the laser dynamics due to modulation can be described by the amplitude of the lasing mode alone. One will, therefore, expect the analysis to be acceptable if the photon round trip time is much shorter than the time period of the modulation. For DFB lasers with a typical 250 μm cavity length, such an analysis should be valid for a modulation of up to 150 GHz. That is obviously beyond the modulation bandwidth of current DFB lasers but not for long, considering ongoing progress.

5.3 Stationary solutions

The application of the above spatially-dependent rate equations requires the stationary solutions of the carrier density $N_0(z)$ and the photon density $S_0(z)$ at the operating point of the DFB laser. Because of the spatial hole burning, optical feedback by the DFB grating varies longitudinally and the solution of photon distribution is no longer available analytically above the lasing threshold. The self-consistent solution $S_0(z)$ with the carrier distribution $N_0(z)$ requires the solution of the longitudinal wave equation (5.1) and the carrier rate equation (5.8) simultaneously. For gain-coupled DFB lasers, the longitudinal dependencies of the effective index of refraction $n(z)$ and the transverse modal confinement factor $\Gamma(z)$ are given by

$$n(z) = n_0 + 2\gamma\Delta n cos(2\beta_0 z + \theta_N) \tag{5.11}$$

$$\Gamma(z) = \Gamma_0[1 + 2\gamma cos(2\beta_0 z + \theta_G)] \tag{5.12}$$

where $\beta_0 = \frac{\pi}{\Lambda}$ is the Bragg wavenumber of the distributed feedback grating and n_0 is the average value of the effective waveguide index. The Fourier constant γ

is determined by the shape of the grating. θ_N and θ_G denote the reference phases for the index grating and gain grating, respectively. For instance, when the phase difference $\theta_N - \theta_G$ is 0 or π, we have either an inphase or antiphase grating.

The general solution of the inhomogeneous wave equation (5.1) is usually assumed to consist of right and left propagating waves $Z_R(z)$ and $Z_L(z)$:

$$Z_0(z) = Z_R(z)e^{-j\beta_0 z} + Z_L(z)e^{j\beta_0 z} \tag{5.13}$$

At the two laser facets, they satisfy the boundary conditions

$$Z_R(0) = r_L Z_L(0) \tag{5.14}$$

$$Z_L(L) = r_R Z_R(L) \tag{5.15}$$

where r_L and r_R are the facet reflectivities at left and right sides, respectively.

Substituting equations (5.11), (5.6) and (5.13) into the wave equation (5.1) and using the slowly-varying envelope approximation, we get the usual coupled-wave equations:

$$\frac{dZ_R}{dz} + j(\beta - \beta_0)Z_R = -jKe^{-j\theta_G}Z_L \tag{5.16}$$

$$\frac{dZ_L}{dz} - j(\beta - \beta_0)Z_L = jKe^{j\theta_G}Z_R \tag{5.17}$$

where the complex coupling coefficient K is given by

$$K = K_r + jK_i = \left\{\pm k_0\Delta n + j\frac{\Gamma_0}{2}[(1 + j\alpha_M)g_0 - \alpha_0]\right\}\gamma \tag{5.18}$$

where k_0 is the wave number in the vacuum and α denotes the waveguide loss in the active region. The signs + and − represent the inphase and antiphase configurations of the index and the gain gratings, respectively. The real part K_r and imaginary K_i part of the coupling coefficient K measure the strength of feedback provided by the index and gain gratings, respectively[1].

[1]We refer to the the cases $K_r > 0$ and $K_r < 0$ as inphase and antiphase optical coupling, respectively.

Above the lasing threshold, spatial hole burning occurs in DFB lasers due to the interaction between the carriers and the photons. Equations (5.16) and (5.17) need to be solved self-consistently with the carrier rate equation at steady-state, i.e.

$$J_0(z) = R[z, N_0(z)] + G[z, N_0(z)]S_0(z) \tag{5.19}$$

In this paper, the transfer matrix method is used for that purpose [16]. The self-consistent solutions can be found by searching the values of the total photon number P_0 and the lasing frequency ω_0 numerically with the condition that the right and left propagating waves satisfy the boundary conditions (5.14) and (5.15) simultaneously at the operating point. Once the total photon number P_0 is determined, the output powers P_R and P_L from the right and left facets can also be calculated from:

$$P_R = v_g \hbar\omega_0 P_0 \frac{(1-|r_R|^2)|Z_R(L)|^2}{\int_L |Z_0(z)|^2 dz} \tag{5.20}$$

$$P_L = v_g \hbar\omega_0 P_0 \frac{(1-|r_L|^2)|Z_L(0)|^2}{\int_L |Z_0(z)|^2 dz} \tag{5.21}$$

where v_g is the light group velocity and $\hbar\omega_0$ is the photon energy.

5.4 Small signal analysis

Although it is well known that the well-behaved semiconductor lasers exhibit a linear light-current characteristic without kinks above threshold, we can see that equations (5.3), (5.4) and (5.8) are essentially nonlinear due to the interaction between carriers and photons, especially when nonlinear gain compression is present. Therefore, under certain circumstances, such as high frequency modulation, harmonic and intermodulation distortions may become significant in the modulation response. To study this behaviour, we perform an extended small signal analysis of

the photon and carrier rate equations by introducing the following expansions:

$$J(z,t) = J_0(z) + J_1(z)e^{j\Omega t} \tag{5.22}$$

$$N(z,t) = N_0(z) + N_1(z)e^{j\Omega t} + N_2(z)e^{j2\Omega t} \tag{5.23}$$

$$P(t) = P_0 + P_1 e^{j\Omega t} + P_2 e^{j2\Omega t} \tag{5.24}$$

With truncated Taylor expansions of $R(N)$ and $G(N,S)$ around the stationary values $N_0(z)$ and $S_0(z)$, the amplitudes of the modulated carrier densities can be obtained by collecting terms with the same harmonic dependency from the carrier rate equation as follows:

$$j\Omega N_1(z) = J_1(z) - \frac{\partial R}{\partial N}N_1(z) - \left\{G_0(z)\frac{P_1}{P_0} + \frac{\partial G}{\partial N}N_1(z) + \frac{\partial G}{\partial P}P_1\right\}S_0(z) \tag{5.25}$$

$$\begin{aligned} j2\Omega N_2(z) = &-\frac{\partial R}{\partial N}N_2(z) - \frac{1}{2}\frac{\partial^2 R}{\partial N^2}N_1^2(z) - \left\{G_0(z)\frac{P_2}{P_0} + \frac{\partial G}{\partial N}N_2(z) + \frac{\partial G}{\partial P}P_2\right. \\ &\left. + \left[\frac{\partial G}{\partial N} + \frac{\partial^2 G}{\partial N \partial P}P_0 N_1(z) + \frac{\partial G}{\partial P}P_1\right]\frac{P_1}{P_0}\right\}S_0(z) \end{aligned} \tag{5.26}$$

In deriving the above formulas, we have assumed that harmonic coefficients of a given order are much smaller than those of the previous order, i.e. $N_1(z) >> N_2(z)$, $P_1 >> P_2$ etc. so as to neglect the higher order terms. Similarly, from the photon rate equations, we get

$$j\Omega P_1 = -R_{sp}\frac{P_1}{P_0} + P_0\int_L \left[G_{Nr}N_1(z) + G_{Sr}(z)S_0(z)\frac{P_1}{P_0}\right]dz \tag{5.27}$$

$$\begin{aligned} j2\Omega P_2 = &-R_{sp}\frac{P_2}{P_0} + P_0\int_L \left[G_{Nr}N_2(z) + G_{Sr}(z)S_0(z)\frac{P_2}{P_0}\right]dz \\ &+P_1\int_L \left[G_{Nr}N_1(z) + G_{Sr}(z)S_0(z)\frac{P_1}{P_0}\right]dz \end{aligned} \tag{5.28}$$

The condition of stationary solution has been used in order to obtain the above equations which include the contribution from spontaneous emission. By substituting equations (5.25) and (5.26) into equations (5.27) and (5.28), the AM response and second-order harmonic distortion for the DFB laser can be obtained after some

algebraic manipulations

$$\frac{P_1}{P_0} = \frac{\int_L \frac{G_{Nr}(z)J_1(z)}{j\Omega + \Gamma_N(z)}dz}{j\Omega + \Gamma_P + \int_L \frac{G_{Nr}(z)S_0(z)\left[G(z) + \frac{\partial G}{\partial P}P_0\right]}{j\Omega + \Gamma_N(z)}dz} \tag{5.29}$$

$$\frac{P_2}{P_1} = \frac{\int_L [G_{Nr}(z)N_1(z) + G_{Sr}(z)S_0(z)\frac{P_1}{P_0}]dz}{j2\Omega + \Gamma_P + \int_L \frac{G_{Nr}(z)S_0(z)\left[G(z) + \frac{\partial G}{\partial P}P_0\right]}{j2\Omega + \Gamma_N(z)}dz} - \frac{\int_L \frac{G_{Nr}S_0(z)}{j2\Omega + \Gamma_N(z)}\left\{\left(\frac{\partial G}{\partial N} + \frac{\partial^2 G}{\partial N \partial P}P_0\right)N_1(z) + \frac{\partial G}{\partial P}P_1\right\}dz}{j2\Omega + \Gamma_P + \int_L \frac{G_{Nr}(z)S_0(z)\left[G(z) + \frac{\partial G}{\partial P}P_0\right]}{j2\Omega + \Gamma_N(z)}dz} \tag{5.30}$$

where

$$\Gamma_P = \frac{R_{sp}}{P_0} - \int_L G_{Sr}(z)S_0(z)dz \tag{5.31}$$

$$\Gamma_N(z) = \frac{\partial R}{\partial N} + \frac{\partial G}{\partial N}S_0(z) \tag{5.32}$$

are defined as the photon and local carrier damping rates, respectively. With the parameters of Table I, they are typically of order of 0.3 GHz and 0.5 GHz, respectively. In equation (5.30), the term related to $N_1^2(z)$ is ignored for simplicity. Such a simplification can be justified under the condition $N_0(z) >> N_1(z)$ and was confirmed by numerical calculations as well.

As we can see, the equations (5.29) and (5.30) include the spatially distributed nonlinearities such as the spatial hole burning, the local carrier damping rate and the nonlinear gain compression explicitly through the distribution functions $G_{Nr}(z)$, $G_{Sr}(z)$, $\Gamma_N(z)$ and $G(z)$. The closed form expressions enable us to analyze their roles in the harmonic distortion and discuss their physical effects in an illustrative manner. For the gain-coupled DFB lasers, the distributed optical feedback is no longer uniform due to the spatial hole burning. Moreover, the periodically distributed

modal gain $G(z)$ can also interfere constructively with the standing wave pattern of the lasing light in the cavity. As a consequence, the spatial inhomogeneities will have more significant effects on the laser dynamic performance as well as on the second-order harmonic distortions in the AM response.

Table I Physical parameters used in the model

Bragg wavelength	λ_B	1.55 μm
group index of refraction	n_g	3.7
effective waveguide index of refraction	n_w	3.25
end-facet reflectivity	R_m	0
waveguide loss	α_0	20 cm^{-1}
differential gain	g_d	6×10^{-16} cm^2
carrier density at transparency	N_0	1.5×10^{18} cm^{-3}
nonradiative recombination coefficient	A	1×10^{-9} s^{-1}
radiative recombination coefficient	B	1×10^{-10} cm^3s^{-1}
Auger recombination coefficient	C	1.3×10^{-28} cm^6s^{-1}
linewidth enhancement factor	α_M	3

At high frequency, that is when $\Omega >> \Gamma_P$ and $\Omega >> \Gamma_N(z)$, the equations (5.29) and (5.30) for the AM response and the second harmonic distortion can be further reduced to the following simpler forms

$$\frac{P_1}{P_0} = \frac{\int_L G_{Nr}(z)J_1(z)dz}{\Omega_R^2 - \Omega^2} \tag{5.33}$$

$$\frac{P_2}{P_1} = -\frac{2\Omega^2}{\Omega_R^2 - 4\Omega^2}\frac{P_1}{P_0} = -\frac{2\Omega^2}{\Omega_R^2 - 4\Omega^2}\frac{\int_L G_{Nr}(z)J_1(z)dz}{\Omega_R^2 - \Omega^2} \tag{5.34}$$

where

$$\Omega_R^2 = \int_L \left\{ G_{Nr}(z)S_0(z)\left[G(z, N_0(z)) + \frac{\partial G}{\partial P}P_0\right]\right\} dz \tag{5.35}$$

is the angular relaxation oscillation or resonance frequency, which actually determines the modulation bandwidth of the DFB lasers. In deriving equation (5.34), we have used equation (5.27).

At low frequency, that is when $\Omega << \Gamma_P$ and $\Omega << \Gamma_N(z)$, the study of the harmonic distortion can be made neglecting Ω in equations (5.29) and (5.30). With equation (5.25), we can obtain the following expression, which explicitly demonstrates the contribution of the various nonlinearities to the harmonic distortion in DFB lasers at low frequency:

$$\begin{aligned}\frac{P_2}{P_1} &= \frac{\frac{R_{sp}}{P_0}\int_L G_{Nr}J_1\tau_N[1-H(z)]dz}{\left[\int_L G_{Nr}S_0\left[G+\frac{\partial G}{\partial P}P_0\right]\tau_N dz\right]^2} + \frac{\int_L G_{Sr}S_0 dz\int_L G_{Nr}J_1H(z)\tau_N dz}{\left[\int_L G_{Nr}S_0\left[G+\frac{\partial G}{\partial P}P_0\right]\tau_N dz\right]^2} \\ &- \frac{P_0\int_L G_{Nr}S_0\frac{\partial G}{\partial P}\tau_N dz\int_L G_{Nr}J_1\tau_N dz}{\left[\int_L G_{Nr}S_0\left[G+\frac{\partial G}{\partial P}P_0\right]\tau_N dz\right]^2} \\ &+ \frac{\int_L G_{Nr}J_1\tau_N dz\int_L G_{Nr}S_0\left[G+\frac{\partial G}{\partial P}P_0\right]H(z)\tau_N dz}{\left[\int_L G_{Nr}S_0\left[G+\frac{\partial G}{\partial P}P_0\right]\tau_N dz\right]^2} \\ &- \frac{\int_L G_{Nr}J_1H(z)\tau_N dz\int_L G_{Nr}S_0\left[G+\frac{\partial G}{\partial P}P_0\right]\tau_N dz}{\left[\int_L G_{Nr}S_0\left[G+\frac{\partial G}{\partial P}P_0\right]\tau_N dz\right]^2}\end{aligned} \tag{5.36}$$

where

$$H(z) = \left[\frac{\partial G}{\partial N} + \frac{\partial^2 G}{\partial N \partial P}P_0\right]\tau_N S_0(z) \tag{5.37}$$

is a spatially distributed function related to the spatial hole burning and $\tau_N(z) = 1/\Gamma_N(z)$. Equation (5.36) contains nonlinear terms of different origin. Although equation (5.36) is somewhat complicated, it is not that difficult to see that the first term is spontaneous emission related and the second and third terms are dominated by the gain compression effect. As for the last two terms with opposite signs, they are governed by the spatial hole burning in DFB lasers.

5.5 Harmonic distortion

Expressions (5.30), (5.34) and (5.36) indicate that although the effects of various nonlinearities on the harmonic distortion are usually not simply superposed in DFB lasers, each nonlinearity can be dominant in different cases. Such a property allows us to investigate their effects on the second-order harmonic distortions, separately. Moreover, the terms in equations (5.30) and (5.36) with different signs reveal that nonlinearities from different origin can compensate each other under certain circumstances. To simplify the discussion, we keep the optical modulation depth (OMD) at low frequency (below 0.1 GHz) to be 20% throughout the discussion in this paper.

5.5.1 Relaxation oscillation effect

Because of its significance, we start the analysis of second-order harmonic distortion from the relaxation oscillation in the gain-coupled DFB laser. As in the conventional semiconductor lasers, the relaxation oscillation of such lasers also occurs at very high frequency. The simplified expressions (5.33) and (5.34) indicate that the modulation efficiency as well as the second-order harmonic distortion of DFB lasers drop sharply when the modulation frequency is higher than the resonance frequency (see Fig. 2). The relaxation oscillation causes the second-order harmonic distortion to increase rapidly and gives rise to two resonance peaks in the frequency spectrum at $\Omega_R/2$ and Ω_R, respectively. The analytical result (5.34) reveals that a 40 dB per decade harmonic distortion is caused by the relaxation oscillation in the vicinity of the resonance frequencies $\Omega_R/2$ and Ω_R (see Fig. 2 also). This agrees well with the conclusion of the numerical analysis of reference [4]. It also indicates that the relaxation oscillation always gives rise to a negative contribution to the second-order harmonic distortion for modulation frequency below $\Omega_R/2$. Between the two resonance peaks at $\Omega_R/2$ and Ω_R, the phase varies from π

to $-\pi$ and reaches zero just halfway. This behaviour is typical and showed up in numerical analyses of the second-order harmonic distortion of the AM response in DFB lasers [4, 17].

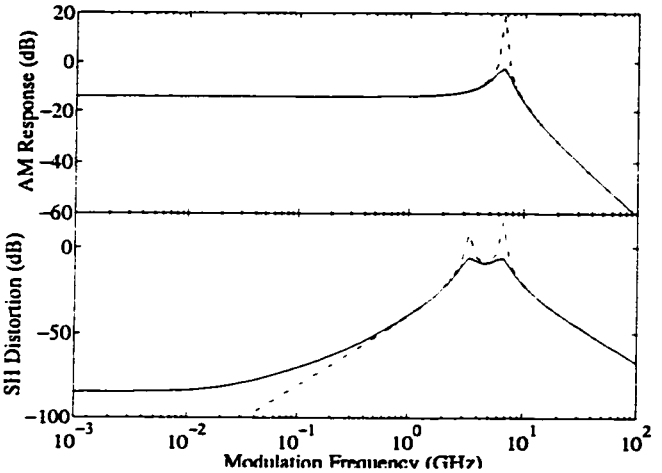

Fig. 2 AM response and second-order harmonic (SH) distortion of gain-coupled DFB laser, where $\gamma = 1/2$ (sinusoidal shape grating), $|K|L = 1.3$ (the least spatial hole burning) and $I = I_{th} + 15\ mA$. Gain compression and spontaneous emission are not included. Other calculation parameters are presented in the Table I. Solid lines: generated from equations (5.29) and (5.30); dashed lines: generated from equations. (5.33) and (5.34).

In expression (5.36), the denominator is proportional to the fourth power of the resonance frequency Ω_R. Thus, the increase of the resonance frequency not only means that the relaxation-oscillation-induced harmonic distortion rises at a higher frequency, but also leads to a substantial improvement to the second-order harmonic distortion of the AM response at low frequency (see Fig. 3). It has been discovered recently that, in the gain-coupled DFB lasers, the periodically-distributed gain grating can interfere with the standing wave pattern of the optical field. Such an interaction enhances the local effective differential gains $G_{Nr}(z)$ and $G_{Sr}(z)$ through the factor $1 + j\alpha_M$ in equation (5.5). Therefore, the resonance frequency Ω_R can be increased and decreased by the inphase and antiphase gain

coupling structures, respectively [18]. However, the numerical results in Fig. 3 show that although the structural enhancement of the resonance frequency increases the modulation bandwidth 2 or 3 times for the antiphase gain-coupled DFB lasers, it does not improve the low frequency harmonic distortion of antiphase gain-coupled DFB lasers. From expression (5.36), we learn that the enhancement is actually cancelled out by the local effective differential gain $G_{N_r}(z)$ in the numerators, which is enhanced as well.

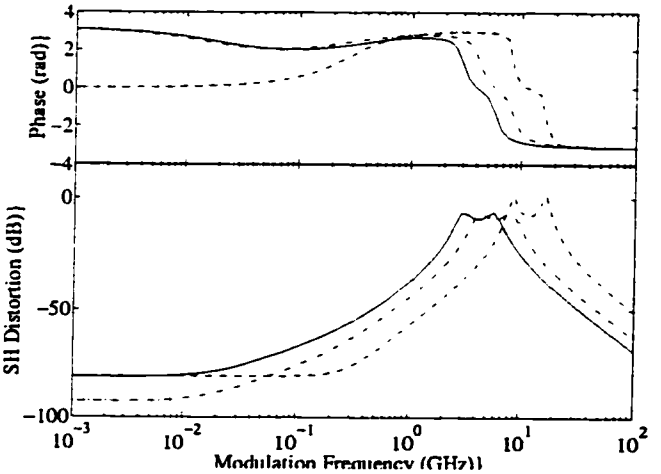

Fig. 3 Harmonic distortion in gain-coupled DFB lasers with different resonance frequency $\Omega_R/2\pi$, where $I = I_{th} + 15\ mA$ and $|\kappa|L = 1.3$. Spontaneous emission and gain compression are not included. Solid line: $g_d = 6 \times 10^{-16}\ cm^2$ with inphase gain-coupling; dash-dotted line: $g_d = 1.2 \times 10^{-15}\ cm^2$ with inphase gain-coupling; dashed line: $g_d = 6 \times 10^{-16}\ cm^2$ with antiphase gain-coupling; dotted line: $g_d = 1.2 \times 10^{-15}\ cm^2$ with antiphase gain-coupling.

5.5.2 Spatial hole burning effect

As we can see from expression (5.36), if the function $H(z)$ is uniform in z or constant, the last two terms with opposite signs can cancel each other out completely. Hence, we can conclude that DFB lasers with less spatial hole burning will generally have a lower second-order harmonic distortion in the low frequency regime. The plots of Figs. 4(b) and 5(b) show that the second-order harmonic distortion at

low frequency increases rapidly with the spatial hole burning in gain-coupled DFB lasers. Although the inphase and antiphase gain-coupled DFB lasers with the same coupling strength $|K|L$ give the same longitudinal photon density distribution $S(z)$, Figs. 4(a) and 5(a) show that antiphase gain coupling generally produces a lower second-order harmonic distortion because it introduces less spatial hole burning [18]. We can see from the figures that, typically, for the coupling strengths $|K|L = 1$ and $|K|L = 2$, the antiphase gain coupling improves the distortion by about 15.5 dB and 12.6 dB, respectively. Similar results have also been obtained by Novak with the transmission line analysis [5]. Our calculations also indicate that, for gain-coupled DFB lasers, the minimum spatial-hole-burning-induced distortion can be obtained with a $|K|L$ value between 1 and 1.5, which correspond to a K_i/K_r value around 1, depending on the grating structure. The inphase and antiphase gain-coupled DFB lasers with the same coupling strength $|K|L$ have the same value of $|K_i/K_r|$ [18].

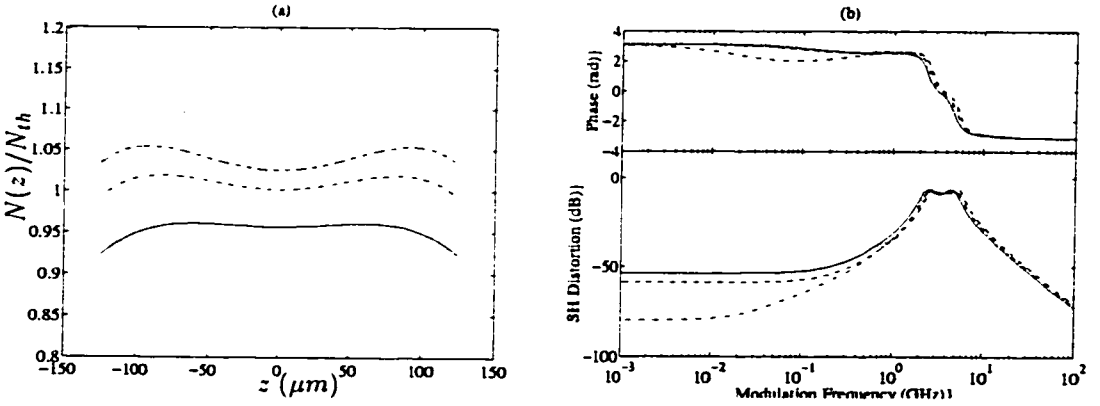

Fig. 4 (a) The carrier density distribution in inphase gain-coupled DFB laser. (b) Spatial hole burning effect on SH distortion, where $\gamma = 1/2$, $I = I_{th} + 15\ mA$. Solid line: $|K|L = 1.0$; dash-dotted line: $|KL| = 1.3$; dashed line: $|KL| = 1.5$; dotted line: $|K|L = 2.0$. The gain compression and spontaneous emission are not included.

A careful comparison of equations (5.36) and (5.30) indicates that the function $H(z)$ actually comes from the numerator of the second term in equation (5.30). Therefore, it will eventually roll off as the modulation frequency approaches the

local carrier damping rate $\Gamma_N(z)$. In other words, the related harmonic distortion is dominated in the low frequency regime only by the spatial hole burning. Moreover, the numerical results show that, in the low frequency regime, the spatial hole burning contributions to the second-order harmonic distortion in the inphase and antiphase gain-coupled DFB lasers are negative and positive, respectively (see Figs. 4(b) and 5(b)). Together with the relaxation-oscillation-induced second-order harmonic distortion, the total harmonic distortion can therefore be increased or reduced in the inphase and antiphase gain-coupled DFB lasers, respectively. Similarly to the discussion in reference [4], such a compensation not only can keep the spectrum of the harmonic distortion flat to a higher frequency, but also causes a dip to appear at high frequency in the spectrum for the antiphase gain-coupled DFB laser with a large spatial hole burning.

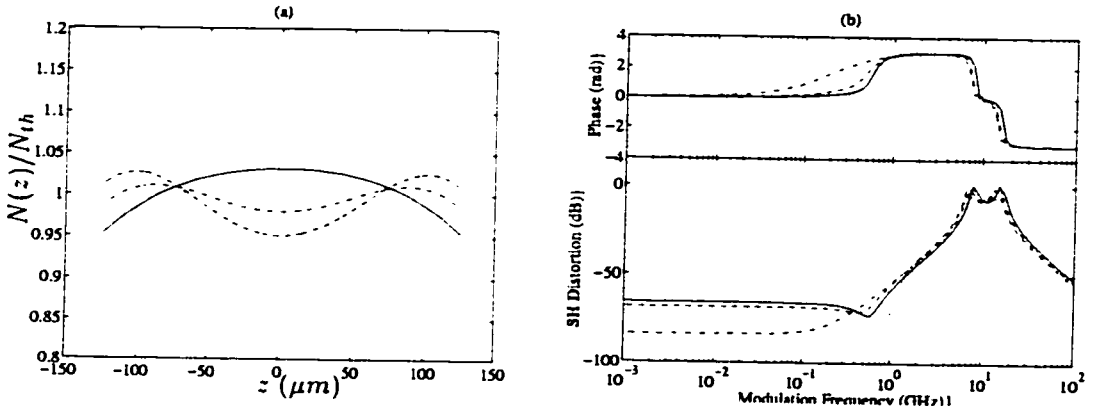

Fig. 5 (a) The carrier density distribution in antiphase gain-coupled DFB laser. (b) Spatial hole burning effect on SH distortion, where $\gamma = 1/2$, $I = I_{th} + 15\ mA$. Solid line: $|K|L = 1.0$; dash-dotted line: $|KL| = 1.3$; dashed line: $|KL| = 1.5$; dotted line: $|K|L = 2.0$. The gain compression and spontaneous emission are not included.

5.5.3 Gain compression effect

Gain compression influences the second-order harmonic distortion of gain-coupled DFB lasers significantly. In similarity with the periodically-distributed modal gain

$G(z, N)$, the distributed gain compression can also interact with the standing wave pattern of lasing light to enhance its effect [18]. Moreover, the effect not only decreases the optical gain, but also reduces the optical feedback of the gain grating. Therefore, the gain compression effect on the second-order harmonic distortion will be different in inphase and antiphase gain-coupled DFB lasers. Numerical results in Figs. 6 show that gain compression affects the spectra of second-order harmonic distortion throughout the whole frequency range. The strong damping of the resonance peaks of the relaxation oscillation caused by increasing gain-compression can also be seen clearly. Because of the enhancement of the local effective differential gain $G_{Sr}(z)$, antiphase gain-coupling gives a much higher photon damping rate Γ_P. The resonance peaks are, therefore, suppressed more in antiphase gain-coupled DFB lasers (see Figs. 6). Although the photon distribution $S_0(z)$ in gain-coupled DFB lasers at threshold depends on the coupling strength $|K|L$ only, this can become different above threshold in inphase and antiphase gain-coupled DFB lasers due to the spatial hole burning effects. In inphase gain-coupled DFB lasers, such a difference generally reduces the optical feedback of the gain grating. Hence, more photons can be produced by the inphase gain-coupled DFB laser with the same $|K|L$ value at threshold, especially when the $|K|L$ value is large. The self-consistent analysis verifies that gain compression effect on the low frequency second-order harmonic distortion is slightly stronger in inphase gain-coupled DFB lasers.

Numerical results also reveal that, by increasing gain compression in the inphase gain-coupled DFB lasers, the sign of second harmonic distortion at low frequency changes from negative to positive in the inphase gain-coupled DFB lasers. This implies that the second term in expression (5.36) dominates the related harmonic distortion for gain-coupled DFB lasers. In other words, for the gain-coupled DFB lasers, the gain-compression-induced second-order harmonic distortion is positive in the low frequency range. Therefore, the gain compression effect can partly cancel

the second-order harmonic distortion induced by spatial hole burning in inphase gain-coupled DFB lasers (see Fig. 6(a)). Because the gain compression effect is much more complicated in gain-coupled DFB laser, the low frequency distortion does not constantly increases by 12 dB with the doubling of the gain compression coefficient as in the F-P lasers [4].

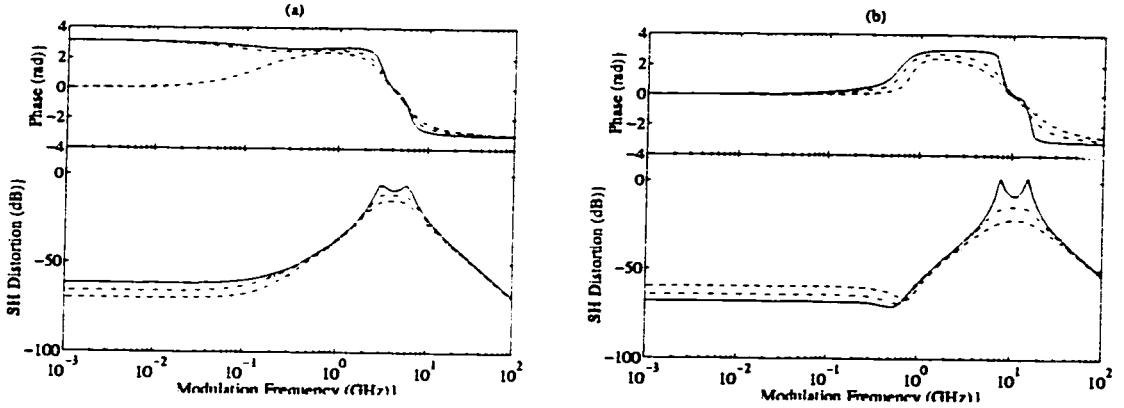

Fig. 6 The influence of gain compression on SH distortion in gain-coupled DFB laser, where $\gamma = 1/2$, $|K|L = 1.5$ and $I = I_{th} + 15\ mA$. (a) inphase gain-coupling; (b) antiphase gain-coupling. Solid line: $\varepsilon_N = 0$; dashed-dotted line: $\varepsilon_N = 3 \times 10^{-17}\ cm^3$; dash line: $\varepsilon_N = 6 \times 10^{-17}\ cm^3$; dotted line: $\varepsilon_N = 9 \times 10^{-17}\ cm^3$. The spontaneous emission is not included.

5.5.4 Spontaneous emission effect

The distributed spontaneous emission R_{sp} has very little effect on the second-order harmonic distortion (see Figs. 7). Our results confirm that it virtually does not contribute to the resonance peaks simply because the term R_{sp}/P_0 is much smaller than the relaxation oscillation frequency Ω_R^2. Formula (5.36) indicates that the spontaneous-emission-induced harmonic distortion is always positive because the function $H(z) < 1$. Since various nonlinear effects produce the second-order harmonic distortions with different signs, the spontaneous emission effect does not always increase the total harmonic distortion in DFB lasers. Figs. 7 show that,

by including the spontaneous emission, the low frequency harmonic distortion of inphase and antiphase gain-coupled DFB lasers are slightly decreased and increased, respectively. Therefore, if the spatial-hole-burning-induced harmonic distortion is negative in the low frequency regime, such as in the inphase gain-coupled DFB laser, the two contributions from different origins are able to compensate each other which leads to a decrease of the total second-order harmonic distortion.

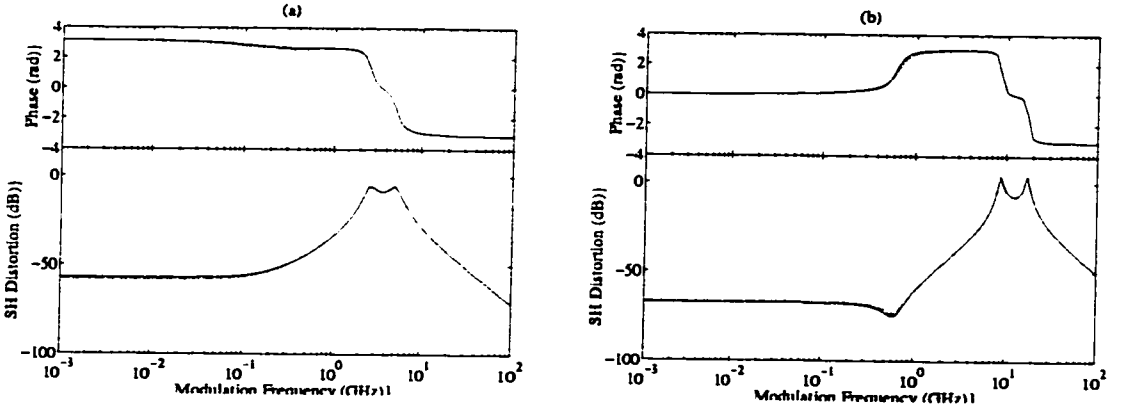

Fig. 7 The spontaneous emission effect on SH distortion in the gain-coupled DFB laser, where $\gamma = 1/2$, $|K|L = 1$ and $I = I_{th} + 15\ mA$. The gain compression is not included. (a) inphase gain-coupling; (b) antiphase gain-coupling. Solid line: $n_{sp} = 0$; dash-dotted line: $n_{sp} = 3$; dashed line: $n_{sp} = 5$; dotted line: $n_{sp} = 10$.

5.5.5 Bias effect

A proper study of the second-order harmonic distortion in gain-coupled DFB lasers needs to include the bias effect. Because of the nonlinear interaction between carriers and photons, the characteristics of the AM response can change at different operating points. For gain-coupled DFB lasers especially, the optical feedback by the gain grating can be altered by the spatial hole burning as well as the gain compression. Hence, bias can affect the second-order harmonic distortion in such lasers. It is well known that spatial hole burning in DFB lasers decreases monotonically with bias current but that gain compression, however, increases (see

equation (5.36)). As a consequence, an optimum operating point must exists for the lowest second-order harmonic distortion in the AM response. For the inphase gain-coupled DFB lasers, the spatial-hole-burning-induced harmonic distortion has a sign opposite to that induced by gain compression. When both are considered simultaneously, the cancellation will result in a harmonic distortion dip at a particular bias level (see Fig. 8). A stronger spatial hole burning can shift such a dip at a higher bias level. Hence, with a proper design, a lower harmonic distortion in low frequency regime at a desired bias level can be obtained for the inphase gain-coupled DFB laser. As for the antiphase gain-coupled DFB lasers, we know from previous analysis that the second-order harmonic distortion caused by spatial hole burning and gain compression have the same sign. That is why a similar dip will not appear in antiphase gain-coupled DFB lasers as we increase the bias current. Moreover, the self-consistent analysis reveals that, because of the positive power feedback mechanism by the spatial hole burning effect, the lasing modes in the antiphase gain-coupled DFB laser are unstable above a given bias point (see Fig. 9). The lasing mode can split into two asymmetric but stable modes. This necessarily deteriorates the modulation response and makes antiphase gain-coupled DFB lasers unsuitable for analog applications at high bias.

5.6 Conclusion

Using the Green's function based spatially-dependent rate equations, we have presented a systematic study of the second-order harmonic distortion in gain-coupled DFB lasers. Salient features of the DFB lasers such as the complex couplings, the spatial hole burning, distributed spontaneous emission and nonlinear gain compression are all included in the formalism. In particular, we have expressed in closed

form the effect of relaxation oscillation and spatial hole burning on the harmonic distortion in DFB lasers. Because of the carrier-dependent complex feedback mechanism and the interference between the standing wave pattern and the gain grating, the spatial effects in the gain-coupled DFB lasers are more important than those in index-coupled DFB lasers.

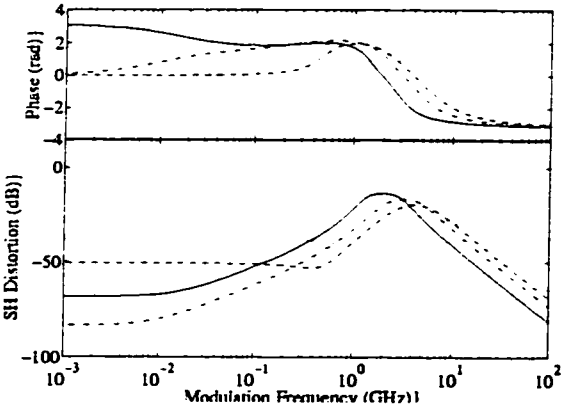

Fig. 8 The effect of bias on the SH distortion in inphase gain-coupled DFB lasers, where $\gamma = 1/2$, $|K|L = 2$ and $\varepsilon_N = 9 \times 10^{-17}\ cm^3$. Solid line: $I = 1.5I_{th}$; dash-dotted line: $I = 2.0I_{th}$; dashed line: $I = 2.6I_{th}$; dotted line: $I = 3.7I_{th}$.

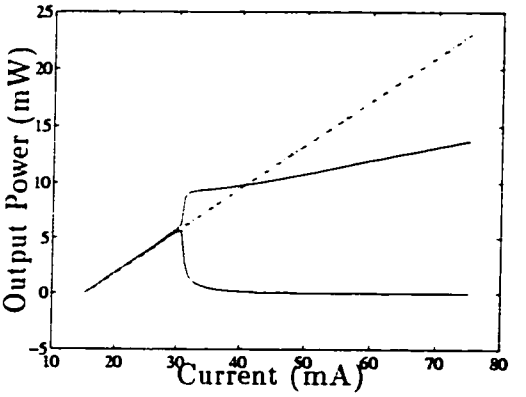

Fig. 9 Power versus current characteristic for the dominant mode in gain-coupled DFB lasers, where $\gamma = 1/2$ and $|K|L = 1.3$. Gain compression and spontaneous emission are not included. Solid line: antiphase (stable mode); dash-dotted line: antiphase (unstable mode); dotted line: inphase.

Antiphase gain coupling significantly increases the DFB laser modulation bandwidth. Depending on the material linewidth enhancement factor α_M, the relaxation oscillation frequency of gain-coupled DFB lasers can be enhanced 2 or 3 times. We have also shown that antiphase gain coupling has a positive spatial-hole-burning-induced harmonic distortion in DFB lasers at low frequency. This causes spatial-hole-burning-induced distortion to cancel that originating from the relaxation oscillation effect and gives about 10 dB to 15 dB improvement in the total harmonic distortion at 1 GHz over the inphase gain-coupled DFB lasers. However, at high bias level, the lasing mode in antiphase gain-coupled DFB lasers can become unstable, which can cause severe harmonic distortion in those lasers.

On the other hand, a stable lasing mode can be obtained in the inphase gain-coupled DFB lasers. Moreover, gain compression affects the inphase gain-coupled DFB lasers less with respect to the second-order harmonic distortion. Since it has a distortion which is opposite in sign to that of the spatial-hole-burning-induced harmonic distortion, a total harmonic distortion as low as 84 dB below 100 MHz can be reached by setting the laser bias properly.

REFERENCES

[1] R. Olshansky , "Subcarrier multiplexed lightwave systems for broadband distribution", IEEE J. Lightwave Technol., pp. 1429–1431, 1989.

[2] T. Hong , Y. Suematsu , S. Chung , and M. Kang , "Harmonic characteristics o laser diodes", J. Opt. Commun., Vol. 3, pp. 42–48, 1982.

[3] M. S. Lin , S. J. Wang , and N. K. Dutta , "Measurements and modelling of th harmonic distortion in InGaAsP distributed feedback lasers", IEEE J. Quantum Electron., Vol. 26, pp. 998–1004, 1990.

[4] G. Morthier , F. Libbrecht , K. David , P. Vankwikelberge , and R. G. Baets , "Theoretical investigation of the second harmonic distortion in the AM response of 1.55 μm F-P and DFB lasers", IEEE J. Quantum Electron., Vol. 27, pp. 1990–2002, 1991.

[5] D. Novak and A. J. Lowery , "Up to 15 dB improvement in second harmon distortion in complex-coupled DFB semiconductor lasers", Electron. Lett. Vol. 29, pp. 1954–1956, 1993.

[6] T. Okuda , H. Yamada , T. Torikai , and T. Uji , "DFB laser intermodulatio distortion analysis taking longitudinal electrical field distribution into account", IEEE Photon. Tech. Lett., Vol. 6, pp. 27–30, 1994.

[7] C. H. Henry , "Theory of spontaneous emission noise in open resonator and it application to lasers and optical amplifiers", IEEE J. Lightwave Technol., Vol. 4, pp. 288–297, 1986.

[8] B. Tromborg , H. Olesen , and X. Pan , "Theory of linewidth for multielectro laser diodes with spatial distributed noise sources", IEEE J. Quantum Electron., Vol. 27, pp. 178–192, 1991.

[9] G. H. Duan , P. Gallion , and G. P. Agrawal , "Dynamic and noise properties tuneable multielectrode semiconductor lasers including spatial hole burning and nonlinear gain", IEEE J. Quantum Electron., Vol. 29, pp. 844–855, 199

[10] T. Makino , "Transfer-matrix theory of the modulation and noise of multielement semiconductor lasers", IEEE J. Quantum Electron., Vol. 29, pp. 2762–2770, 1993.

[11] J. Hong , W. P. Hunag , and T. Makino , "Static and dynamic simulation for ridge waveguide MQW DFB lasers", IEEE J. Quantum Electron., Vol. 41, 1995.

[12] G. P. Li , T. Makino , R. Moore , N. Puetz , K. Leong , and H. Lu , "Partly gain-coupled 1.55μm strain-layer multi-quantum- well DFB lasers", IEEE J. Quantum Electron., Vol. 29, pp. 1736–1742, 1993.

[13] W. T. Tsang , M. C. Wu , Y. K. Chen , F. S. Choa , R. A. Logan , S. N. G. Chu A. M. Sergent , P. Magill , K. C. Reichmann , and C. A. Burrus , "Long-wavelength InGaAsP/InP multiquantum well distributed feedback and distributed bragg reflector lasers grown by chemical bean epitaxy", IEEE J Quantum Electron., Vol. 30, pp. 1370–1379, 1994.

[14] K. Kudo , S. Arai , and J. I. Shim , "Reduction of effective linewidth enhancement factor α_{eff} of DFB lasers with complex coupling coefficients", IEEE Photon. Tech. Lett., Vol. 4, pp. 531–534, 1992.

[15] L. M. Zhang and J. E. Carroll , "Enhanced AM and FM modulation response of complex coupled DFB lasers", IEEE Photon. Tech. Lett., Vol. 5, pp. 506–508, 1993.

[16] T. Makino , H. Lu , and G. P. Li , "Transfer-matrix dynamic model of partly gain-coupled 1.55 μm DFB lasers with a strained-layer MQW active grating", IEEE J. Quantum Electron., Vol. 30, pp. 2443–2448, 1994.

[17] J. L. Bihan and G. Yabre , "FM amd IM intermodulation distortions in directly modulated single-mode semiconductor lasers", IEEE J. Quantum Electron., Vol. 40, pp. 899–904, 1994.

[18] J. Chen , R. Maciejko , A. Champagne , and T. Makino , "Relaxation oscillati frequency of DFB lasers with gain coupling", IEEE J. Quantum Electron., Vol. 31, pp. 1955–1963, 1995.

CHAPTER 6

Large Signal Dynamics in Gain-Coupled DFB Lasers

The small-signal analysis of the modulation response presented in the previous chapters is useful for predicting the parameter dependency, but is not enough. In optical communication systems, semiconductor lasers are generally biased close to threshold and the modulation depth can be well beyond the range assumed in the small-signal analysis. The nonlinear effects then play an important role, and some new features arise during the transient period. To study those phenomena, a numerical analysis of the laser large signal dynamics is therefore necessary.

Side mode suppression is the key to ensure dynamic single mode oscillation in DFB lasers. Although the frequency dependent DFB feedback provides an effective mechainsm for the selection of the lasing mode, the side mode powers may fluctuate significantly during the transient period because of the spatial hole burning effect. Spatial hole burning perturbs the modal resonance conditions in DFB lasers and causes the powers to change as well as the frequencies to chirp. Transient side mode suppression must be analyzed in greater detail. In gain-coupled DFB lasers, the carrier-dependent feedback structure adds complexity to the process.

Submitted to IEEE J. Quantum Electron.

Transient Side Mode Suppression in Gain-Coupled DFB Lasers

Jianyao Chen, Roman Maciejko, *Senior Member, IEEE*
and Toshihiko Makino, *Senior Member, IEEE*

Abstract

Based on the spatially dependent multimode rate equations, we investigate the transient side mode suppression in gain-coupled DFB lasers. A simplified but accurate multimode dynamic analysis of gain-coupled DFB lasersis developed. To the first order of perturbation approximation, the study includes various spatial effects, such as the distributed complex coupling, the nonuniform carrier distribution and the nonlinear gain compression. It is found that gain coupling introduces high decay rates for the side modes, which effectively suppresses their transient fluctuation and shortens the rise time of the transient side mode suppression ratio ($SMSR$).

J. Chen, and R. Maciejko are with the Optoelectronics Laboratory, Department of Engineering Physics, École Polytechnique, P. O. Box 6079, Station "Centre-ville", Montréal, Québec Canada H3C 3A7

T. Makino is with Northern Telecom (Nortel), P. O. Box 3511, Station C, Nepean, Ontario, Canada K1Y 4H7

6.1 Introduction

DFB lasers with gain coupling are characterized by a stable single mode operation with a remarkably high side mode suppression ratio, which is very important for the reduction of the system transmission penalty caused by fiber dispersion at 1.55 μm [1]. Based on a threshold gain analysis, it has been shown that the suppression of side modes in gain-coupled DFB lasers is caused by a reduction of the interaction between the side mode Bloch waves and the gain medium [2].

The high speed modulation of the DFB laser induces strong carrier density fluctuations in the cavity. The conventional rate equation analysis of Fabry-Perot lasers indicates that the side mode spectrum can broaden significantly during transients [3]. Coupled with spatial hole burning and the nonlinear gain compression, the dynamic carrier variation in gain-coupled DFB lasers not only modifies the index of refraction in the laser cavity, but also changes the feedback of the DFB grating. Those effects perturb the lasing resonance condition and the side mode suppression. They can therefore bring about complex modal interactions in gain-coupled DFB lasers during the transient period. In order to gain a more detailed knowledge into the design of DFB lasers with a high dynamic single-mode performance, a careful analysis of the transient side mode suppression including the effects of various spatial nonuniformities becomes therefore necessary.

Several numerical approaches have been developed to model the transient dynamics or the so-called 'large signal dynamics' of DFB semiconductor lasers. Using the analogy between the laser waveguide and the transmission line in electric circuit theory, Lowery successfully adapted the transmission line technique to model the large signal dynamics of DFB lasers [4]. Also, by transforming the scalar travelling wave equations into an F-matrix and using the concept of instantaneous frequency, Tsang and his coworkers recently proposed a 'time domain model' to simulate the

transient response of DFB lasers [5]. Zhang and Carroll, on the other hand, developed a 'power matrix method' for the large signal analysis of DFB lasers, which transforms the field equations into power equations and determines the modal powers from the amplified spontaneous emission [6]. Even though those approaches are easily adaptable to the study of arbitrary laser geometries, their inherently numerical nature makes the study of various underlying physical effects less transparent. For a long time, rate equation analysis has been used to derive simple and insightful closed form results. Based on the approximation of threshold modal fields, this paper therefore investigates the transient side mode suppression in gain-coupled DFB lasers using the spatially dependent multimode rate equations. This approach offers both relatively straightforward physics and significant advantages in numerical computation. Our analysis shows that the gain coupling increases the decay rate of the side modes and hence effectively improves the transient side mode suppression in DFB lasers.

6.2 The model

In the standing wave formalism, the temporal and spatial dependencies of the optical fields in DFB lasers are separable. We assume the laser waveguide to be single-mode in the transverse direction and apply the effective index approximation to determine the interaction between the DFB modes and the active medium [7]. Since intermodal couplings induced by spatial hole burning and nonlinear gain compression are negligible in the single-contact DFB lasers, a set of multimode rate equations for the modal photon number $I_i(t)$ and the phase fluctuation $\phi_i(t)$ can be obtained from the wave equation [8, 9, 10]:

$$\frac{dI_i}{dt} = \left\{-\gamma_i + v_g \int_L Re[C_i(z)]\Delta g(z,t)dz\right\} I_i(t) + R_{sp}^i \qquad (6.1)$$

$$\frac{d\phi_i}{dt} = \frac{v_g}{2}\int_L Im[C_i(z)]\Delta g(z,t)dz \tag{6.2}$$

where

$$C_i(z) = (1+j\alpha_M)\frac{Z_i^2(z)\Gamma(z)}{\int_L Z_i^2(z)dz} \tag{6.3}$$

$$R_{sp}^i = n_{sp}v_g\frac{\int_L |Z_i(z)|^2 dz \int_L |Z_i(z)|^2 \Gamma(z)g(z)dz}{\left|\int_L Z_i^2(z)dz\right|^2} \tag{6.4}$$

are the enhancement factor of the modal dynamic differential gain [11] and the spontaneous emission rate coupled to the corresponding mode. v_g is the group velocity of light in the semiconductor laser and γ_i represents the decay rate of the DFB mode. $\Delta g(z,t) = g[N(z,t), S(z,t)] - \bar{g}[N_0(z), S_0(z)]$ and gives the local deviation of the gain distribution from the reference value $\bar{g}(z)$. N and S are the distributions of the carrier and photon densities in the laser. For the gain-coupled DFB lasers discussed in this paper, we assume that the thickness of the active layer is etched to form the gain grating. The variation of the index $n(z)$ and the modal confinement factor $\Gamma(z)$ for such a structure can be written as:

$$n(z) = n_0 + 2c_g\Delta n\cos(2\beta_0 z) \tag{6.5}$$

$$\Gamma(z) = \Gamma_0 \pm 2c_g\Delta\Gamma\cos(2\beta_0 z) \tag{6.6}$$

where β_0 denotes the Bragg wavenumber of the DFB grating. n_0 denotes the average value of the effective waveguide index and Δn gives the maximum effective index variations due to the index grating. Similarly, Γ_0 and $\Delta\Gamma$ are the average and maximum variation of the gain confinement factor, respectively. c_g is the Fourier coefficient determined by the shape of the gain grating. The sign $\pm$ corresponds to the inphase and antiphase gain coupling structures respectively.

The modal field functions $Z_i(z)$ in the rate equations (6.1) and (6.2) have the

usual form:

$$Z_i(z) = Z_i^+(z)e^{-j\beta_0 z} + Z_i^-(z)e^{j\beta_0 z} \tag{6.7}$$

where Z_i^+ and Z_i^- are the amplitudes for the forward and backward propagating waves, respectively. They are governed by the following coupled wave equations [9]:

$$\frac{dZ_i^+}{dz} + j[\beta_i(z) - \beta_0 + j\frac{\gamma_i}{2v_g}]Z_i^+ = -jK_i(z)e^{-j\theta}Z_i^- \tag{6.8}$$

$$-\frac{dZ_i^-}{dz} + j[\beta_i(z) - \beta_0 + j\frac{\gamma_i}{2v_g}]Z_i^- = -jK_i(z)e^{j\theta}Z_i^+ \tag{6.9}$$

where

$$\beta_i(z) = k_i n_0 + j\frac{\Gamma_0}{2}[(1 + j\alpha_M)g(N,S) - \alpha_{in}] \tag{6.10}$$

$$K_i(z) = \left\{k_i\Delta n \pm j\frac{\Delta\Gamma}{2}[(1 + j\alpha_M)g(N,S) - \alpha_{in}]\right\}c_g \tag{6.11}$$

are the modal propagation constants and the DFB coupling coefficients, respectively. $\gamma_i/2v_g$ in equations (6.8) and (6.9) can be regarded as the effective net gain for the longitudinal modes. It should be pointed out that γ_i is an important parameter in this multimode rate equation approach. As can be seen from the rate equations (6.1), (6.2) and the coupled wave equations (6.8), (6.9), γ_i actually provides the link between the temporal and spatial dependencies of DFB modes.

The carrier rate equation reads

$$\frac{\partial N}{\partial t} = J(z,t) - R(z,N) - \frac{v_g}{A_c}g(N,S)S(z,t) \tag{6.12}$$

where $J(z,t)$ is the pumping rate and $R(z,N)$ represents the Shockley-Read-Hall, spontaneous and Auger carrier recombination rates. A_c gives the area of laser waveguide cross section.

$$S(z,t) = \sum_i \frac{|Z_i(z)|^2}{\int_L |Z_i(z)|^2\,dz} I_i(t) \tag{6.13}$$

gives the total photon density distribution in the DFB cavity [12]. Equations (6.1), (6.2), (6.8) and (6.9), form a complete system for the analysis of the static and

dynamic characteristics of general DFB semiconductor lasers with various spatial nonuniformities. A rigorous study implies the self-consistent solution of those equations, which is numerically difficult and time consuming due to the extremely low decay rate γ of the lasing mode [9]. Especially during modulation, the carrier density and the photon population experience a wide range of fluctuations in a short period, which significantly complicates the solution of equations (6.1), (6.2), (6.8), (6.9) and (6.12).

Table I Physical parameters used in the model

Bragg wavelength	λ_B	1.55 μm
waveguide width	w	1.5 μm
thickness of active layer	d	0.1 μm
cavity length	L	350 μm
group index of refraction	n_g	3.7
effective waveguide index of refraction	n_w	3.23
end-facet reflectivity	r_L, r_R	0
waveguide loss	α_0	20 cm^{-1}
transverse modal confinement factor	Γ_0	0.1
differential gain	g_d	6×10^{-16} cm^2
carrier density at transparency	N_0	1.5×10^{18} cm^{-3}
nonradiative recombination coefficient	A	1×10^{-9} s^{-1}
radiative recombination coefficient	B	1×10^{-10} cm^3s^{-1}
Auger recombination coefficient	C	1.3×10^{-28} cm^6s^{-1}
spontaneous emission factor	n_{sp}	3
linewidth enhancement factor	α_M	3

Since spatial hole burning induces a weak change of the index of refraction in the cavity and since, above threshold, the dynamic variation of the carrier density is clamped at about its threshold value, we assume that the distributions of the modal fields do not change much with the carrier fluctuation. Under such a perturbation approximation, the solution of equations (6.1), (6.2), (6.8), (6.9) and (6.12) can be simplified significantly. We first solve the coupled wave equations (6.8) and (6.9) at

the threshold of the first mode. Then, setting the time derivatives in rate equations (6.1), (6.2) and (6.12) to zero and solving them simultaneously, we can easily obtain the stationary solutions for the photon and carrier density distributions at any given bias level. Then, using the stationary solution as initial distributions for the photons and the carriers, the dynamic solutions of the time-dependent rate equations (6.1), (6.2) and (6.12) for a given modulation signal can be found with the help of the Runge-Kutta method.

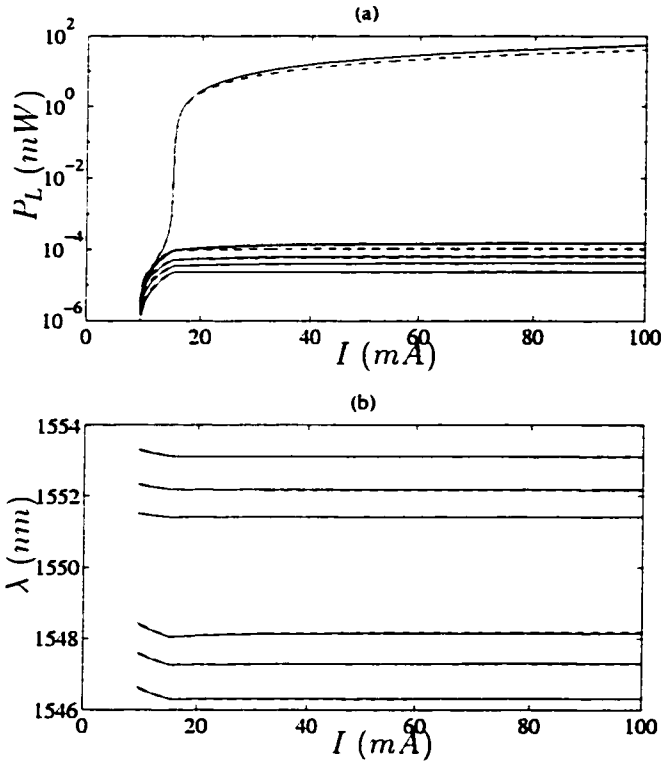

Fig. 1 Comparison of the modal power (a) and the wavelength (b) of antiphase gain-coupled DFB lasers with $|K|L = 4$. Solid lines: produced by perturbation analysis; dashed line: produced by self-consistent analysis.

The validity of such a perturbation approach can be verified by comparing the results with a rigorous self-consistent analysis [9]. Fig. 1 presents the multimode light-current curves and the adiabatic modal wavelength transition in an antiphase

gain-coupled DFB laser. The key laser parameters are listed in Table I. The results produced by the perturbation analysis show a fairly good agreement with those of the self-consistent analysis. Slight discrepancies appear when the injection current is above threshold. It is also worth pointing out that the perturbation analysis only takes 200 steps to complete the curves. Considering that 50 thousand steps are needed for the self-consistent analysis in the same calculation, we obtain a very significant improvement with reliable results.

6.3 Multimode dynamics

Because of the nature of carrier recombination and photon generation, the dynamic modulation of DFB lasers can cause the carrier and photon distributions to fluctuate in the cavity. Under a step-function injection, Fig. 2 exhibits an example of the transient responses of carrier and photon distributions in gain-coupled DFB lasers[1]. After the laser is turned on, the carrier density in the laser cavity appears to have a nearly linear increase, while the photon density grows relatively slowly. Since the number of photons in all the longitudinal modes in still low at this stage, spatial hole burning is not yet visible in the carrier distribution. When the carrier density or the laser gain reach the threshold of the first mode, the stimulated emission rises up rapidly. This sharp increase causes the carrier density to drop. With a large number of photons in the laser, spatial hole burning becomes pronounced. Because of a non-vanishing material linewidth enhancement factor, such a carrier nonuniformity causes a distributed index change along the laser cavity and hence influences the dynamic behaviour of the longitudinal modes. The smooth variation of the distributions of the carrier and photon densities implies that all the longitudinal modes oscillate at the same frequency and the effect of the side modes is minimal.

[1] $S(z,t)$ is defined by expression (6.13).

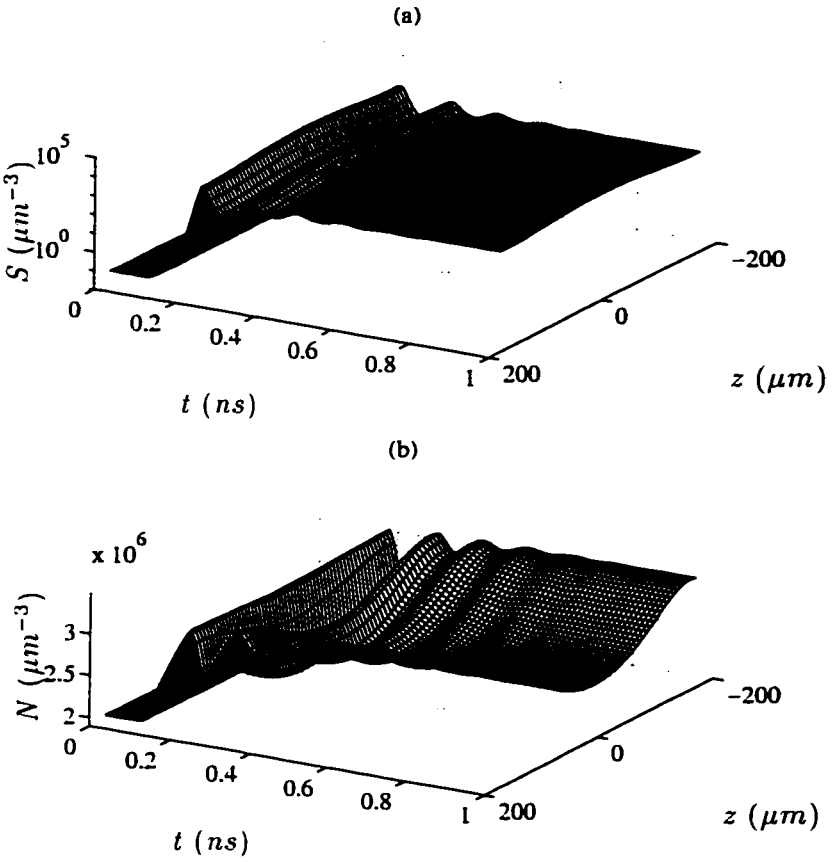

Fig. 2 Step function response of inphase gain-coupled DFB lasers with $|\kappa|L = 3$, where $I_{off} = I_{th} - 2\ mA$ and $I_{on} = I_{th} + 50\ mA$. (a) photon density distribution; (b) carrier density distribution.

The rate equation analysis yields the multimode power response and the dynamic wavelength chirp in a straightforward manner. Fig. 3 depicts the temporal evolution of the longitudinal modes in an inphase gain-coupled DFB laser. In order to ensure a sufficient accuracy, six longitudinal modes are considered in the calculation. As we can see, the fundamental mode on the long wavelength side of the Bragg stopband rises up predominantly after the laser is turned on. Meanwhile, the side modes on both sides of the Bragg stopband, strongly suppressed by the gain coupling effect, all oscillate at a low power level with the same relaxation oscillation frequency. They all reach their highest values at the first peak of oscillation and decay quickly as

the laser evolves towards the stationary state. The results further indicate that the modes on the long wavelength side of the Bragg stopband have higher powers with stronger wavelength chirp. Physically, this is because the intensities of the long and short wavelength Bloch modes in DFB lasers are in phase and in antiphase with the index grating, respectively [2]. Since the carrier induced index change is concentrated in the high gain regions, which coincide with the high index sections of the grating in inphase gain-coupled DFB lasers, the resonance conditions of the long wavelength modes are affected more, which causes their power to fluctuate more in the transient period. Similarly, when an antiphase gain-coupled DFB laser is considered, the modes on the short wavelength side of the Bragg stopband are chirped more and carry more power (see Fig. 4) since the high gain sections are in phase with the low index sections [2].

According to the threshold gain analysis, which assumes a uniform carrier distribution in the cavity, the gain coupling induces a strong mode selection mechanism which suppresses the side modes [13]. Using the multimode rate equations (6.1) and (6.2), we find that gain coupling is effective in suppressing transient side mode oscillations. In the transient regime, the peaks of the photon numbers for side modes $\hat{I}_i$ are located where the derivatives of rate equations (6.1) vanish. Therefore,

$$\hat{I}_i = \frac{R_{sp}^i}{\gamma_i - v_g \int_L Re[C_i(z)]\Delta g(z,\hat{t})dz} \tag{6.14}$$

Since the carrier density $N(z,t)$ or the laser gain $g(z,t)$ oscillate around their stationary values in the transient state, we infer from (6.14) that the peaks of sided mode oscillations $\hat{I}_i$ also coincide with the carrier fluctuation $\Delta N(z,t)$. In the single-mode dominant DFB lasers, which is the case for gain-coupled DFB lasers, this also means that all side modes oscillate in phase but not with the lasing mode, since the carrier fluctuation is mainly determined by the lasing mode. It is well known that the lasing mode does not oscillate in phase with carrier distribution. Therefore,

the transient side mode suppression ratio will oscillate at the relaxation oscillation frequency after the laser is turned on.

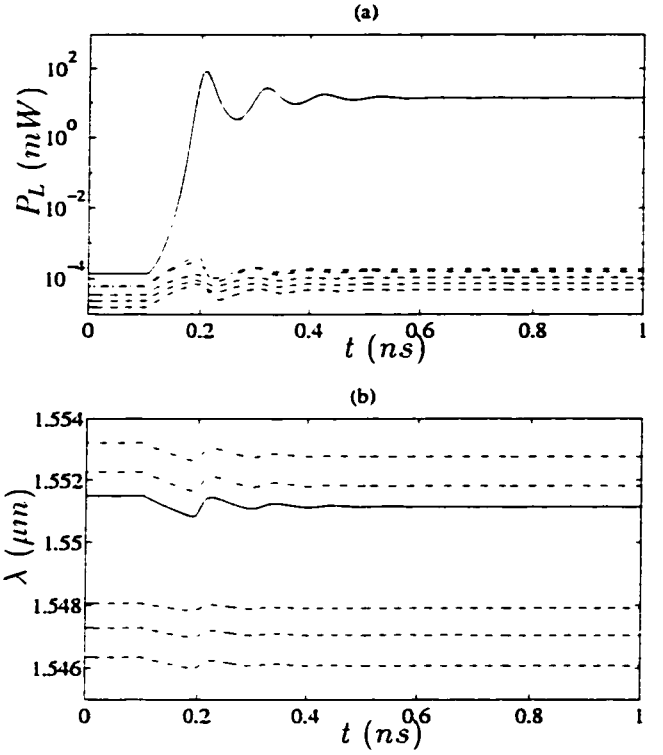

Fig. 3 Transient response of modal power (a) and wavelength (b) of inphase gain-coupled DFB laser with $|K|L = 4$ by step function signal, where $I_{off} = I_{th} - 2\ mA$ and $I_{on} = I_{th} + 50\ mA$. Solid line: lasing mode; dash-dotted lines: long wavelength mode; dashed lines: short wavelength mode.

The side modes reach their maximum values at the first peaks of the relaxation oscillation. From the above analysis, we know that the first peak of $N(z,t)$ occurs at the threshold of the lasing mode and it is distributed almost uniformly in the DFB cavity. Since we use the threshold state as the reference state for the perturbation analysis, the maximum for the photon number of the side modes can be determined approximately from:

$$\max\{I_i(t)\} \approx \frac{R_{sp}^i}{\gamma_i} \tag{6.15}$$

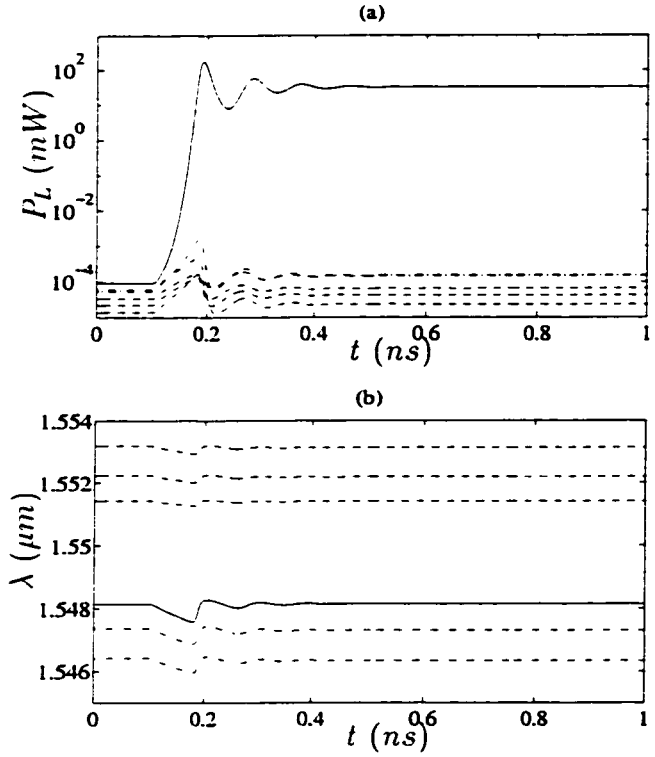

Fig. 4 Transient response of modal power (a) and wavelength (b) of antiphase gain-coupled DFB laser with $|\kappa|L = 4$ by step function signal, where $I_{off} = I_{th} - 2\ mA$ and $I_{on} = I_{th} + 50\ mA$. Solid line: lasing mode; dash-dotted lines: short wavelength mode; dashed lines: long wavelength mode.

which is inversely proportional to the modal decay rate. This indicates explicitly that, by increasing the decay rate of the side modes, we can suppress the transient variation of the side modes. The results of Fig. 5 show that the decay rates of the side modes are high when the gain coupling is strong. According to the Bloch wave analysis, we can understand that the gain grating reduces the interactions between the side modes and the gain medium, especially for the modes on the side of the Bragg stopband opposite to the lasing mode [2]. By increasing gain coupling, we can obtain a higher decay rate γ_i of the side modes to suppress their fluctuations in the transient state. Fig. 6 shows clearly that a high gain coupling not only reduces the power of the side modes, but also shortens the rise time of the lasing mode since

more photons are transferred into that mode.

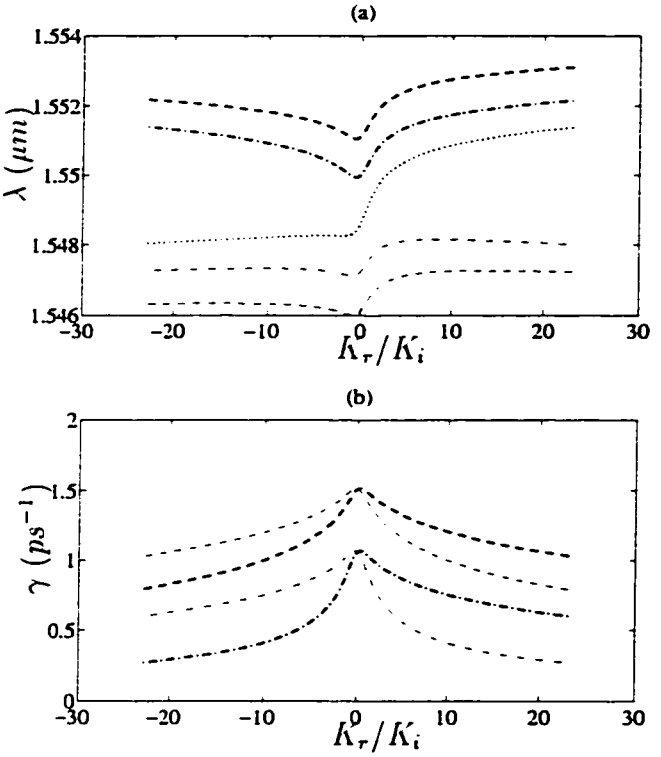

Fig. 5 Dependency of the modal wavelength (a) and the decay rate (b) on the complex coupling coefficient $K = K_r + jK_i$ in gain-coupled DFB lasers, Thicker lines: long wavelength side mode; thiner lines: short wavelength side mode. Dotted line: lasing mode.

6.4 The transient side mode suppression

If we neglect the spontaneous emission rate R_{sp}^i in equations (6.1), a simple expression for the transient side mode suppression ratio can then be obtained as follows[2]:

$$SMSR(t) = SMSR(0)\exp\left\{\gamma_s t + v_g \int_L Re[C_m(z) - C_s(z)] \int_0^t \Delta g(z,t)dtdz\right\} \tag{6.16}$$

[2] $\gamma_m = 0$ since we choose the reference state at the threshold of the lasing mode.

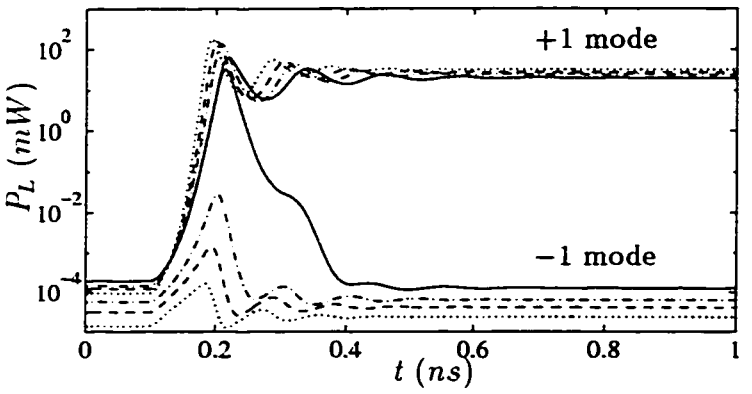

Fig. 6 Effect of the gain coupling on the side mode suppression in antiphase gain-coupled DFB lasers, where $|K|L = 4$, $I_{off} = I_{th} - 2$ mA and $I_{on} = I_{th} + 50$ mA. Solid line: $\Delta\Gamma/\Gamma_0 = 0$ (index-coupled); dash-dotted line: $\Delta\Gamma/\Gamma_0 = 0.5$; dashed line: $\Delta\Gamma/\Gamma_0 = 0.75$; dotted line: $\Delta\Gamma/\Gamma_0 = 1$

where the subscripts m and s denote the main mode and the highest side mode, respectively. This closed form result indicates that a large side mode decay rate γ_s enhances the transient $SMSR$ by shortening the rise time. Moreover, the results in Fig. 7 show that the gain coupling enhances the effective dynamic differential gain of the lasing mode and, at the same time, suppresses that of the side modes (Although only the results for the ± 1 modes are presented here, one can show that the suppression mechanism applies to the other side modes as well.). Since the carrier density grows linearly initially, the second term in the exponential of expression (6.16) grows parabolically with time. Therefore, through the difference of the enhanced dynamic differential gain $Re[C_m(z) - C_s(z)]\frac{\partial g}{\partial N}$, the transient $SMSR$ of gain-coupled DFB lasers can increase rapidly after the laser is turned on. Together with the high side mode decay rate γ_s, this leads to a significant improvement of the transient $SMSR$ of gain-coupled DFB lasers. Because of the relaxation oscillation, the transient $SMSR$ also reaches a stationary value when the photon number in the lasing mode becomes high. A detailed analysis indicates that the decay rate of the

envelope of the transient $SMSR$ oscillation is determined by the carrier damping rate Γ_N[3], which is strong when the photon density of the lasing mode is high.

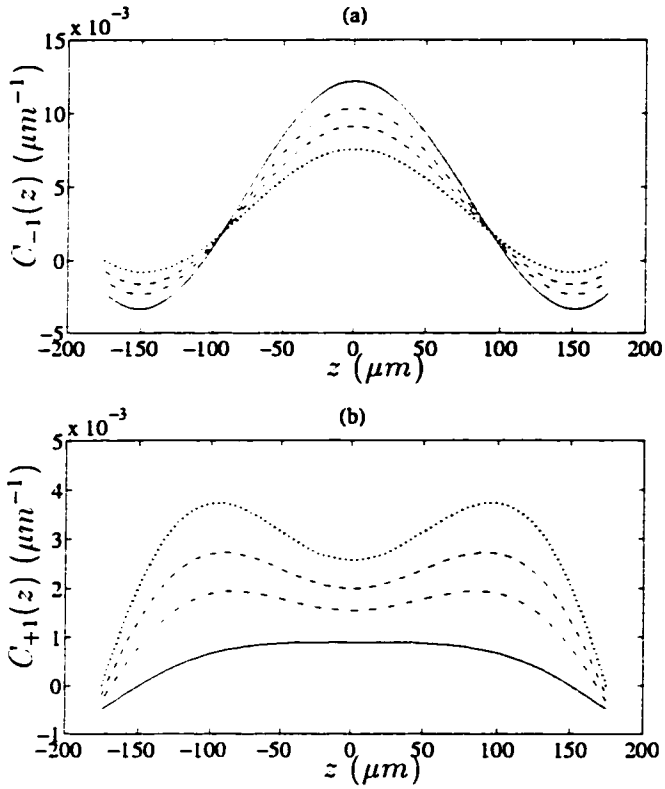

Fig. 7 Dependency of $C_i(z)$ on the modulation depth of the gain grating in inphase gain-coupled DFB lasers. (a) long wavelength fundamental mode; (b) short wavelength fundamental mode. Solid line: $\Delta\Gamma/\Gamma = 1$; dash-dotted line: $\Delta\Gamma/\Gamma = 0.75$; dashed line: $\Delta\Gamma/\Gamma = 0.5$; dotted line: $\Delta\Gamma/\Gamma = 0.25$.

Both expressions (6.14) and (6.16) indicate that a high side mode decay rate γ_s is crucial to enhance the transient $SMSR$ in DFB lasers. It is known that a frequency dependent DFB coupling induces a strong modal discrimination in DFB lasers. One can therefore expect that a high $|K|L$ value can help produce a high decay rate γ_s. The numerical results of Fig. 8 show that, in both inphase and antiphase gain-

[3] $\Gamma_N = \frac{\partial R}{\partial N} + \frac{v_g}{A_c}\frac{\partial g}{\partial N}S(z,t)\Gamma(z)$ [11].

coupled DFB lasers, a high $|K|L$ value not only gives a higher $SMSR$ at steady-state, but also a higher decay rate for the envelope of the transient $SMSR$ oscillation after the laser is turned on. Since more photons are transferred to the lasing mode, a high $|K|L$ also causes the transient $SMSR$ to oscillate at a higher frequency with a smaller amplitude. Compared with an inphase gain-coupled DFB laser with the same $|K|L$ value, we see from Fig. 8 that the antiphase gain-coupled DFB lasers give a better transient $SMSR$. This is because the feedback strength of the DFB grating in antiphase gain-coupled DFB lasers is enhanced by the carrier induced change of the index of refraction. Consequently, the spatial hole burning effect in antiphase gain-coupled DFB lasers is relatively weaker and the carrier distribution also fluctuates less in the laser cavity during the transient period.

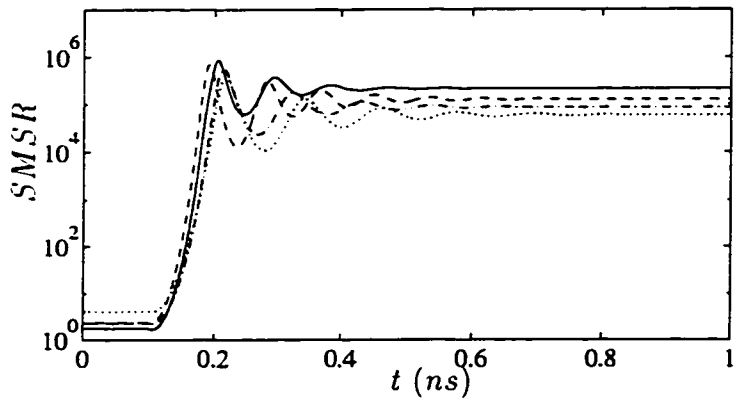

Fig. 8 Effect of the coupling strength on the side mode suppression in gain-coupled DFB lasers, where $I_{off} = I_{th} - 2\ mA$ and $I_{on} = I_{th} + 50\ mA$. Solid line: antiphase gain-coupled with $|K|L = 4$; dash-dotted line: inphase gain-coupled with $|K|L = 4$; dashed line: antiphase gain-coupled with $|K|L = 3$; dotted line: inphase gain-coupled with $|K|L = 3$.

The bias-dependent carrier distribution modifies the condition of the DFB laser cavity. Similarly to the Fabry-Perot lasers, the injection bias can affect the $SMSR$ of DFB lasers. The results of Fig. 9 show that, when the OFF bias I_{off} is set

below threshold, it basically influences the initial $SMSR$ only. By setting I_{off} closer to threshold, the initial value of the side mode suppression ratio $SMSR(0)$ is increased and the rise time of the transient $SMSR$ is shortened. When I_{off} is set above threshold, it will not only affect the initial $SMSR$, but also the oscillation of the transient $SMSR$. This behaviour is similar to what Marcuse described in Fabry-Perot lasers [3]. By setting I_{off} above threshold, we can significantly narrow the width of the initial side mode spectrum and dampen the envelope of the relaxation oscillation of the transient $SMSR$. Fig. 9 also shows that a high ON bias current increases the frequency of the relaxation oscillation and gives a high $SMSR$ in the final stationary state. This is because the amplitudes of the side modes are clamped by the effects of the complex DFB coupling and the high injection current provides more photons to the lasing mode. Since the carrier damping rate Γ_N is increased as well, a high I_{on} also causes the relaxation oscillation of the transient $SMSR$ to decay in a relatively shorter period. A high ON bias current I_{on} also shortens the rise time of the transient $SMSR$ in gain-coupled DFB lasers.

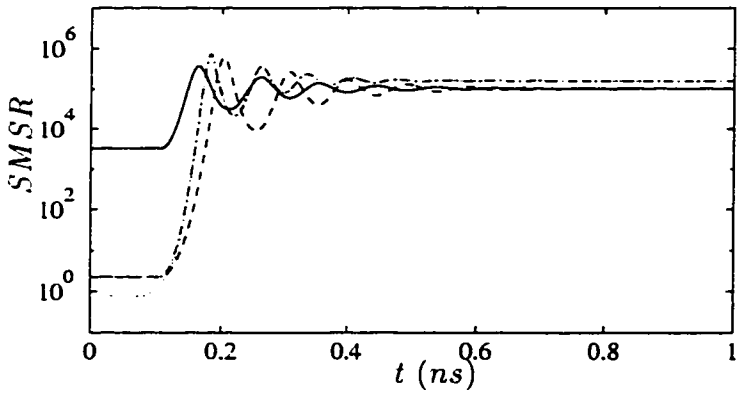

Fig. 9 Effect of the bias on the side mode suppression in antiphase gain-coupled DFB lasers with $|K|L = 3$. Solid line: $I_{off} = I_{th} + 1$ mA and $I_{on} = I_{th} + 40$ mA; dash-dotted line: $I_{off} = I_{th} - 2$ mA and $I_{on} = I_{th} + 50$ mA; dashed line: $I_{off} = I_{th} - 2$ mA and $I_{on} = I_{th} + 40$ mA; dotted line: $I_{off} = I_{th} - 8$ mA and $I_{on} = I_{th} + 65$ mA.

Nonlinear gain compression induces another distributed perturbation in gain-coupled DFB lasers. Multimode rate equation analysis, however, shows in Fig. 10 that the effect only influences the transient $SMSR$ by damping the relaxation oscillation. It does not change the rise time of the transient $SMSR$ since the effect only appears when the light intensity is high enough in the laser cavity. Despite of the same gain deviation $\Delta g(z,t)$, the detailed results show that nonlinear gain compression reduces the power of the lasing mode more and causes an apparent decrease of the $SMSR$ at high power. Physically, this can be understood because the lasing mode is dominant in gain-coupled DFB lasers from the gain coupling effect and the perturbation induced by the nonlinear gain compression is concentrated in the regions where the intensity of lasing mode is high. This, in return, affects the lasing mode most. Because of the stronger enhancement factor of the modal dynamic differential gain $C_i(z)$ [11], Fig. 10 shows that the nonlinear gain compression dampens the $SMSR$ more strongly in antiphase gain-coupled DFB lasers.

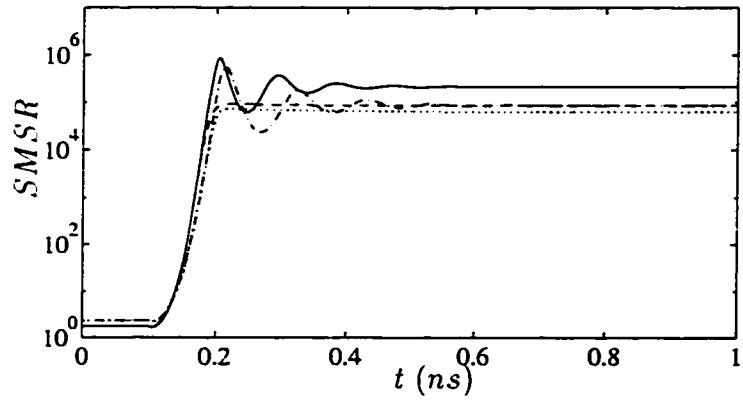

Fig. 10 Effect of the nonlinear gain compression on the side mode suppression in gain-coupled DFB lasers with $|K|L = 4$. Solid line: antiphase gain-coupled with $\varepsilon_N = 0\ cm^3$; dash-dotted line: inphase gain-coupled with $\varepsilon_N = 0\ cm^3$; dashed line: antiphase gain-coupled with $\varepsilon_N = 3 \times 10^{-17}\ cm^3$; dotted line: inphase gain-coupled with $\varepsilon_N = 3 \times 10^{-17}\ cm^3$.

6.5 Conclusion

Based on a spatially dependent multimode rate equation analysis, the transient side mode suppression in gain-coupled DFB lasers has been investigated. By introducing a modal decay rate γ_i into the rate equations, we have studied the side mode dynamics in some details. To first order of perturbation approximation, the study has included various spatially depended features of gain-coupled DFB lasers. Detailed analysis including closed form results has revealed that the transient side mode suppression in DFB lasers depends crucially on the modal decay rate. The gain coupling effectively increases the decay rates of the side modes and hence improves the transient side mode suppression significantly.

REFERENCES

[1] G. P. Li, T. Makino, R. Moore, N. Puetz, K. Leong, and H. Lu, "Partly gain-coupled 1.55 μm strained-layer multi-quantum-well DFB lasers", IEEE J. Quantum Electron., Vol. 29, pp. 1736–1742, 1993.

[2] J. Chen, A. Champagne, R. Maciejko, and T. Makino, "Improvement of single-mode gain margin in gain-coupled DFB lasers", IEEE J. Quantum Electron., Vol. 33, pp. 33–40, 1997.

[3] D. Marcuse, and T. P. Lee, "On approximate analytical solutions of rate equations for studying transient spectra of injection lasers", IEEE J. Quantum Electron., Vol. 19, pp. 1397–1406, 1983.

[4] A. J. Lowery, "New dynamic model for multimode chirp in DFB semiconductor lasers", IEE Proc. Optoelectron., Vol. 137, pp. 293–300, 1990.

[5] C. F. Tsang, D. D. Marcenac, J. E. Carroll, and L. M. Zhang, "Comparison between 'power matrix model' and 'time domain model', in modelling large signal responses of DFB lasers", IEE Proc. Optoelectron., Vol. 141, pp. 89–96, 1994.

[6] L. M. Zhang, and J. E. Carroll, "Large-signal dynamic model of the DFB lasers", IEEE J. Quantum Electron., Vol. 28, pp. 604–611, 1992.

[7] T. Makino, "Effective-index matrix analysis of distributed feedback semiconductor lasers", IEEE J. Quantum Electron., Vol. 28, pp. 434–440, 1992.

[8] J. Chen, R. Maciejko, and T. Makino, "Dynamic properties of push-pull DFB semiconductor lasers", IEEE J. Quantum Electron., Vol. 32, pp. 2156–2165, 1996.

[9] J. Chen, R. Maciejko, and T. Makino, "Self-consistent analysis of side mode suppression in gain-coupled DFB semiconductor lasers", submitted to IEEE J. Quantum Electron..

[10] W. P. Huang, X. Li, and T. Makino, "Analytical formulas for modulation responses of semiconductor DFB lasers", IEEE J. Quantum Electron., Vol. 31, pp. 842–851, 1995.

[11] J. Chen, R. Maciejko, A. Champagne, and T. Makino , "Relaxation oscillation frequency of DFB lasers with gain coupling", IEEE J. Quantum Electron., Vol. 31, pp. 1955–1963, 1995.

[12] X. Pan, B. Tromborg, and H. Olessen, "Complex pole expansion approach to multimode DFB laser modelling", IEE Proc. Optoelectron., Vol. 141, pp. 271–264, 1994.

[13] T. Makino, "Side-mode suppression mechanism of gain-coupled DFB lasers with periodically etched quantum wells", IEEE Photon. Technol. Lett., Vol. 8, pp. 602–604, 1996.

CHAPTER 7

Push-Pull Modulation in Gain-Coupled DFB Lasers

A characteristic feature of semiconductor lasers is that intensity or amplitude modulation (AM) leads simultaneously to phase or frequency modulation (FM). The interdependency between AM and FM under direct current modulation is governed by the linewidth enhancement factor α_M encountered in the previous chapters. It has its origin in the index change that invariably occurs when the optical gain changes in response to variations in the carrier population. Because of the dispersive nature of optical fibers at 1.55 μm, such a phenomenon can cause severe transmission penalties in the high bit-rate and long-haul optical communication systems.

Multicontact push-pull modulation provides new possibilities to modify the DFB semiconductor laser dynamics. Because of the highly localized carrier injection, the frequency dependent feedback and the stable gain coupling, push-pull modulation can cause the lasing mode to couple strongly with particular side modes and hence introduce various new features in the dynamics of DFB semiconductor lasers. The purpose of this chapter is, using the spatially-dependent, coupled, multimode rate equations, to study the behaviours of two-electrode push-pull modulation in gain-coupled DFB lasers. This approach also provides various closed-form results which add physical insight into the modulation mechanism.

Published in IEEE J. Quantum Electron., vol. 32, pp. 2156-2165, 1996

Dynamic Properties of Push-Pull DFB Semiconductor Lasers

Jianyao Chen, Roman Maciejko, *Senior Member, IEEE*
and Toshihiko Makino, *Senior Member, IEEE*

Abstract

Using the spatially-dependent multimode rate equations, we present a systematic study of small signal dynamics of push-pull DFB lasers. The various spatial effects such as the longitudinal spatial hole burning, nonlinear gain compression, side mode contribution and push-pull modulation are all analyzed in a self-consistent manner. With the closed form expressions for the AM and FM responses, we show explicitly that the resonance frequency and the first cut-off frequency of push-pull DFB lasers are determined by the frequency spacing and the threshold gain difference between the lasing mode and its closest antisymmetric side mode, respectively. Numerical results reveal that a high modulation speed with a very low frequency chirp can be achieved with the push-pull DFB lasers.

J. Chen, and R. Maciejko are with the Optoelectronics Laboratory, Department of Engineering Physics, École Polytechnique, P. O. Box 6079, Station "Centre-ville", Montréal, Québec Canada H3C 3A7

T. Makino is with Northern Telecom (Nortel), P. O. Box 3511, Station C, Nepean, Ontario, Canada K1Y 4H7

7.1 Introduction

Although single-mode DFB semiconductor lasers have been the most popular lightwave sources used in the current optical communication systems, their large dynamic frequency chirp under direct modulation combined with the dispersion in optical fibers at 1.55 μm where the loss is the minimum can cause severe transmission penalties in the high bit-rate and long-haul applications. Chirp is caused by the change in the index of refraction induced by carrier injection during modulation as well as the power-dependent photon intensity distribution along the laser cavity. In order to overcome this problem, several methods have been proposed, which include the use of external modulators [1], coupling the laser to an external high-Q resonator [2], master-slave injection locking [3], and shaping the waveform of the injection current [4]. While providing solutions to the problem, those approaches, however, also add to both cost and complexity. Hence, a direct laser modulation technique with low chirp is very desirable for high frequency applications.

It has been reported recently that push-pull modulation can be an effective alternative to achieve low chirp with high-speed modulation of DFB lasers [5]. As illustrated in Fig. 1, the concept of the device is to use two electrical contacts to drive the laser. A uniform bias brings the laser above threshold. Optical power modulation can be achieved by increasing the injection current at one end of the device, while simultaneously decreasing the same amount of injection current at the other end. Since a constant total injection current is maintained in the DFB laser, it gives a very low variation of the mean refractive index induced by the longitudinal spatial hole burning. Hence, the dynamic frequency chirp can be minimized. A diagram illustrating the photon density along the cavity for both 'ON' and 'OFF' states is shown in Fig. 2. Mirror symmetry indicates that both states give the same lasing frequency.

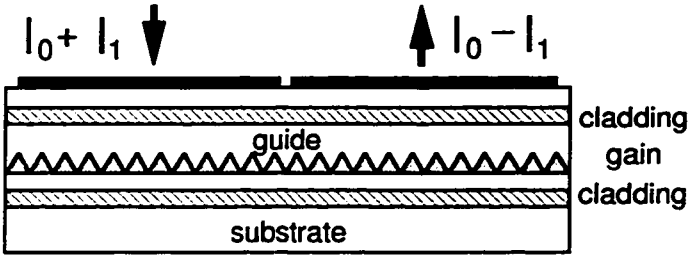

Fig. 1 Schematic structure of a two-contact push-pull DFB laser.

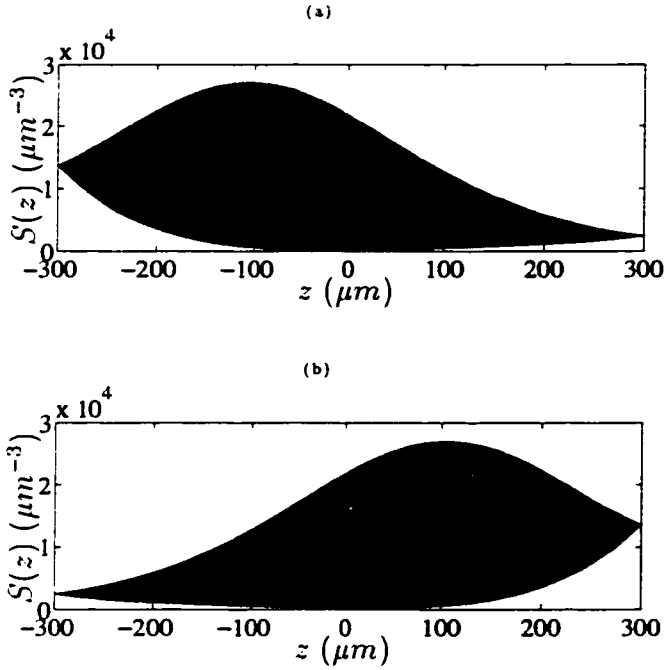

Fig. 2 Photon density distribution in the symmetric gain-coupled push-pull DFB laser. (a) 'ON' state; (b) 'OFF' state.

The push-pull modulation also changes the high frequency performance of DFB lasers. Instead of modulating the photon population globally as in the single contact lasers, push-pull modulation displaces the photon concentration back and forth by changing the carrier population in the two sections. It has been suggested that the modulation bandwidth of the push-pull DFB laser can be much higher than that of the conventional single-contact DFB laser [6, 7].

So far, the theoretical study of push-pull DFB lasers is still very limited and most of the previous analysis was based on travelling wave equations [5, 6, 7]. Closed form results can help us gain more physical insight into the operation of the device and the rate equation analysis is an effective method for the study of the dynamics of push-pull DFB lasers. In this paper, we propose a two-mode interference model. Using the spatially-dependent multimode rate equations, we include the essential features of push-pull DFB lasers such as longitudinal variations of the carrier and photon density distributions, spatially dependent nonlinear gain compression and push-pull current injection rigorously. By performing the small signal analysis, closed form expressions for the AM and FM responses as well as the first cut-off frequency and the structure-dependent resonance frequency are all derived. The results show that the first cut-off frequency and the resonance frequency are determined by the threshold gain difference and the frequency spacing between the lasing mode and its closest antisymmetric mode, respectively.

7.2 Multimode rate equations

We consider general DFB semiconductor lasers in which the waveguide may have an arbitrary type of grating corrugation, including phase shift and facet condition. Moreover, the injection current may also be nonuniformly distributed. To simplify the analysis, we assume that the laser is transversely single-moded and optical fields propagate along z direction. The scalar wave equation can, therefore, be written as:

$$\frac{d^2 E_\omega(z)}{dz^2} + k^2 \varepsilon(z) E_\omega(z) = F_\omega(z) \tag{7.1}$$

where $k = \omega/c$ is the wave number in vacuum. $F_\omega(z)$ represents the Langevin term generating the spontaneous emission. $\varepsilon(z)$ gives the complex dielectric constant including the periodic variation of the Bragg grating. Generally, it can be written

as:

$$\varepsilon(z) = \left\{ n(z) + j\frac{1}{2k}\left[(1 + j\alpha_M)g(N,S) - \alpha_{int}\right]\Gamma(z) \right\}^2 \tag{7.2}$$

where $n(z)$ and $\Gamma(z)$ give the longitudinally dependent index of refraction and transverse modal confinement factor along the DFB grating, respectively. α_M denotes the material linewidth enhancement factor. $g(N,S)$ and α_{int} represent the material gain and waveguide loss in the active region.

Because of the spatial hole burning and the nonlinear gain compression effects in the active region, the dynamic modulation of the DFB laser can cause the complex dielectric constant $\varepsilon(z,N,S)$ to deviate from the stationary value $\bar{\varepsilon}(z,N_0,S_0)$. If we separate the distribution term from $\varepsilon(z)$ and move it to the right hand side of equation (7.1), we get

$$\frac{d^2E_\omega(z)}{dz^2} + k^2\bar{\varepsilon}(z)E_\omega(z) = F_\omega(z) - k^2\Delta\varepsilon(z)E_\omega(z) \tag{7.3}$$

where, to the first order approximation,

$$\Delta\varepsilon(z) = \frac{\partial\varepsilon}{\partial N}\Delta N(z) + \frac{\partial\varepsilon}{\partial S}\Delta S(z) \tag{7.4}$$

$\Delta N(z)$ and $\Delta S(z)$ denote the local deviations of the carrier and photon densities from the steady-state values, $N_0(z)$ and $S_0(z)$.

If we treat the terms on the right hand side of equation (7.3) as a distributed excitation source for the optical field inside DFB lasers, the Green's function analysis gives the solution to the wave equation (7.1) as follows:

$$E_\omega(z) = \int_L G(z,z')[F_\omega(z') - k^2\Delta\varepsilon(z')E_\omega(z')]dz' \tag{7.5}$$

where $G(z,z')$ is the Green's function. In the multimode DFB lasers, we can write the Green's function as [8]:

$$G(z,z') = \sum_i \frac{Z_i(z)Z_i(z')}{W_i} \tag{7.6}$$

where the $Z_i(z)$ are the eigensolutions of the homogeneous wave equation (7.1) and can be regarded as the longitudinal modal field functions. The following orthogonality relation can be shown to hold,

$$\int_L Z_i(z')Z_j(z')dz' = 0 \qquad i \neq j \tag{7.7}$$

W_i in the denominator is defined as

$$W_i = \int_L [k^2\bar{\varepsilon}(\omega) - k_i^2\bar{\varepsilon}(\omega_i)]Z_i^2(z')dz' \tag{7.8}$$

where $k_i = \omega_i/c$. ω_i is the angular resonance frequency of the ith longitudinal mode in the DFB laser and it may be complex if the mode is below the lasing threshold. Complex resonance frequency has been widely used to describe the characteristics of modes in DFB lasers that are under threshold [9]. Its imaginary part represents the gain difference needed to reach threshold for the mode: $\Delta g_{th}^i = 2Im\{\omega_i\}/v_g$ [10].

For small perturbations around the stationary state, an expansion of W_i can be written as:

$$W_i = (\omega - \omega_i)\frac{\partial W_i}{\partial \omega} \tag{7.9}$$

where

$$\frac{\partial W_i}{\partial \omega} = \frac{2k_i}{v_g}\int_L n(z')Z_i^2(z')dz' \tag{7.10}$$

Also, without loss of generality, the total optical field $E(z)$ in the DFB laser can be expanded using the modal eigenfields as follows:

$$E_\omega(z) = \sum_i A_i(\omega + \Delta\omega_i)Z_i(z) \tag{7.11}$$

where $\Delta\omega_i = \omega_0 - Re\{\omega_i\}$. ω_0 is the reference frequency or can be the lasing frequency of the fundamental mode of the DFB laser. We also define

$$A_i(t) = \frac{1}{2\pi}\int_0^\infty A_i(\omega)e^{j(\omega-\omega_0)t}d\omega \tag{7.12}$$

Substituting expressions (7.9) and (7.11) into the equation (7.5) and then applying orthogonality (7.7), we can derive the following set of equations:

$$(\omega-\omega_i)\frac{\partial W_i}{\partial \omega}A_i(\omega+\Delta\omega_i) = -\sum_j A_j(\omega+\Delta\omega_j)\int_L k_i^2\Delta\varepsilon(z')Z_i(z')Z_j(z')dz' + \int_L Z_i(z')F_\omega(z')dz' \tag{7.13}$$

Taking the inverse Fourier transform of the equations, a set of rate equation for the field amplitude $A_i(t)$ can be obtained as follows:

$$\frac{dA_i}{dt} + Im\{\omega_i\}A_i(t) = \sum_j e^{jRe\{\omega_j-\omega_i\}t}A_j(t)\int_L\left[G_N^{ij}(z')\Delta N(z',t)+G_S^{ij}(z')\Delta S(z',t)\right]dz' + F_i(t) \tag{7.14}$$

where the spatial weight functions $G_X^{ij}(z)$ $(X = N,\ S)$ can be regarded as the effective local gain coupling coefficient with respect to changes in carrier and photon densities, respectively. With formulae (7.2) and (7.10), they can be expressed as follows:

$$G_X^{ij}(z) = \frac{1}{2}(1+j\alpha_M)\frac{\partial G}{\partial X}\frac{Z_i(z)Z_j(z)}{\int_L Z_i^2(z')dz'} \tag{7.15}$$

where $G(z,N,S) = v_g\Gamma(z)g(N,S)$ is the stimulated emission rate. The term $F_i(t)$ gives the Langevin noise contribution to the field amplitude

$$F_i(t) = \frac{j}{2\pi}\int_0^\infty \frac{v_g}{2k_i}\frac{\int_L F_\omega(z')Z_i(z')dz'}{\int_L n(z')Z_i^2(z')dz'}e^{jRe\{\omega-\omega_i\}t}d\omega \tag{7.16}$$

Although the time dependency of the carrier and photon densities $\Delta N(z,t)$ and $\Delta S(z,t)$ is not considered in deriving equation (7.14), the result can be justified [11]. An even more rigorous derivation from the time dependent Maxwell's equations can also be made using the Floquet-Bloch expansion approach.

Compared with the conventional multimode photon rate equations [12], it is not difficult to see that the rate equations (7.14) are different since the longitudinal modal couplings have been included explicitly into the variation of the modal photon number. In general, due to the various spatial nonuniformities in DFB lasers, the carrier and photon densities under dynamic modulation can change nonuniformly along the DFB cavity, which may cause the modal orthogonality (7.7) to break down and hence induce couplings between the DFB modes. However, in the single-contact semiconductor lasers, such a modal coupling, because of a uniform injection, is rather weak, i.e.

$$\left|A_i \int_L \left[G_N^{1i}(z')\Delta N(z',t) + G_S^{1i}(z')\Delta S(z',t)\right] dz'\right| << \left|A_1 \int_L \left[G_N^{11}(z')\Delta N(z',t) + G_S^{11}(z')\Delta S(z',t)\right] dz'\right| \qquad (7.17)$$

especially between the symmetric lasing mode and antisymmetric side modes. Moreover, within the single-mode bias range, the large threshold gain difference Δg_{th}^i, produced by DFB structure, also causes the side modes, excited by the spatial gain coupling, to attenuate quickly with a very high decay rate $-Im\{\omega_i\}$. This strongly suppresses the side mode influence on the modulation response of the DFB laser. In that case, the laser dynamics is dominated by the behaviour of a single lasing mode. In the push-pull and other multielectrode DFB lasers, however, a highly localized injection can introduce highly nonuniform variations in the carrier and photon densities in the DFB cavity, which causes modal couplings to become important and hence affect the laser dynamics in a non trivial way as shown below.

7.3 Push-pull DFB laser

In the symmetric push-pull DFB lasers, the uniform bias puts the symmetric fundamental mode above its lasing threshold. The push-pull modulation is akin to

an antisymmetric carrier injection into the laser, which causes the closest antisymmetric side mode to couple strongly with the fundamental mode. Therefore, instead of having an amplitude modulation of the fundamental mode, the power output of the push-pull DFB laser is determined by the interference between the symmetric lasing mode and antisymmetric side mode. Since the bias is set within the single mode operation range, the antisymmetric side mode is still under threshold but nevertheless affects the laser operation! The lasing wavelength is, therefore, determined by the fundamental lasing mode.

For the study of the dynamic properties of the push-pull DFB lasers, we need to include the carrier rate equation as follows:

$$\frac{\partial N}{\partial t} = J(z,t) - R(z,N) - G(z,N,S)S(z,t) \tag{7.18}$$

where

$$J(z,t) = J_0(z) + \delta J(z,t) \tag{7.19}$$

is the laser pumping rate. $J_0(z)$ and $\delta J(z,t)$ correspond to the bias and push-pull modulation, respectively. $R(z,N)$ gives the spontaneous carrier recombination rate. $G(z,N,S)$ is the net rate of the stimulated emission and $S(z,t)$ is the photon density distribution in the laser.

In most of the multimode analysis of semiconductor lasers found in the literature, only the modal intensities interact with the gain function in the carrier rate equation: the contributions from the modal intereference terms are ignored [9, 10, 12]. Such a treatment is justified in conventional DFB lasers, as long as

$$Im\{\omega_i\}|A_i| >> \left| A_1 \int_L \left[G_N^{i1}(z')\Delta N(z',t) + G_S^{i1}(z')\Delta S(z',t) \right] dz' \right| \tag{7.20}$$

since the DFB modes oscillate almost independently in the cavity. The interference effects are smoothed out because the phases are random. In push-pull DFB lasers,

however, the antisymmetric injection induces a strong coupling between the symmetric and antisymmetric modes which causes the closest antisymmetric side mode to oscillate coherently with the lasing mode. The modal interference not only has a strong impact on the modal interaction between the DFB modes, but also influences the stimulated photon emission and hence the laser dynamics strongly, as shown in greater detail by our analysis.

As usual, we denote the optical fields of the symmetric (1) and antisymmetric (2) modes in the push-pull DFB laser as follows:

$$Z_1(z) = Z_1^+(z)e^{-j\beta_0 z} + Z_1^-(z)e^{j\beta_0 z} \tag{7.21}$$

$$Z_2(z) = Z_2^+(z)e^{-j\beta_0 z} + Z_2^-(z)e^{j\beta_0 z} \tag{7.22}$$

where $\beta_0 = \frac{\pi}{\Lambda}$ is the Bragg wavenumber of DFB grating. Then, the photon density distribution inside the push-pull DFB lasers can be written as:

$$S(z,t) = \left|A_1(t)Z_1(z) + e^{-jRe\{\omega_1-\omega_2\}t}A_2(t)Z_2(z)\right|^2 \tag{7.23}$$

Consequently, the output of the push-pull DFB laser is expressed as:

$$P_L = v_g\hbar\omega_1\left[1-|r_m|^2\right]\left|A_1(t) + e^{-jRe\{\omega_1-\omega_2\}t}A_2(t)\right|^2 \tag{7.24}$$

where r_m is the facet reflectivity. For simplicity, we have chosen $Z_1^-(0) = Z_2^-(0) = 1$ at the $z = 0$ facet.

If we denote

$$A_1(t) = [a_0 + \delta a_1(t)]e^{j\phi_1(t)} \tag{7.25}$$

$$e^{-jRe\{\omega_1-\omega_2\}t}A_2(t) = \delta a_2(t)e^{j\phi_2(t)} \tag{7.26}$$

the amplitude and frequency responses of the small-signal modulation on push-pull DFB lasers can be obtained as follows:

$$h_a(t) = 2\frac{\delta a_1}{a_0} + \frac{\delta a_2}{a_0}e^{j\Delta\phi} + \frac{\delta a_2}{a_0}e^{-j\Delta\phi} \tag{7.27}$$

$$h_f(t) = \frac{d\phi_1}{dt} + \frac{j}{2}\frac{d}{dt}\left[\frac{\delta a_2}{a_0}e^{j\Delta\phi} - \frac{\delta a_2}{a_0}e^{-j\Delta\phi}\right] \tag{7.28}$$

since $a_0 >> \delta a_1(t)$ and $a_0 >> \delta a_2(t)$, where

$$\Delta\phi(t) = \phi_1(t) - \phi_2(t) \tag{7.29}$$

The responses are different from the conventional expressions for the amplitude and frequency responses [13, 14, 15]. Equations (7.27) and (7.28) not only include the variation of the lasing mode, but also take into account the contribution from the modal interference, which will be shown next to be significant for push-pull DFB lasers.

By performing the small signal expansion on equations (7.14) and (7.18) and using formulae (7.27) and (7.28), we can derive the amplitude and frequency modulation responses as follows (see Appendix):

$$\frac{\delta a_1(s)}{a_0} = 0 \tag{7.30}$$

$$s\phi_1(s) = 0 \tag{7.31}$$

and

$$H_a(s) = \frac{X_{11}(s)B_1(s) + X_{22}(s)B_2(s)}{X_{11}(s)X_{22}(s) - X_{11}(s)X_{21}(s) - X_{22}(s)X_{12}(s)} \tag{7.32}$$

$$H_f(s) = s\frac{j}{2}\frac{[X_{22} - 2X_{21}(s)]B_2(s) - [X_{11}(s) - 2X_{12}(s)]B_1(s)}{X_{11}(s)X_{22}(s) - X_{11}(s)X_{21}(s) - X_{22}(s)X_{12}(s)} \tag{7.33}$$

where $s = j\Omega$ and

$$X_{11}(s) = s + j(\omega_2^* - \omega_1) \tag{7.34}$$

$$X_{22}(s) = s - j(\omega_2 - \omega_1) \tag{7.35}$$

$$X_{12}(s) = a_0^2 \int_L \left[G_S^{21^*} - \frac{G_N^{21^*}}{s + \Gamma_N}\left(G_0 + \frac{\partial G}{\partial S}|Z_1|^2 a_0^2 \right) \right] Z_1 Z_2^* dz \tag{7.36}$$

$$X_{21}(s) = a_0^2 \int_L \left[G_S^{21} - \frac{G_N^{21}}{s + \Gamma_N}\left(G_0 + \frac{\partial G}{\partial S}|Z_1|^2 a_0^2 \right) \right] Z_1^* Z_2 dz \tag{7.37}$$

$$B_1(s) = \int_L \frac{G_N^{21}\delta J(s)dz}{s + \Gamma_N} \tag{7.38}$$

$$B_2(s) = \int_L \frac{G_N^{21^*}\delta J(s)dz}{s + \Gamma_N} \tag{7.39}$$

Formulae (7.30) and (7.31) indicate that the push-pull modulation hardly modulates the symmetric lasing mode (i.e., up to higher order effects). Hence, the frequency chirp under dynamic modulation can be significantly reduced confirming previous results. Moreover, based on the formulae (7.27) and (7.28), our results also indicate clearly that modal interference plays a dominant role in push-pull DFB laser dynamics since the variation on the lasing main mode contributes very little to the laser modulation responses.

At high frequency, since $s >> \Gamma_N$, formulae (7.32) and (7.33) can be further reduced to

$$H_a(s) = \frac{2s\int_L Re\{G_N^{21}\}\delta J(s)dz + 2\int_L Im\{(\omega_2-\omega_1)G_N^{21^*}\}\delta J(s)dz}{s^3+s^2\gamma_p+s\Omega_R^2+\Omega_C\Omega_R^2} \quad (7.40)$$

$$H_f(s) = \frac{\int_L \left[s^2 Im\{G_N^{21}\}+sRe\{(\omega_2-\omega_1)G_N^{21^*}\}+sA_S+A_N\right]\delta J(s)dz}{s^3+s^2\gamma_p+s\Omega_R^2+\Omega_C\Omega_R^2} \quad (7.41)$$

where

$$\gamma_p = 2Im\{\omega_2\} - 2a_0^2\int_L Re\{G_S^{21}Z_1^*Z_2\}dz \quad (7.42)$$

$$A_S = -2a_0^2 Im\left\{G_N^{21}\int_L G_S^{21^*}Z_1Z_2^*\left[G_0+\frac{\partial G}{\partial S}|Z_1|^2a_0^2\right]dz\right\} \quad (7.43)$$

$$A_N = 2a_0^2 Im\left\{G_N^{21}\int_L G_N^{21^*}Z_1Z_2^*\left[G_0+\frac{\partial G}{\partial S}|Z_1|^2a_0^2\right]dz\right\} \quad (7.44)$$

and

$$\Omega_R^2 = |\omega_2-\omega_1|^2 - 2a_0^2\int_L Im\{(\omega_2-\omega_1)G_S^{21^*}Z_1Z_2^*\}dz + 2a_0^2\int_L Re\{G_N^{12}Z_1^*Z_2\}\left[G_0+\frac{\partial G}{\partial S}|Z_1|^2a_0^2\right]dz \quad (7.45)$$

$$\Omega_C = \frac{2a_0^2}{\Omega_R^2}\int_L Im\{(\omega_2-\omega_1)G_N^{21^*}Z_1Z_2^*\}\left[G_0+\frac{\partial G}{\partial S}|Z_1|^2a_0^2\right]dz \quad (7.46)$$

which can be regarded as the angular resonance frequency and the first cutoff frequency of push-pull modulated DFB laser, respectively.

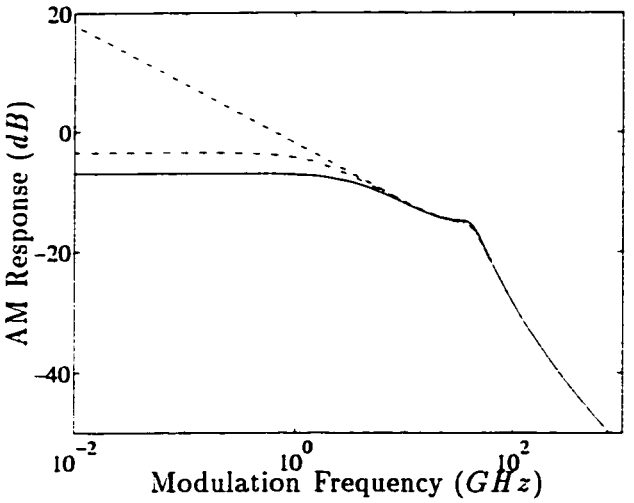

Fig. 3 Comparison of the AM responses of push-pull DFB lasers. Solid line: generated by Eq. (7.32); dash-dotted line: generated by Eq. (7.40); dashed line: generated by Eq. (7.40) with $\Omega_C = 0$.

The above results show that the characteristics of the push-pull modulation response at high frequency is determined by the resonance frequency Ω_R and the first cut-off frequency Ω_C. To verify that numerically, Fig. 3 presents a comparison of intensity modulation response for a gain-coupled DFB laser ($|K|L = 6$, where $K = K_r + jK_i$ is the complex coupling coefficient) using formulae (7.32) and (7.40), respectively. A close agreement between the curves at high frequency demonstrates that both formulae give the same resonance frequency Ω_R at 40 GHz. The dashed line in the figure is obtained by setting $\Omega_C = 0$ in formula (7.40), which reveals that the bend in the solid and dash-dotted curves at around 1 GHz comes from the first cut-off frequency Ω_C. Therefore, we can conclude that formulae (7.45) and (7.46) determine the resonance frequency and the first cut-off frequency for push-pull DFB lasers, respectively.

Because the first term in expression (7.45) is much larger than the second and third terms, we obtain that the resonance frequency and the first cut-off frequency of the push-pull DFB laser are determined by the frequency spacing $Re\{\omega_1 - \omega_2\}$

and the threshold gain difference $2Im\{\omega_1 - \omega_2\}/v_g$ between the lasing mode and its closest antisymmetric side mode, respectively. Since a high frequency AM spectrum requires both a high resonance frequency Ω_R and a high first cut-off frequency Ω_C, we expect that a shorter DFB cavity with a higher threshold gain difference between the lasing mode and the closest antisymmetric side mode is preferred.

7.4 Dynamic behaviour

To clarify the discussion, we analyze a 1.55 μm antireflection-coated DFB laser with an active cross-section of 0.1×1.5 μm^2. The modal confinement factor is assumed to be 0.1. For a stable single-mode operation, we choose an inphase gain-coupled structure for the DFB grating [16]. The waveguide loss is 20 cm^{-1}. The material differential gain equals 6×10^{-16} cm^2; the transparency carrier density, $N_0 = 1.5 \times 10^{18}$ cm^{-3}; the linear carrier lifetime, bimolecular and Auger recombination coefficient, 1 ns, 1×10^{-10} $cm^3 s^{-1}$ and 1.3×10^{-28} $cm^6 s^{-1}$, respectively. The modal index of refraction is 3.23 and the group index of refraction is 3.7.

Using that DFB waveguiding structure, the results of Fig. 4 demonstrate the difference in the small signal responses between the single-contact [15, 17] and push-pull driven lasers. As we can see, push-pull modulation not only suppresses the frequency modulation significantly, but also increases the resonance frequency. After the first cut-off frequency Ω_C at around 1 GHz, a 10 dB per decade fall-off appears in the intensity modulation response and frequency modulation response starts to increase simultaneously. When the modulation frequency approaches the resonance frequency Ω_R at around 40 GHz, a resonance peak appears in the frequency response. This behaviour agrees well with the results presented in reference [7] based on the travelling wave analysis. Beyond the resonance frequency Ω_R, the intensity

modulation efficiency starts to decrease rapidly at 30 dB per decade. Therefore, the characteristics of the push-pull DFB lasers are very promising for the high speed low chirp applications.

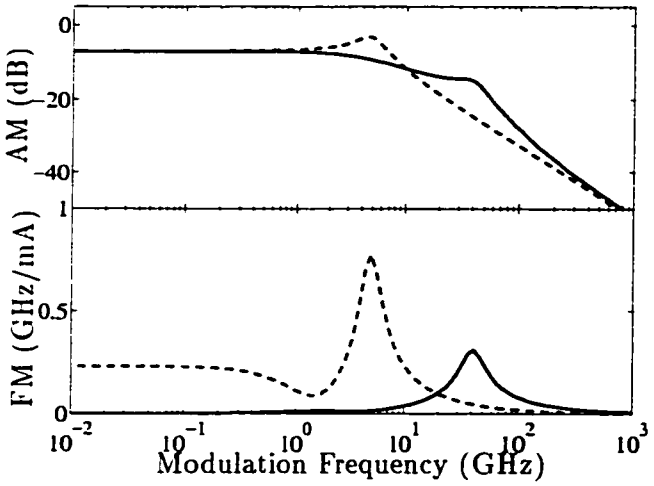

Fig. 4 Comparison of the AM and FM responses between the same DFB device modulated as a single-contact laser (dashed line) or a two-contact push-pull laser (solid line), where $|K|L = 6$, $L = 600$ μm and $I_0 = I_{th} + 20$ mA.

7.4.1 Bias dependency

Formula (7.46) shows that the first cut-off frequency Ω_C is proportional to a_0^2, which indicates that it depends on the optical power linearly. Therefore, by increasing the bias current, Ω_C will also increase, which leads to a higher modulation bandwidth of the push-pull DFB laser [6]. Moreover, Fig. 5(b) shows that the frequency modulation efficiency around the first cut-off frequency Ω_C is also lower at a higher bias current. Both effects contribute to improving the high frequency AM response of push-pull DFB lasers at a high bias current. On the other hand, the curves in the vicinity of the resonance peak in Fig. 5(b) indicate that the position of the resonance frequency Ω_R of push-pull DFB laser does not vary much with

optical power as we indicated above. Although the third term in formula (7.45) is optical power dependent, a careful examination reveals that its variation is typically within a few GHz. Such a difference is not much apparent on the plot because of the scale. The first term, therefore, predominantly determines the resonance frequency Ω_R of the push-pull DFB laser. Below the first cut-off frequency, a careful examination reveals that the frequency modulation efficiency increases slightly at first, then decreases again as the bias current increases further. Such a behaviour is probably related to the longitudinal spatial hole burning in DFB lasers. Although a constant total injection current is kept by the push-pull modulation, the local spatial hole burning will still induce some frequency change as the injection modulates the carrier population.

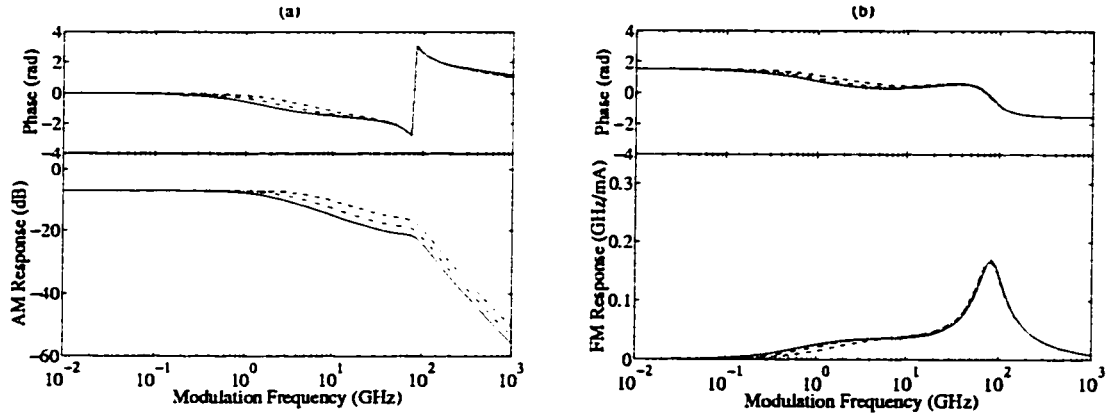

Fig. 5 Modulation responses of push-pull DFB lasers at different bias levels, where $\varepsilon_N = 0$, $|K|L = 3$ and $L = 450\ \mu m$. Solid line: $I_0 = I_{th} + 10\ mA$; dash-dotted line: $I_0 = I_{th} + 20\ mA$; dashed line: $I_0 = I_{th} + 40\ mA$; dotted line: $I_0 = I_{th} + 70\ mA$.

One also notices that the phase of the AM response starts to change at the first cut-off frequency Ω_C, which indicates that possibly a higher group delay distortion may appear when the push-pull DFB laser is modulated at high frequency. Therefore, although it reduces frequency chirp very efficiently, push-pull modulation may not perform better than the conventional single contact modulation at very high bit

rates. Fig. 5 shows that a higher bias current is preferable for improving the AM phase response of push-pull DFB lasers at high frequency.

7.4.2 Coupling coefficient dependency

The grating coupling coefficient plays a major role in determining the characteristics of DFB lasers. It is well known that the DFB grating provides a frequency dependent feedback to the different longitudinal modes. According to the coupled-wave analysis, the threshold gain difference between the modes of DFB lasers increases with the grating coupling coefficient [12]. Therefore, push-pull DFB lasers with a higher coupling coefficient will give a higher first cut-off frequency Ω_C (see Fig. 6). For gain-coupled DFB lasers, however, the increase of the coupling strength of the index grating will reduce the threshold gain of DFB lasers, which leads to a decrease in the coupling strength of the gain grating. Therefore, as the ratio of the real to imaginary parts of the coupling coefficient, K_r/K_i, increases, the first cut-off frequency Ω_C of the gain-coupled push-pull DFB lasers will decrease at first to reach a lowest first cut-off frequency and then increase again (see Fig. 7). Detailed numerical analysis reveals that the lowest first cut-off frequency corresponds to the least amount of spatial hole burning in the gain-coupled DFB lasers. It appears that the nonuniformity of optical field helps to displace the photon population by push-pull modulation. A high coupling coefficient $|K|$ also improves the phase spectrum of the amplitude modulation around the first cut-off frequency Ω_C.

Both Figs. 6 and 7 also show that an increase in the grating coupling coefficient $|K|$ (a higher ratio K_r/K_i corresponds to a higher $|K|$) brings the lasing mode and its side mode closer and decreases the structure-dependent resonance frequency Ω_R monotonically. It appears that a DFB laser with a low coupling strength $|K|L$, in which the photon density is concentrated more at both ends of the laser, will have a higher resonance frequency Ω_R in the case of push-pull modulation. Considering the

effect on the first cut-off frequency Ω_C at same time, one faces a trade-off between those two frequencies for optimizing the high frequency AM response.

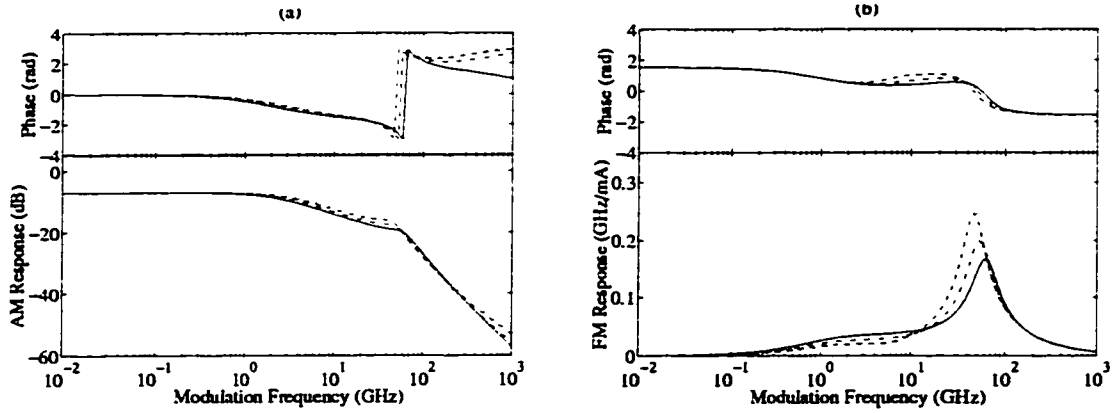

Fig. 6 Modulation responses of push-pull DFB laser with different coupling strengths $|K|L$, where $\varepsilon_N = 0$, $I_0 = I_{th} + 20\ mA$ and $L = 600\ \mu m$. Solid line: $|K|L = 3$; dash-dotted line: $|K|L = 4$; dashed line: $|K|L = 5$; dotted line: $|K|L = 6$.

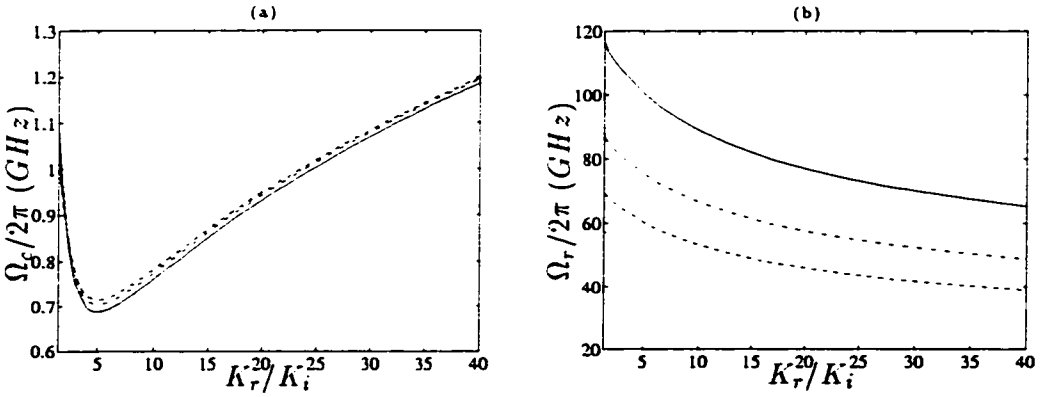

Fig. 7 Dependency of the first cut-off frequency $F_C = \Omega_C/2\pi$ (a) and the resonance frequency $F_R = \Omega_R/2\pi$ (b) on the complex coupling coefficient $K = K_r + jK_i$. Solid line: $L = 450\ \mu m$; dash-dotted line: $L = 600\ \mu m$; dashed line: $L = 750\ \mu m$; dotted line: $L = 900\ \mu m$.

In the case of frequency modulation, a high $|K|$ increases the resonance peak significantly. However, it reduces the frequency modulation efficiency in the range between the first cut-off frequency Ω_C and the resonance frequency Ω_R. Detailed

numerical analysis indicates that the least amount of spatial hole burning in the DFB laser gives the lowest resonance peak in the frequency modulation response. line:

7.4.3 Cavity length dependency

Since the frequency spacing between the DFB cavity modes is inversely proportional to the length of the DFB laser cavity, choosing a shorter cavity length will increase the spacing between the lasing mode and its side mode. Hence, the laser resonance frequency Ω_R can increase rapidly as we reduce the DFB cavity length. Fig. 8 shows that, by increasing the cavity length from 900 μm to 450 μm, the resonance frequency Ω_R increases from from 40 GHz to 85 GHz. Such results confirm that the structure resonance plays an important role in determining the resonance frequency Ω_R.

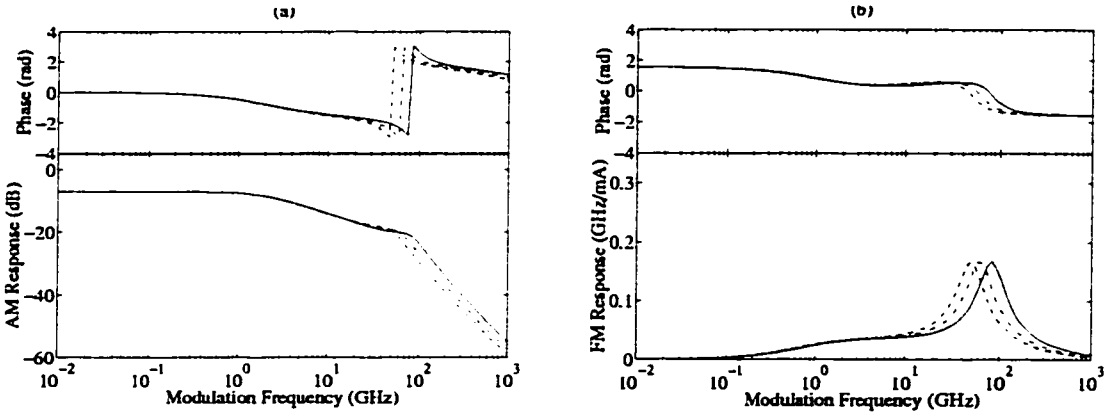

Fig. 8 Modulation responses of push-pull DFB laser with different cavity lengths, where $\varepsilon_N = 0$, $|K|L = 3$ and $I_0 = I_{th} + 20\ mA$. Solid line: $L = 450\ \mu m$; dash-dotted line: $L = 600\ \mu m$; dashed line: $L = 750\ \mu m$; dotted line: $L = 900\ \mu m$.

However, the first cut-off frequency Ω_C shows very little dependency on the DFB cavity length. Both intensity and frequency modulation responses in Fig. 8 show that, in spite of a large change in the length of the DFB cavity, a nearly constant first

cut-off frequency Ω_C is obtained when the coupling strength $|K|L$ is kept constant (see Fig. 7 also). In other words, the first cut-off frequency Ω_C is determined by the coupling strength $|K|L$, while the resonance frequency Ω_R is more sensitive to the cavity length L. We therefore conclude that a short DFB cavity with a high coupling coefficient $|K|$ will be preferred for the improvement of the high frequency performance of push-pull DFB lasers.

7.4.4 Gain compression coefficient dependency

Gain compression increases the damping term γ_p (see (7.42)). Therefore, as we can see from Fig. 9, the intensity modulation response of the push-pull DFB laser with a larger gain compression coefficient falls off more rapidly after the first cut-off frequency. The phase of the intensity modulation response also varies more in presence of a higher gain compression coefficient. In contrast to the conventional single-contact driven DFB lasers, gain compression increases the structure-dependent resonance frequency Ω_R slightly. The second term in expression (7.45) indicates that effect more clearly. Moreover, because of (7.46), this can also cause the first cut-off frequency Ω_C to decrease.

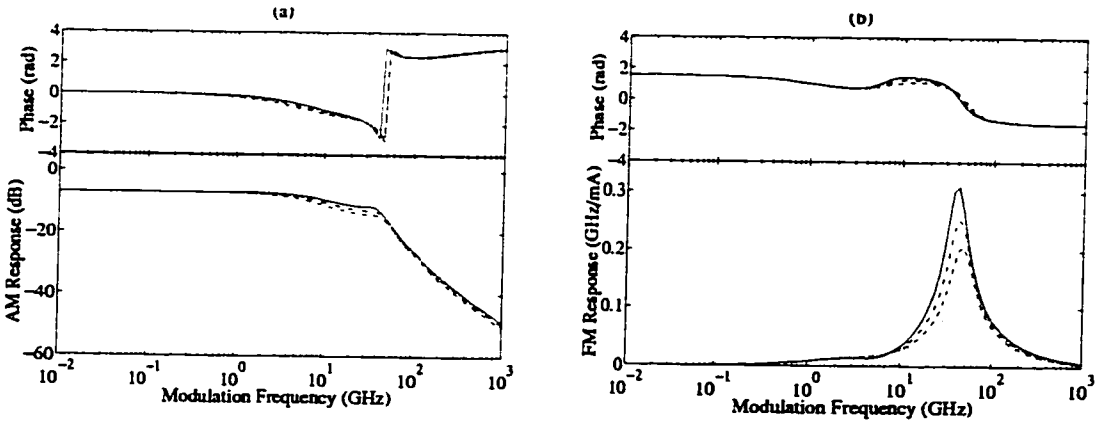

Fig. 9 Modulation responses of push-pull DFB laser with different gain compression coefficient ε_N, where $I_0 = I_{th} + 40\ mA$, $|K|L = 6$ and $L = 600\ \mu m$. Solid line: $\varepsilon_N = 0$; dash-dotted line: $\varepsilon_N = 3$; dashed line: $\varepsilon_N = 6$; dotted line: $\varepsilon_N = 10$.

In the frequency modulation response, the peak around the resonance frequency Ω_R also decreases significantly as the gain compression coefficient increases. Since a very low variation of the mean index of refraction is obtained with the push-pull modulation in DFB lasers and since gain compression always has a tendency to homogenize the carrier distribution, very little effect is seen in the frequency modulation response around the first cut-off frequency Ω_C.

7.5 Conclusion

We have presented a systematic study of the small signal dynamics of push-pull DFB lasers. A two-mode interference model is proposed to understand the operation of the device. Using the spatially-dependent multimode rate equations based on the Green's function analysis, the dynamical properties of push-pull DFB lasers are investigated analytically and numerically. The closed form expressions for the intensity and frequency modulation responses indicate that the high frequency performance of push-pull DFB lasers is characterized by the first cut-off frequency and the structure dependent resonance frequency. We have also shown that the first cut-off frequency and the resonance frequency of push-pull DFB lasers are determined by the threshold gain difference and the frequency spacing between the lasing mode and its closest antisymmetric side mode, respectively. Both our analytical and numerical results agree well with previously published travelling wave analysis [7], which supports the view that the two-mode interference model is an effective approach to investigate the dynamic performance of push-pull DFB lasers. The discussion of the various spatially dependent effects shows that direct push-pull modulation of DFB lasers can produce a very low frequency chirp in high frequency applications.

APPENDIX

In our study of the dynamics of push-pull DFB lasers, we neglect the Langevin noise terms in the rate equations and assume that the small signal carrier density can be written as follows:

$$N(z,t) = N_0(z) + \delta N_1(z,t) + \delta N_2(z,t) \tag{7.47}$$

where the functions $J_0(z)$, $N_0(z)$, $\delta N_1(z,t)$ are symmetric and $\delta J(z,t)$, $\delta N_2(z,t)$ are antisymmetric function of z relative to the laser center. Together with equations (7.25) and (7.26) and the truncated Taylor expansions of $R(N)$ and $G(N,S)$ about the stationary values $N_0(z)$ and $S_0(z)$, the amplitudes of the modulated carrier densities can be obtained from the carrier rate equations (7.18) as follows:

$$\frac{d\delta N_1}{dt} = -\Gamma_N \delta N_1 - 2a_0\delta a_1 \left[G_0 + \frac{\partial G}{\partial S}|Z_1|^2 a_0^2\right] |Z_1|^2 \tag{7.48}$$

$$\frac{d\delta N_2}{dt} = \delta J - \Gamma_N \delta N_2 - a_0\delta a_2 \left[G_0 + \frac{\partial G}{\partial S}|Z_1|^2 a_0^2\right] \left[Z_1 Z_2^* e^{j\Delta\phi} + Z_1^* Z_2 e^{-j\Delta\phi}\right] \tag{7.49}$$

where

$$\Gamma_N = \frac{\partial R}{\partial N} + \frac{\partial G}{\partial N}|Z_1(z)|^2 a_0^2 \tag{7.50}$$

Similarly, from the photon rate equations (7.14), we also get

$$\frac{d}{dt}\frac{\delta a_1}{a_0} = \int_L \left[Re\{G_N^{11}\}\delta N_1 + 2a_0\delta a_1 Re\{G_S^{11}\}|Z_1|^2\right] dz \tag{7.51}$$

$$\frac{d\phi_1}{dt} = \int_L \left[Im\{G_N^{11}\}\delta N_1 + 2a_0\delta a_1 Im\{G_S^{11}\}|Z_1|^2\right] dz \tag{7.52}$$

and

$$\left[\frac{d}{dt} + j(\omega_1 - \omega_2)\right] \frac{\delta a_2}{a_0} e^{-j\Delta\phi} = \int_L \left[G_N^{21}\delta N_2 + a_0\delta a_2 G_S^{21}\left(Z_1 Z_2^* e^{j\Delta\phi} + Z_1^* Z_2 e^{-j\Delta\phi}\right)\right] dz \tag{7.53}$$

$$\left[\frac{d}{dt} - j(\omega_1 - \omega_2^*)\right] \frac{\delta a_2}{a_0} e^{j\Delta\phi} = \int_L \left[G_N^{21^*}\delta N_2 + a_0\delta a_2 G_S^{21^*}\left(Z_1 Z_2^* e^{j\Delta\phi} + Z_1^* Z_2 e^{-j\Delta\phi}\right)\right] dz \tag{7.54}$$

To obtain the equations (7.51)-(7.54), we have used the symmetry of the functions $G_N^{ij}(z)$ and $\delta N_i(z,t)$. The higher order terms are also neglected in the derivation in order to linearize the equations. Finally, by taking the Laplace transform of the above time-dependent equations (7.48)-(7.54) and using formulae (7.27) and (7.28), we can obtain the amplitude and frequency modulation responses (7.32) and (7.33) as well as (7.30) and (7.31) for push-pull DFB lasers.

REFERENCES

[1] I. Kotaka , K. Wakita , M. Okamoto , H. Asai , and Y. Kondo , "A low-drive-voltage, high-speed monolithic multiple-quantum-well modulator/DFB laser light source", IEEE Photon. Tech. Lett., Vol. 5, pp. 61–63, 1993.

[2] J. C. Cartledge, "Improved transmission performance resulting from the reduced chirp of a semiconductor laser coupled to an external high-Q resonator", IEEE J. Lightwave Technol., Vol. 8, pp. 716-721, 1990.

[3] J. C. Cartledge , "Theoretical performance of multigigabit-per-second lightwaves system using injection-locked semisonductor lasers", IEEE J. Lightwave Technol., Vol. 8, pp. 1017–1022, 1990.

[4] L. Bickers and L. D. Westbrook , "Reduction of laser chirp in 1.55 μm DFB laser by modulation pulse shaping", Electron. Lett., Vol. 21, pp. 103–104, 1985.

[5] M. C. Nowell , L. M. Zhang , J. E. Carroll , and M. J. Fice , "Chirp reduction using push-pull modulation of three-contact lasers", IEEE Photon. Tech. Lett., Vol. 5, pp. 1368–1370, 1993.

[6] D. D. Marcenac , M. C. Nowell , and J. E. Carroll , "Theory of enhanced amplitude modulation bandwidth in push-pull modulation DFB lasers", IEEE Photon. Tech. Lett., Vol. 6, pp. 1309–1311, 1994.

[7] M. C. Nowell , J. E. Carroll , R. G. S. Plumb , D. D. Marcenac , M. J. Robertson , H. Wickes , and L. M. Zhang , "Low chirp and enhanced-resonant frequency by direct push-pull modulation of DFB lasers", IEEE J. Selected Topics in Quantum Electron., Vol. 1, pp. 433–441, 1995.

[8] C. H. Henry , "Theory of spontaneous emission noise in open resonator and it application to lasers and optical amplifiers", IEEE J. Lightwave Technol., Vol. 4, pp. 288–297, 1986.

[9] X. Pan, B. Tromborg, and H. Olesen, "Complex pole expansion approach to multimode DFB laser modelling", IEE Proc. Optoelectron., Vol. 141, pp. 271–274, 1994.

[10] R. Bonello, and I. Montrosset, "Analysis of multisection and multielectrode semiconductor lasers", IEEE J. Lightwave Technol., Vol. 10, pp. 1890–1900, 1992.

[11] H. Wenzel and H. J. Wunsche , "An equation for the amplitudes of the modes in semiconductor lasers", IEEE J. Quantum Electron., Vol. 30, pp. 2073–2080, 1994.

[12] G. P. Agrawal and N. K. Dutta , *Long-Wavelength Semiconductor Lasers.* New York: Van Nostrand Reinhold, 1986.

[13] B. Tromborg , H. Olesen , and X. Pan , "Theory of linewidth for multielectrode laser diodes with spatial distributed noise sources", IEEE J. Quantum Electron., Vol. 27, pp. 178–192, 1991.

[14] T. Makino, "Transfer-matrix theory of the modulation and noise of multielement semiconductor lasers", IEEE J. Quantum Electron., Vol. 29, pp. 2762–2770, 1993.

[15] W. P. Huang, X. Li, and T. Makino, "Analytical formulas for modulation responses of semiconductor DFB lasers", IEEE J. Quantum Electron., Vol. 31, pp. 842–851, 1995.

[16] A. J. Lowery, B. Jonsson, H. Olesen, and D. Novak, "Mode instabilities in complex-coupled DFB semiconductor lasers", Electron. Lett., Vol. 31, pp. 40–41, 1995.

[17] J. Chen, R. Maciejko, A. Champagne and T. Makino, "Relaxation oscillation frequency of DFB lasers with gain coupling", IEEE J. Quantum Electron., Vol. 31, pp.1443–1450, 1995.

CHAPTER 8

Conclusion

8.1 Summary

As fundamental building blocks with the most promising performance in optical fiber communication systems, distributed feedback (DFB) semiconductor lasers need to be studied in depth for further design improvement. The goal of this dissertation was, through a comprehensive modelling and analysis, to reach a thorough understanding of the gain coupling effect including various spatial features on the properties of advanced DFB semiconductor lasers.

The first step was to develop a versatile mathematics model for efficient and accurate simulation of gain-coupled DFB lasers. To retain the beauty of the rate equation analysis which leads to closed-form results, the standing wave formalism was extended to multimode and full bias range modelling (from below to above threshold). Using both the Green's function analysis and the coupled mode expansion, a set of spatially dependent multimode rate equations were derived for the first time. With such a formalism, the calculations are separated into two steps. Step one concentrates on the DFB modal field analysis, which can be achieved by solving the coupled wave equations or the transfer matrix of the local normal wave analysis. Various spatial features, such as the asymmetric facet reflection, the multiple phase shift, and the distributed complex coupling are included at this step. Step

two concentrates on the analysis of the temporal variation in DFB lasers. By solving the photon rate equations with the carrier rate equation simultaneously, the modal amplitude fluctuations and the frequency chirp can be simulated for an arbitrary time-dependent injection modulation. Following the need, the formalism can be performed either self-consistently or perturbatively.

The second part of this research was to apply the developed model to investigate the practical features of gain-coupled DFB laser. The study performed in this dissertation covered a wide range of DFB laser physics. With the help of rate equation analysis, various simple and insightful closed-form results were derived. Special attention was paid to several characteristics of DFB semiconductor laser and led to significant contributions, summarized as follows:

1. A systematic investigation of the single-mode condition in gain-coupled DFB lasers has been conducted. The study provided an intuitive explanation of the distributed single-mode selection mechanism of gain-coupled DFB lasers and revealed for the first time that the unequal section lengths of the gain grating have a significant effect on the single-mode yield of DFB lasers in terms of the gain margin. The influence of various structural and material parameters on the laser threshold condition were also analyzed in detail.

2. Based on the analysis of a discrete coupled mode expansion, a self-consistent multimode modelling of gain-coupled DFB lasers has been provided. By introducing the modal net gain parameter into the coupled-wave equations, a set of spatially-dependent, multimode, photon rate equations was derived for the first time. Various spatial effects, including inphase or antiphase gain coupling, spatial hole burning and the effect of nonlinear gain compression on the side mode suppression ratio in gain-coupled DFB lasers were investigated systematically.

3. A comprehensive analysis of the relaxation oscillation frequency of gain-coupled DFB lasers has been performed. By including spatial hole burning, nonlinear gain compression, and gain saturation effects simultaneously, it provides a generalized analysis of all types of semiconductor lasers. The study successfully explained the mechanism of modulation bandwidth broadening in gain-coupled DFB lasers. Thanks to closed-form results, the impact of the material linewidth enhancement factor α_M on the relaxation oscillation frequency of gain-coupled DFB lasers was also revealed for the first time.

4. Using the spatially dependent rate equations, an analysis of the second-order harmonic distortion in gain-coupled DFB lasers was performed. The study is useful for device applications in analog optical communications. The effects of inphase and antiphase gain coupling, including various spatial feature, were discussed systematically. The results showed analytically that spatial hole burning and the relaxation oscillation dominate in the second-order harmonic distortions at low and high frequency, respectively. Also, the possible cancellations of harmonic distortions between different nonlinearity sources were shown clearly.

5. The extension of rate equation analysis to the transient dynamics of gain-coupled DFB lasers including various spatially dependent features has been accomplished successfully. The study systematically investigated the side mode fluctuations in gain-coupled DFB lasers during the transient period. It was shown for the first time that the high decay rate and the low dynamic differential gain contribute significantly to the transient side mode suppression in gain-coupled DFB lasers. The model also provided significant advantages in numerical computation.

6. A new theoretical model was proposed for the analysis of push-pull gain-coupled DFB lasers. In this model, the interference between the lasing mode and its closest antisymmetric side mode is included in the analysis of the laser dynamics. Using the spatially dependent multimode rate equations, the analysis proved analytically that the laser response is characterized by the power-dependent first cut-off frequency and the structure-dependent resonance frequency. Various analytical and numerical results contributed to an in-depth understanding of push-pull DFB lasers in high frequency applications.

8.2 Recommendations

Although successful modelling and analysis of gain-coupled DFB lasers has been reached in this dissertation, the deep potential and sophisticated features of those devices are far from being exhausted. The following improvements could be considered in the future:

1. The analysis of gain-coupled DFB lasers in this dissertation assumed a uniform carrier injection under the contacts in order to simplify device modelling, it does not consider the effect of the longitudinal variation of the quasi-Fermi level separation in the active region. It has been shown that this effect causes a nonuniform carrier injection and reduces the spatial hole burning in DFB lasers [Bandelow *et al.*, 1992]. With a periodically varying active layer, such an effect may impact the performance of gain-coupled DFB lasers. Although it is straightforward to extend the multimode model to nonuniform carrier injection, a computer-effective approach needs to be developed for self-consistency.

2. Carrier transport should also be considered for the multiple quantum well DFB lasers. The effect is related to the carrier nonuniformity in quantum

wells, barriers and confinement layers [Nagaranjan *et al.*, 1992]. Although the effect is confined mainly to the transverse dimension, it can be related to the longitudinal carrier dynamics because of the spatial hole burning effect and the nonuniform quasi-Fermi level separation in the active regions. For gain-coupled DFB lasers, the direct etching of the active layer also induces carrier side-injection into high-gain regions. Such an effect can also influence gain coupling as well as gain dynamics in the DFB lasers [Champagne *et al.*, 1996].

3. An more accurate material gain model should be used to replace the frequency independent phenomenalogical expression adopted in this dissertation. Especially for the multiple quantum well DFB lasers, a narrower gain spectrum, a nonlinear carrier density dependency and a nonuniform carrier distributions all bring new characteristics to the static and dynamic characteristics of gain-coupled DFB lasers. Although it is not very realistic to attempt doing this from first principle, it is possible to find a compromise between efficiency and complexity [Makino, 1996].

4. So far, in most of the literature, including this dissertation, only guided-modes were considered in the analysis. Such a treatment is justified for the first-order-grating feedback lasers since there are no high-order refraction beams involved in the light emission process. In some applications, however, high order grating feedback is utilized because of application requirements and fabrication ease. To simulate such DFB lasers, it is necessary to include the radiative modes since a significant amount of the optical power is radiated away by the high order beams. For gain-coupled high-order DFB lasers, such a study could be very interesting.

5. Our preliminary analysis of two-contact push-pull DFB lasers also suggests that more advanced features can be obtained by applying multicontact modulation to DFB lasers, if done properly. With a compact structure and new design flexibility, multicontact modulation can be expected to become important in high frequency application of DFB lasers, especially for gain-coupled DFB lasers.

In conclusion, gain coupling introduces many advantageous features for the improvement of DFB lasers. As new applications emerge and device fabrication technologies develop, gain-coupled DFB lasers with new advanced features will certainly appear and play an increasingly important role in the future of optical communication systems. Following this progress modelling and analysis of gain-coupled DFB lasers will become even more challenging.

BIBLIOGRAPHY

ADAMS, D. M., MAKINO, T., CHAMPAGNE, A., CHEN, J., and MACIEJKO, R., 1996, *Yield enhancement due to carrier-injection behavior in truncated-well truncated-well gain-coupled DFB's*, CLEO '96, Anaheim, U. S. A., June.

AGRAWAL, G. P. and DUTTA, N. K., 1993, *Semiconductor Lasers*, New York, Van Nostrand Reinhold.

BANDELOW, U., WENZEL, H., and WÜNSHE, H. J., 1992, "Influence of inhomogeneous injection on sidemode suppression in strongly coupled DFB semiconductor lasers", *Electron. Lett.*, vol. 28, p. 1324–1326.

CHAMPAGNE, A., MACIEJKO, R., and MAKINO, T., 1996, "Enhanced carrier injection efficiency from lateral current injection in multiple-quantum-well DFB lasers", *IEEE Photon. Tech. Lett.*, vol. 8, p. 749–751.

CHEN, J., CHAMPAGNE, A., MACIEJKO, R., and MAKINO, T., 1996, *Threshold condition of single-mode gain-coupled DFB lasers*, ICAPT '96, Montreal, Canada, July.

CHEN, J., CHAMPAGNE, A., MACIEJKO, R., and MAKINO, T., 1997, "Improvement of single-mode gain margin in gain-coupled DFB lasers", *IEEE J. Quantum Electron.*, vol. 33, p. 33–40.

CHEN, J., MACIEJKO, R., , and MAKINO, T., 1995, *A Green's function analysis of second harmonic distortion in gain-coupled DFB lasers*, CAM '95, Quebec, Canada, June.

CHEN, J., MACIEJKO, R., CHAMPAGNE, A., and MAKINO, T., 1995, *Enhanced resonance frequency of gain-coupled DFB lasers*, CLEO '95, Baltimore, U. S. A., May.

CHEN, J., MACIEJKO, R., CHAMPAGNE, A., and MAKINO, T., 1995, "Relaxation oscillation frequency of DFB lasers with gain coupling", *IEEE J. Quantum Electron.*, vol. 31, p. 1955–1963.

CHEN, J., MACIEJKO, R., and MAKINO, T., "Self-consistent analysis of side mode suppression in gain-coupled DFB semiconductor lasers", *Submitted to IEEE J. Quantum Electron.*

CHEN, J., MACIEJKO, R., and MAKINO, T., "Transient side mode suppression in gain-coupled DFB lasers", *Submitted to IEEE J. Quantum Electron.*

CHEN, J., MACIEJKO, R., and MAKINO, T., 1995, "Second-order harmonic distortion in AM response of gain-coupled DFB lasers", *Intl. J. of Optoeletron.*, vol. 10, p. 139–149.

CHEN, J., MACIEJKO, R., and MAKINO, T., 1996, "Dynamic properties of push-pull DFB semiconductor lasers", *IEEE J. Quantum Electron.*, vol. 32, p. 2156–2165.

CHEN, J., MACIEJKO, R., and MAKINO, T., 1996, "High resonance frequency of push-pull distributed feedback lasers", *J. Appl. Phys.*, vol. 79, p. 8914–8916.

CHEN, J., MACIEJKO, R., and MAKINO, T., 1996, *High side mode suppression in gain-coupled DFB lasers*, LEOS '96, Boston, U. S. A., Nov.

CHEN, J., MACIEJKO, R., and MAKINO, T., 1996, *Mode proximity and frequency response of push-pull DFB lasers*, CLEO '96, Anaheim, U. S. A., June.

COST 240 Group, 1994, "Comparison of different DFB laser models within the Eroupean COST 240 collaboration", *IEE Proc. -Optoeletron.*, vol. 141, p. 82–88.

DAVID, K., MORTHIER, G., VANKWIKELBERGE, P., and BAETS, R. G., 1991, "Gain-coupled DFB lasers versus index-coupled and phase-shifted DFB lasers: a comparison based on spatial hole burning corrected yield", *IEEE J. Quantum Electron.*, vol. 27, p. 1714–1723.

DOI, A., FUKUZAWA, T., NAKAMURA, M., ITO, R., and AIKI, K., 1979, "InGaAsP/InP distributed feedback injection lasers fabricated by one-step liquid phase expitaxy", *Appl. Phys. Lett.*, vol. 35, p. 441–443.

HAUS, H. A. and SHANK, C. V., 1976, "Antisymmetric taper of distributed feedback lasers", *IEEE J. Quantum Electron.*, vol. 12, p. 532–539.

HENRY, C. H., 1986, "Theory of spontaneous emission noise in open resonator and its application to lasers and optical amplifiers", *IEEE J. Lightwave Technol.*, vol. 4, p. 288–297.

HUANG, W. P., LI, X., and MAKINO, T., 1995, "Analytical formulas for modulation responses of semiconductor DFB lasers", *IEEE J. Quantum Electron.*, vol. 31, p. 842–851.

KOGELNIK, H. and SHANK, C. V., 1971, "Stimulated emission in a periodic structure", *Appl. Phys. Lett.*, vol. 18, p. 152–154.

KOGELNIK, H. and SHANK, C. V., 1972, "Coupled-wave theory of distributed feedback lasers", *J. Appl. Phys.*, vol. 43, p. 2327–2335.

KUDO, K., ARAI, S., and SHIM, J. I., 1993, "Linewidth reduction of dsm lasers due to effects of composite cavity and distributed reflectors", *IEEE J. Quantum Electron.*, vol. 29, p. 1769–1781.

LEE, T. P., 1991, "Recent advances in long-wavelength semiconductor lasers for optical fiber communications", *Proc. of IEEE*, vol. 79, p. 253–275.

LI, G. P. and MAKINO, T., 1993, "Single-mode yield analysis of partly gain-coupled multiquantum-well DFB lasers", *IEEE Photon. Tech. Lett.*, vol. 5, p. 1282–1284.

LI, G. P., MAKINO, T., MOORE, R., PUETZ, N., LEONG, K., and LU, H., 1993, "Partly gain-coupled 1.55 μm strained-layer multi-quantum-well DFB lasers", *IEEE J. Quantum Electron.*, vol. 29, p. 1736–1742.

LOWERY, A. J., 1990, "New dynamic model for multimode chirp in DFB semiconductor lasers", *IEE Proc. -Optoeletron.*, vol. 137, p. 293–300.

LU, H., BLAAUW, C., BENYON, B., LI, G. P., and MAKINO, T., 1995, "High-power and high-speed performance of $1.3 - \mu m$ strained MQW gain-coupled DFB lasers", *IEEE J. Selected Topics in Quantum Electron.*, vol. 1, p. 375–381.

LU, H., MAKINO, T., and LI, G. P., 1995, "Dynamic properties of partly gain-coupled $1.55 - \mu m$ DFB lasers", *IEEE J. Quantum Electron.*, vol. 31, p. 1443–1450.

LUO, Y., NAKANO, Y., TADA, K., INOUE, T., HOSOMATSU, H., and IWAOKA, H., 1991, "Fabrication and characteristics of gain-coupled DFB lasers with a corrugated active layer", *IEEE J. Quantum Electron.*, vol. 27, p. 1724–1731.

MAKINO, T., 1993, "Transfer-matrix theory of the modulation and noise of multielement semiconductor lasers", *IEEE J. Quantum Electron.*, vol. 29, p. 2762–2770.

MAKINO, T., 1996, "Analytical formulas for the optical gain of quantum wells", *IEEE J. Quantum Electron.*, vol. 32, p. 493–501.

NAGARANJAN, R., ISHIKAWA, M., FUKUSHIMA, T., GEELS, R. S., and BOWERS, J. E., 1992, "High-speed quantum-well lasers and carrier transport effects", *IEEE J. Quantum Electron.*, vol. 28, p. 1990-2008.

NAKAMURA, M., AIKI, A., UMEDA, J., and YARIV, A., 1975, "CW operation of distributed feedback GaAs-GaAlAs diode lasers at temperatures up to 300 K", *Appl. Phys. Lett.*, vol. 27, p. 403–405.

NAKAMURA, M., AIKI, A., UMEDA, J., YARIV, A., YEN, H. W., and MORIKAWA, T., 1974, "GaAs-GaAlAs double-heteostructure distributed feedback diode lasers", *Appl. Phys. Lett.*, vol. 25, p. 487–488.

NAKAMURA, M., YARIV, A., YEN, H. W., and SOMEKH, S., 1973, "Optically pumped GaAs surface laser with corrugation feedback", *Appl. Phys. Lett.*, vol. 22, p. 515–516.

NAKANO, Y., DEGUCHI, Y., IKEDA, K., LUO, Y., and TADA, K., 1991, "Reduction of excess intensity noise induced by external reflection in gain-

coupled distributed feedback semicondutor lasers", *IEEE J. Quantum Electron.*, vol. 27, p. 1732–1735.

NAKANO, Y., LUO, Y., and TADA, K., 1989, "Facet reflection independent, single longitudinal mode oscillation in a GaAlAs/GaAs distributed feedback laser equipped with a gain-coupled mechanism", *Appl. Phys. Lett.*, vol. 55, p. 1606–1608.

NAKANO, Y., UCHIDA, Y., and TADA, K., 1992, "Highly efficient single longitudinal-mode oscillation capability of gain-coupled distributed feedback semiconductor lasers - advantage of asymmetric facet coating", *IEEE Photon. Tech. Lett.*, vol. 4, p. 308–311.

SCIFRES, D. R., BURNHAM, D. R., and STREIFER, W., 1974, "Distributed feedback single heterostructure laser", *Appl. Phys. Lett.*, vol. 25, p. 203–205.

SEKARTEDJO, K., EDA, N., FURUYA, K., SUEMATSU, Y., KOYAMA, F., and TANBUN-EK, T., 1984, "1.5 μm phase-shifted DFB lasers for single mode operation", *Electron. Lett.*, vol. 20, p. 80–81.

SODA, H., KOTAKI, Y., SUDO, H., ISHIKAWA, H., YAMAKOSHI, S., and IMAI, H., 1987, "Stability in single longitudinal mode operation in GaInAsP/InP phase-adjusted DFB lasers", *IEEE J. Quantum Electron.*, vol. 23, p. 804–814.

STREIFER, W., BURNHAM, R., and SCIFRES, D. R., 1975, "Effect of external reflectors on longitudinal modes of distributed feedback lasers", *IEEE J. Quantum Electron.*, vol. 11, p. 154–161.

SUEMATSU, Y., IGA, K., and ARAI, S., 1992, "Advanced semiconductor lasers", *Proc. of IEEE*, vol. 80, p. 383–397.

TROMBORG, B., OLESEN, H., and PAN, X., 1991, "Theory of linewidth for multielectrode laser diodes with spatial distributed noise sources", *IEEE J. Quantum Electron.*, vol. 27, p. 178–192.

TSANG, C. F., MARCENAC, D. D., CARROLL, J. E., and ZHANG, L. M., 1994, "Comparison between 'power matrix model' and 'time domain model', in modelling large signal responses of DFB lasers", *IEE Proc. -Optoeletron.*, vol. 141, p. 89–96.

TSANG, W. T., WU, M. C., CHEN, Y. K., CHOA, F. S., LOGAN, R. A., CHU, S. N. G., SERGENT, A. M., MAGILL, P., REICHMANN, K. C., and BURRUS, C. A., 1994, "Long-wavelength InGaAsP/InP multiquantum well distributed feedback and distributed bragg reflector lasers grown by chemical bean epitaxy", *IEEE J. Quantum Electron.*, vol. 30, p. 1370–1379.

UTAKA, K., AKIBA, S., and MATSUSHIMA, Y., 1984, "$\lambda/4$-shifted InGaAsP/InP DFB lasers by simultaneous holographic exposure of positive and negative photoresisters", *Electron. Lett.*, vol. 20, p. 1008–1010.

VANKWIKELBERGE, P., MORTHIER, G., and BAETS, R., 1990, "Cladiss-a longitudinal multimode model for the analysis of the static, dynamic and stochastic behavior of diode lasers with distributed feedback", *IEEE J. Quantum Electron.*, vol. 26, p. 1728–1740.

ZHANG, L. M. and CARROLL, J. E., 1992, "Large-signal dynamic model of the DFB laser", *IEEE J. Quantum Electron.*, vol. 28, p. 604–611.

IMAGE EVALUATION TEST TARGET (QA-3)

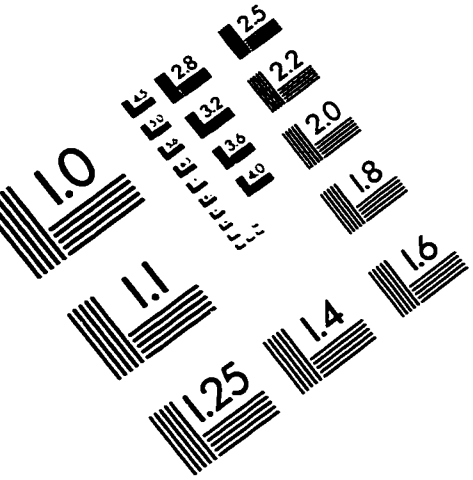

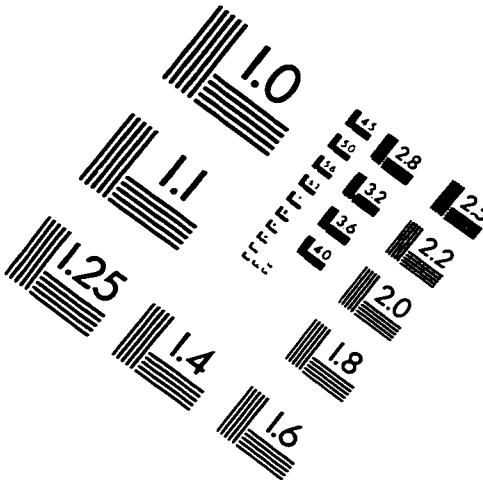

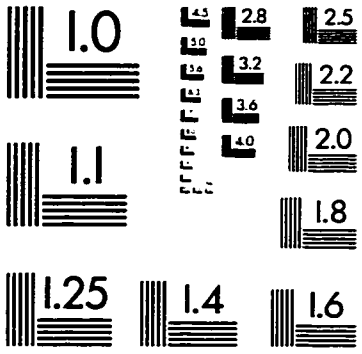

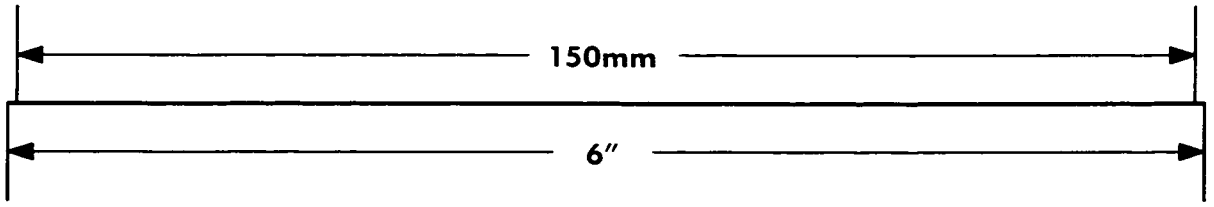

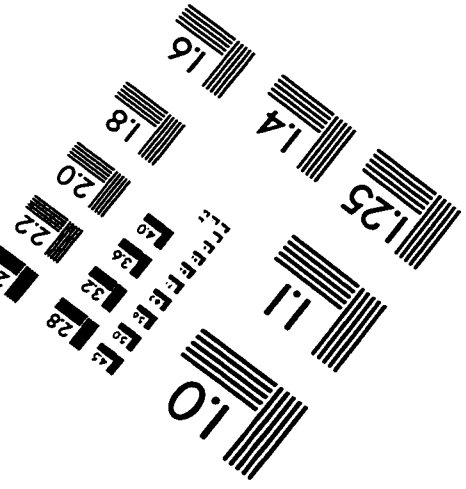

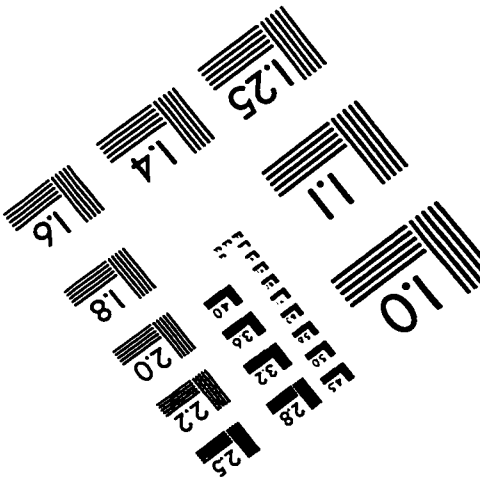

APPLIED IMAGE, Inc
1653 East Main Street
Rochester, NY 14609 USA
Phone: 716/482-0300
Fax: 716/288-5989